CHARACTERIZATION OF NOVEL GENES REGULATING THE SYNAPTIC VESICLE CYCLE IN *DROSOPHILA*

By

Ashleigh Long

Dissertation

Submitted to the Faculty of the Graduate School of Vanderbilt University

Submitted in partial fulfillment of the requirements for the degree of

Doctor of Philosophy

In

Biological Sciences

August, 2010

Nashville, Tennessee

Approved:

Professor Todd Graham

Professor Kendal Broadie

Professor David Miller

Professor Donna Webb

ACKNOWLEDGMENTS

This work could not have been possible without the guidance, support and assistance of many people. I'd like to begin by thanking my advisor, Dr. Kendal Broadie, for his guidance (and patience!) while I was a student in his lab, and for creating a lab with numerous resources so that I can pursue this work. Second, Dr. Jeff Rohrbough has been a wealth of technical assistance, patience, and guidance. Dr. Scott Phillips, Dr. Luyuan Pan, Dr. Nick Trotta, and Ms. Emma Rushton have also provided me with their technical expertise and moral support , for which I am truly grateful. I'd like also thank Qing Xia Chen for maintaining many of the lab instruments and fly stocks that we use in the lab, and Mr. Elvin Woodruff for his contributions of electron microscopy to this work, and for his friendship. Lastly, my family has been an amazing source of love, kindness, and moral support. I could not have done this without their support.

TABLE OF CONTENTS

Page

LIST OF FIGURES AND TABLES

Table

LIST OF ABBREVIATIONS

Ω	Ohms
µM	micrometer
ACh	acetylcholine
AChe	acetylcholinesterase
Arc	activity-regulated cytoskeleton associated protein
AZ	active zone
Ca^{2+}	calcium
CAMKII	calcium/calmodulin-dependent protein kinase II
CNS	central nervous system
DLG	discs large protein
dRich	*Drosophila* Rich protein
EJC	excitatory junctional current
EMS	ethyl methyl sulfonate
ERG	electroretinogram
Fusl	Fuseless
GABA	γ-aminobutyric acid
GAP	GTPase
Gbb	Glass bottom boat
GFP	green fluorescent protein
GluRIIa	ionotropic glutamate receptor type IIa
HRP	horse radish peroxidase
PKA	protein kinase A

PNS	peripheral nervous system
mEJC	miniature excitatory junctional current
mRNA	messenger RNA
mV	millivolts
nA	nanoamp
NMJ	neuromuscular junction
NonC	no-on-and-no-off-transient C
RNA	ribonucleic acid
RNAi	RNA interference
SCAMP	secretory carrier membrane protein
SEM	standard error of mean
SV	synaptic vesicle
TEVC	two electrode voltage clamp
TRP	Transient Receptor Potential
VGCC	voltage-gated calcium channel
Wsp	Wiskott-Aldrich Syndrome Protein
WT	Wild-type

CHAPTER I
Introduction

I. Synaptic Transmission

Chemical synaptic transmission involves a secreted signal from a neuron to a target (neuron, muscle or secretory cell) across intercellular space (Katz and Miledi, 1965). This communication occurs when an action potential travels to the synapse and causes depolarization of the presynaptic bouton. This depolarization opens voltage-gated calcium channels (VGCC) within active zones (specialized sites of vesicular fusion). Presynaptic calcium entry triggers the fusion of docked neurotransmitter-containing vesicles to the presynaptic membrane (exocytosis), and the transmitter then travels across the synaptic cleft to bind postsynaptic receptors. Activated receptors can then function as ion channels or second-messenger systems to modulate the activity of the postsynaptic cell.

Chemical synaptic transmission mechanisms vary in temporal dynamics. “Fast” chemical synapses release transmitter that binds directly to ligand-gated ion channels in the postsynaptic membrane to change their permeability, and this creates ionic flux, across the membrane (Katz and Miledi, 1965). “Slow” chemical synapses release neurotransmitter which also binds to receptors on the postsynaptic membrane; however, these receptors then activate a second messenger system within the target cell that can activate or inhibit ion channels in the postsynaptic membrane (Katz and Miledi, 1965). The phenomenon of synaptic communication between motor neurons and their corresponding postsynaptic muscle targets was initially well characterized by Bernard Katz and his students, who formulated the “Quantal Hypothesis” (Katz and Miledi, 1968), which postulated that the release of neurotransmitter occurs

in discrete “packets” or quanta. We now consider these quanta to be synaptic vesicles.

II. Neurotransmitter and Vesicle Cycles

The cell biological events that orchestrate the release of transmitter from vesicles at the synaptic nerve terminal can be described in terms of two partially overlapping cycles, the *Neurotransmitter Cycle*, which regulates transmitter biosynthesis, storage, reuptake and degradation, and the *Vesicle Cycle,* where components of the synaptic vesicle are recycled via sequential, defined, and repeated steps of membrane trafficking, exocytosis and endocytosis (Figure 1.2).

Neurotransmiter Cycle

Modulation of the neurotransmitter cycle can impact neurotransmitter release and chemical signaling in at least two distinct ways. First, it can affect signaling qualitatively by determining the site and mode of transmitter release. No feature more clearly defines the phenotype of a neuron than the identity of its neurotransmitter (Sudhof, 2001; Sudhof, 2004; Sudhof, 2008). Transmitter identity depends on the expression of specific biosynthetic, storage, reuptake, and degradation machinery (Sudhof, 2001; Sudhof, 2004; Sudhof, 2008). The localization of this machinery within neurons in turn determines the site and mode of neurotransmitter release, as the machinery differs substantially for distinct classes of neurotransmitters, reflecting differences in their mode of action (Fon and Edwards, 2001). Second, modulatory changes to the neurotransmitter cycle can exert a profound influence on the magnitude of signaling by regulating the quantity of neurotransmitter available for release (Fon and Edwards, 2001). Additionally, regulation of the neurotransmitter cycle (at the level of presynaptic vesicle filling) has gained recent attention as a modulator of quantal size. Once considered invariant, it is now generally accepted that the postsynaptic response to

single packets of neurotransmitter may show wide variation in amplitude (Bekkers et al., 1990; Raastad et al., 1992; Liu et al., 1999; Hartveit and Veruki, 2007; Bukaharaeva et al., 2007). This large quantal variability can be observed even under conditions in which the responses arise from a single synaptic bouton isolated by local stimulation (Liu and Tsien, 1995a; Liu et al., 1999; Hartveit and Veruki, 2007; Bukaharaeva et al., 2007). Further evidence has ascribed the variation in postsynaptic response size to variability in the amount of neurotransmitter released (Frerking et al., 1995; Silver et al., 1996; Liu et al., 1999; DiAntonio, 2006; Collins and DiAntionio, 2007) suggesting regulation of postsynaptic activity through differential SV filling.

a. Biosynthesis, Storage, and Reuptake of Neurotransmitter

Classical fast neurotransmitters (γ-aminobutyric acid (GABA), glutamate, and acetylcholine (ACh)) are synthesized in the cytoplasm and therefore need to be packaged into the lumen of SVs prior to release. Relative to the cytoplasm, vesicles contain large amounts of neurotransmitter (Fon and Edwards, 2001; Sudhof, 2004; Sudhof, 2008; Onoa et al., 2010; Messa et al., 2010), requiring active transport by specialized multimeric ATPases. In addition, plasma membrane reuptake systems recycle the exocytotically released neurotransmitter, and the recycled neurotransmitter generally contributes more to SV filling than newly synthesized transmitter (Jones, 1998; Sudhof, 2004; Bruneau and Akaaboune, 2006; Sudhof, 2008; Onoa et al., 2010; Messa et al., 2010). At the *Drosophila* glutamatergic neuromuscular junction (NMJ) synapse, for example, glutamate recycles locally in the nerve terminal, where it can be accumulated using active transport across the membrane of the vesicle (Featherstone et al., 2005; DiAntonio, 2006; Collins and DiAntionio, 2007; Morimoto et al., 2010). These transport and storage activities rely on the proton electrochemical gradient generated by a vacuolar pump, whose activity establishes an electrochemical gradient across the vesicle

membrane (Maycox et al., 1988). The proton pump is approximately 20nm in size, and is composed of a larger peripheral complex called V_1, which engages in ATPase activity, and an integral membrane complex called V_0, which mediates proton translocation. The two subunits operate together to establish the electrochemical gradient that drives neurotransmitter uptake (Fykse and Fonnum, 1996). Vesicular uptake is mediated by at least seven different transporters, representing four distinct uptake systems. At the glutamatergic synapse, glutamate is taken up into synaptic vesicles by three differentially expressed transporters (Fremeau et al., 2002; Gras et al., 2002; Schafer et al., 2002; Collins and DiAntonio, 2007); monoamines (catecholamines, histamine, serotonin), are transported by two differentially expressed transporters (Liu et al., 1992; Elbaz et al., 2010); and single transporters have been identified for GABA and glycine (Sagne et al., 1997; McIntyre et al., 2002; Elbaz et al., 2010), and for acetylcholine (Alfonso et al., 1993; Roghani et al., 1994; Khare et al., 2010). However, most vesicles contain only a single proton pump (Stadler and Tsukita, 1984), suggesting that expression of the particular transporter type is probably a major determinant of the type of neurotransmitter used by a neuron.

b. Neurotransmitter Cycle as a Regulator of Quantal Size

At the NMJ, Bernard Katz described that each quantum of released neurotransmitter from the vesicle triggers a unitary physiological electrical response, or "miniature endplate potential" (Katz and Miledi, 1968) within the target muscle fiber, allowing for muscular contraction to occur in response to transmitter release. Classically, at any particular synapse, the amount of neurotransmitter stored in individual SVs has generally been considered constant (Katz and Miledi, 1965). Recent work, however, suggests neurotransmitter content of vesicles is in fact variable, even within the same synaptic terminal, challenging this long-held view (Liu et al., 1999 DiAntonio, 2006; Collins and DiAntionio, 2007). For example, at

the glutamatergic synapse, it has been shown by Richard Tsien's lab that glutamate receptors are, in general, not saturated during unitary excitatory post synaptic currents (EPSCs) and that trial-to-trial variations in unitary event size are largely due to variations in glutamate concentration (Liu and Tsien, 1995a; Liu et al., 1999; DiAntonio, 2006; Collins and DiAntionio, 2007). Individual steps within the neurotransmitter cycle may therefore also serve an additional role in regulating the amount of neurotransmitter released (Goda and Sudhof, 1997, Farsad and DeCamilli, 2002; DiAntonio, 2006; Collins and DiAntionio, 2007; Edwards, 2007).

c. Neurotransmitter Degradation at the Synapse

After each synaptic release event, neurotransmitter activity must be inactivated to prevent prolonged synaptic activity. This outcome may be accomplished through a variety of means. At the vertebrate NMJ, acetylcholinesterase (AChE), the enzyme that hydrolyzes ACh, is localized within the synaptic cleft. AChE converts ACh into the inactive metabolites choline and acetate, and its role in rapidly clearing free ACh from the synapse is essential for proper muscle function (Gawron and Keil, 1960; Wilson and Alexander, 1962; Gearhart et al., 1980; Sudhof, 2008). Blocking the function of AChE causes excessive ACh to accumulate in the synaptic cleft. The excess Ach causes neuromuscular paralysis (i.e, prolonged muscle contractions) (Gearhart et al., 1980; Sudhof, 2008). Conversely, GABA is inactivated by degradation to succinate in a two-step mechanism involving the enzymes GABA-glutamate transaminase and succinate semialdehyde dehydrogenase (Sudhof, 2004; Sudhof, 2008; Zhang et al., 2010) At the glutamatergic synapse, (for example, the *Drosophila* NMJ), synaptically-released glutamate is taken up by glia, converted to glutamine, and then delivered back to the neuron for conversion to glutamate (reviewed in: Sudhof, 2004; Sudhof, 2008).

Figure 1.1 Differential Vesicle Pools in the Nerve Terminal. The synaptic vesicles are organized in distinct populations or 'pools': the readily releasable pool (the first vesicles released upon stimulation), seen in green; the reserve pool, (RP) (which is called into action only upon strong physiological stimulation), seen in red; and the recycling pool, (those vesicles being reused after fusion to replenish the vesicle pools), seen in yellow.

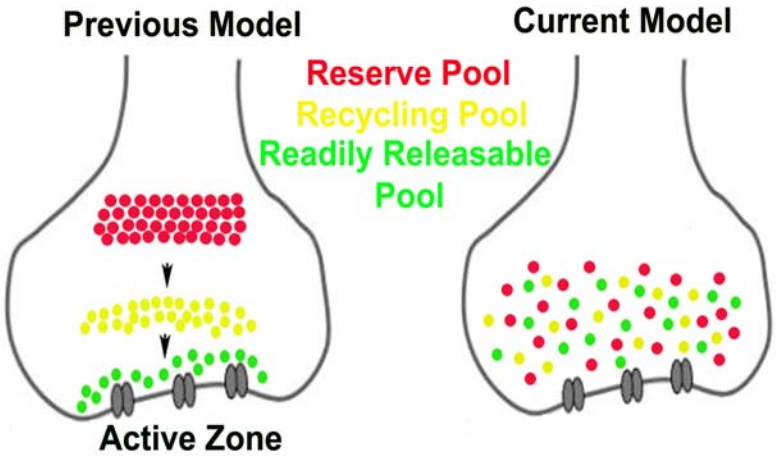
Previous Model
Current Model
Reserve Pool
Recycling Pool
Readily Releasable Pool
Active Zone

The Vesicle Cycle

a. Vesicle Pool Formation

Overall, synaptic vesicles may be similar in terms of their ultrastructure and biochemistry (Sudhof, 2000; Sudhof, 2004; Sudhof, 2008), but for several decades, investigators have proposed that “pools” of vesicles exist, with distinct functional properties. In this view, each vesicle can be assigned to one of at least three pools: the Readily Releasable Pool (RRP), the Recycling Pool and the Reserve Pool (Figure 1.1). The RRP is defined as vesicles that are immediately available to fuse upon neuronal stimulation. These vesicles are generally thought to be docked to the presynaptic active zone and primed for release (Fdez and Hilfiker, 2007, Pang and Sudhof, 2010). The Recycling Pool contains vesicles that maintain cyclic release upon moderate stimulation. Physiological stimulations cause this pool to recycle continuously, and it is constantly refilled by newly recycled vesicles (Sudhof, 2004; Pang and Sudhof, 2010). The reserve pool consists of synaptic vesicles from which release is triggered only during intense stimulation (Virmani et al., 2003; Sudhof, 2004; Bronk et al., 2007; Sudhof, 2008). This pool constitutes the majority of vesicles in most presynaptic terminals, and it is possible that they are seldom or never recruited during routine physiological activity (Virmani et al., 2003; Sudhof, 2004; Bronk et al., 2007; Sudhof, 2008). Many of the molecular mechanisms underlying vesicle trafficking are not clear. However, contributing to the physiological distinction of these vesicle pools are synapsins, a multi-gene family of neuron-specific phosphoproteins. Synapsins are known to modulate neurotransmitter release at the pre-synaptic terminal by reversibly tethering SVs to the actin cytoskeleton, creating the reserve pool (Rohrbough and Broadie, 2005; Bronk et al., 2007; Sudhof, 2008; Cesca et al., 2010; Messa et al., 2010). The N-terminal domain of synapsin I can be phosphorylated by Protein Kinase A (PKA) and calcium/calmodulin dependent kinase II (CAMKII),

releasing the SV from synapsin and the actin meshwork, and presumably allowing the SV to be translocated from the reserve pool to the readily releasable pool (Greengard et al., 1994; Hosaka et al., 1999; Rohrbough and Broadie, 2005; Bronk et al., 2007; Sudhof, 2008; Cesca et al., 2010; Messa et al., 2010). Traditionally, vesicle pools have been depicted as being morphologically segregated into distinct clusters. For example, the RRP must, by definition, lie at or close to the presynaptic membrane. However, recent evidence indicates that, at least in some preparations, vesicles in the recycling and reserve pools are intermixed to a considerable degree (Opazo and Rizzoli, 2010; Li et al., 2010) Figure 1.2.

Underlying the formation of the RRP are vesicles that are “docked” at the active zone, which create the pool of vesicles associated with the plasma membrane. Docked vesicles (Figure 1.2) are defined as those vesicles that appear closely apposed to the plasma membrane of the axon terminal in electron micrographs (Sudhof, 2000; Weimer et al., 2003). The quantitative criterion used to score docked vesicles varies slightly between studies, although most score vesicles whose membrane is within a defined distance of the plasma membrane (e.g., <30nm). For many years, it was debated whether docked vesicles in electron micrographs were a pool of vesicles engaged in distinct molecular interactions, or simply forced into membrane proximity by the high density of vesicles in the reserve pool (Sudhof, 2000; Richmond and Broadie, 2002). The spatial specificity of docking (the clustering of synaptic vesicles around the presynaptic specialization), implies that a protein recognition mechanism likely mediates the attachment of the vesicle to the membrane, rather than crowding by the reserve pool (Richmond and Broadie, 2002; Bronk et al., 2007). Of all the steps of the vesicle cycle, perhaps the least understood is vesicle docking. One reason for this lack of understanding is the difficulty in assaying synaptic vesicle docking. Observation of single synaptic vesicles, via FM dye loading, reveals that synaptic vesicles approach the

plasma membrane, become associated with the membrane for an interval of time, and then detach and drift away (Murthy and Stevens, 1999; Sudhof, 2000; Bronk et al., 2007). It was originally proposed that interactions between the SNARE proteins provided the spatial specificity of docking (Sollner et al., 1993b). Since the SNARE family members are localized to distinct subcellular compartments within the cell, they represent a kind of "molecular tag" at each compartment (Weimer and Richmond, 2005; Sudhof, 2008; Pang and Sudhof, 2010). Thus, formation of SNARE complexes between pathway-specific SNARE proteins may act as a mechanism to ensure the correct anchoring of vesicles to target compartments in the cell. However, subsequent biochemical and genetic characterization of SNARE family members have, thus far, failed to support such a role for the SNARE proteins at the synapse (Weimer and Richmond, 2005; Sudhof, 2008; Lin et al., 2010). When mutants were made of the neuronal Sec1-related protein unc-18 in *C.elegans* (a protein first identified in a screen for "uncoordinated" behavioral phenotypes), the proportion of vesicles docked near release sites is reduced, suggesting a role for unc-18 in docking (Weimer et al., 2003). Additionally, in mice, munc-18 physically interacts with the vesicle associated protein Doc2 (Verhage et al., 1997; Weimer and Richmond, 2005; Groffen et al., 2006; Friedrich et al., 2010), making Doc2 a potentially interesting candidate for docking (Weimer and Richmond, 2005; Groffen et al., 2006; Friedrich et al., 2010). If Doc2 is involved in vesicle docking, via an interaction with munc-18, one might expect to see enhanced docking when Doc2 is overexpressed. Consistent with this, Doc2 overexpression in rat medulla PC12 cells leads to enhanced transmitter release (Groffen et al., 2006; Friedrich et al., 2010), though no ultrastructural analyses have, to this date, been performed, and Doc2's role in vesicle docking is still under investigation.

Figure 1.2 The Vesicle Cycle. The Synaptic Vesicle (SV) Cycle can be divided into seven steps. 1) Docking. SVs that have filled with neurotransmitters dock at the active zone; 2) Priming. After docking, SVs go through a maturation process that makes them competent for Ca^{2+} triggered membrane fusion; 3) Fusion/Exocytosis. Primed SV membranes are stimulated for rapid fusion/exocytosis by a Ca^{2+} spike during an action potential. 4) Endoyctosis. Empty SV membranes are largely internalized by way of clathrin coated pits (aqua color) which become coated vesicles; but also alternatively by the 'kiss and stay' pathway (blue color), or the 'kiss and run' pathway (green color). 5) Translocation. a) Direct Route: coated vesicles shed their coats, acidify, and translocate into the interior, becoming recycling SVs; b) Indirect Route: Recycling SVs fuse with early endosomes, and SVs are regenerated primarily by budding from endosomes. 6) Neurotransmitter Uptake. SVs accumulate neurotransmitters by active transport driven by an electrochemical gradient created by a proton pump. 7) SVs filled with neurotransmitters translocate back to the active zone either by diffusion or by a cytoskeleton-based transport process.

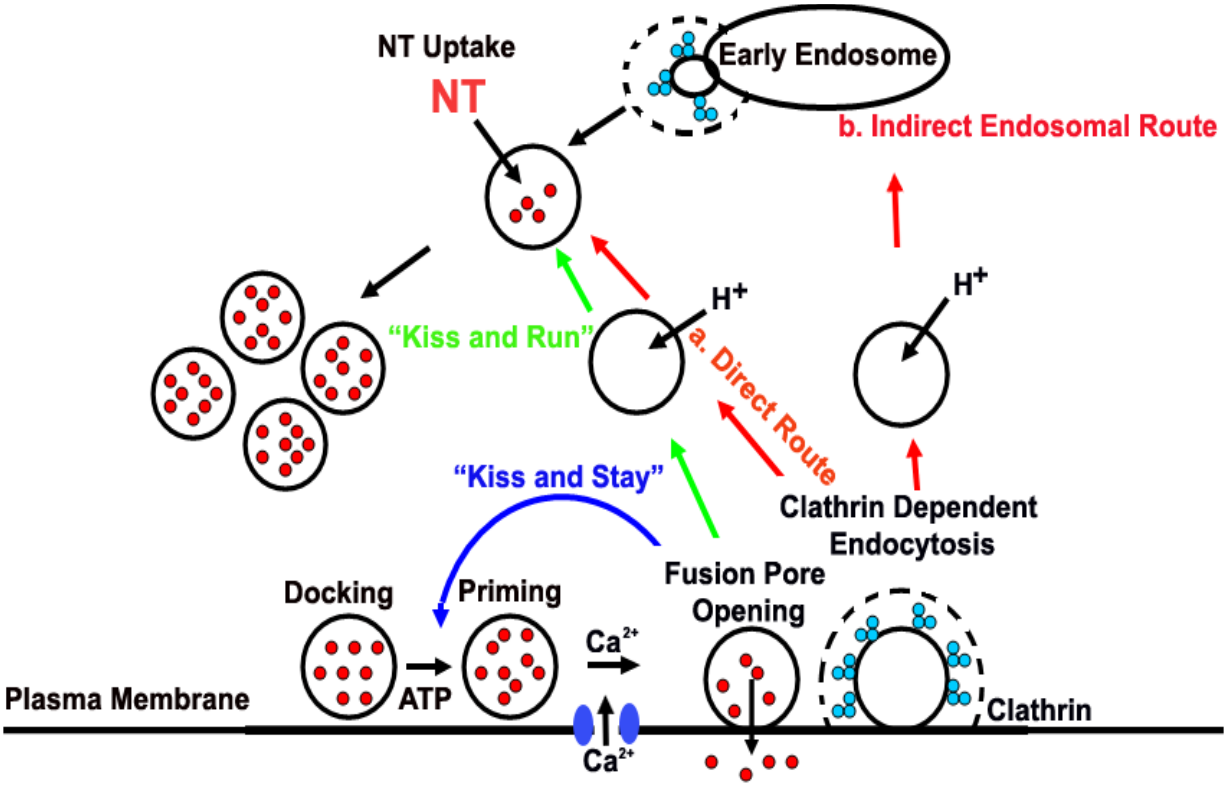
NT Uptake
NT
Early Endosome
b. Indirect Endosomal Route
H+
H+
"Kiss and Run"
a. Direct Route
"Kiss and Stay"
Clathrin Dependent
Endocytosis
Fusion Pore
Opening
Docking
Priming
Ca2+
ATP
Plasma Membrane
Clathrin
Ca2+

Other studies have revealed in yeast that the Rab family of small GTPases proteins may also regulate vesicle docking. In *C.elegans* Rab3 mutants, synaptic vesicles are diffusely distributed at presynaptic nerve terminals with fewer vesicles clustered near active zones (Nonet et al., 1997). Overexpression of Rab3 increases the number of dense core vesicles morphologically docked at the plasma membrane in *C.elegans* and mice (Martelli et al., 2000; Cheviet et al., 2005; Graham et al., 2008; Burgoyne et al., 2009). When bound to GTP, Rab3 directly associates with the presynaptic proteins Rabphilin, a cytoplasmic protein that associates with synaptic vesicles in a Rab3 - dependent manner (Stahl et al., 1996; Sudhof, 2001; Sudhof; 2004), and RIM, an active zone protein (Wang et al., 1997; Sudhof, 2001; Sudhof, 2004; Juranek et al., 2006; Kiyonaka et al., 2007; Sudhof, 2008). Potentially, the interaction between Rab3 and RIM could anchor vesicles at active zones, and Rabphilin could modulate the interaction (Sudhof, 2001; Sudhof, 2004; Juranek et al., 2006; Kiyonaka et al., 2007; Sudhof, 2008). Clearly, a deeper understanding of vesicle docking will require a full characterization of unc-18, Doc2, and Rab3 protein interactions at the synapse, including detailed morphometric and functional analyses.

b. Priming, Fusion, and Assembly of the SNARE Complex

Priming

Priming of the vesicle occurs subsequent to docking; it is the process that makes the vesicle competent for Ca^{2+} - dependent release (Sudhof, 2001; Sudhof, 2004; Verhage and Sorenson, 2008; Sudhof, 2008) (Figure 1.2). Priming is widely accepted to involve the transition of the integral presynaptic plasma membrane protein syntaxin from a “closed” to “open” conformation. Specifically, while in the closed conformation, syntaxin associates with unc-18 (reviewed in Sudhof, 2001; Sudhof, 2004; Sudhof, 2008). In mice, it has been shown that Unc-18-1 forms a complex with closed syntaxin and may inhibit SNARE complex

assembly (Dulubova et al., 1999; Yang et al., 2000), thereby negatively regulating the transition to an open confirmation. However, unc-18-1 is also essential for SV fusion by an unknown mechanism (Verhage et al., 2000; Rizo and Sudhof, 2002; Sudhof, 2004). Additionally, it has been shown that unc-13, a diacylglycerol (DAG) binding protein, can displace unc-18 binding (Richmond et al., 1999; Richmond et al., 2001; Aravamudan and Broadie, 2003; Madison et al., 2005), and that the carboxy (C) terminus of unc-13 interacts with syntaxin in its open state (Maruyama and Brenner, 1991; Betz et al., 1998; Sudhof, 2008). Potentially, unc-13 could thus mediate and/or stabilize an open syntaxin state for assembly of the SNARE complex and subsequent fusion. During SNARE complex formation, target membrane protein syntaxin is thought to initially form a binary complex with vesicle protein synaptobrevin (VAMP) to form a tertiary complex (Sutton et al., 1998; Sudhof, 2004; Sudhof, 2008), or to vesicle-localized synaptotagmin (Rickman et al., 2005; Sudhof, 2004; Sudhof, 2008), which would force the SV into close proximity to the active zone membrane for fusion (Augustin et al., 1999; Jahn and Sudhof, 1999; Lin and Scheller, 2000; Sudhof, 2004; Aravamudan et al., 1999; Richmond et al., 1999). Indeed, unc-13 knockouts in *Drosophila* and *C. elegans* eliminate evoked transmission, and exhibit an inability of docked vesicles to fuse (Richmond et al., 1999; Richmond et al., 2001; Aravamudan and Broadie, 2003; Madison et al., 2005). In *C. elegans*, these defects can be rescued through the transgenic expression of a constitutively “open” syntaxin conformation in an unc-13 null background. This demonstrates that unc-13 functions in the priming mechanism for vesicle fusion competency. In addition, unc-13 is known to exist in both soluble and insoluble forms (Betz et al., 2001). The soluble form of unc-13 can be recruited to the plasma membrane in a DAG-dependent manner (Betz et al., 1998; Ashery et al., 2000) to help form a pool of fusion competent SVs, characterized by low release probability dynamics, and fast refilling rates, which may be the major source

neurotransmitter release during stimulation by high frequency action potentials (Brose and Rosenmund, 2002; Rhee et al., 2002). Conversely, insoluble unc-13 is tightly associated with the cytoskeletal matrix of the active zone by proteinaceous linker, and is proposed to establish a basal, fusion competent SV pool that possesses high release probability but slow refilling rate (Rhee et al., 2002). Additionally, it has been shown that tomosyn, a syntaxin binding protein, inhibits SV priming. Tomosyn contains a SNARE motif, which forms an inhibitory SNARE complex with syntaxin and SNAP-25 (McEwen et al., 2006; Gracheva et al., 2006; Sudhof, 2008). Mutants lacking tomosyn have increased synaptic transmission, an enlarged pool of primed vesicles, and increased abundance of unc-13 at synapses (McEwen et al., 2006; Gracheva et al., 2006; Sudhof, 2008). Thus, priming is modulated by the balance between tomosyn and unc-13, presumably by regulating the availability of open syntaxin (McEwen et al., 2006; Gracheva et al., 2006, Sudhof, 2008).

Fusion

Synaptic transmission requires the fusion of neurotransmitter-filled vesicles with the presynaptic membrane, in a rapid (<50μs), Ca^{2+} influx-driven process, which involves regulated fusion pore opening and expansion (Figure 1.2). The protein machinery responsible for this process includes a core set of proteins, the SNARE proteins (reviewed in Jahn and Sudhof, 1999; Lin and Scheller, 2000), which form an extremely stable complex, shown to be sufficient to promote in vitro membrane fusion in liposomes (Weber et al., 1998), facilitated *in concert* with additional proteins and lipids acting as cofactors (Weber et al., 1998; Jahn and Sudhof, 1999; Lin and Scheller, 2000; Sudhof, 2004; Tucker et al., 2004; Sudhof et al. 2008). This complex is formed by synaptobrevin (VAMP) (Trimble et al., 1988), and syntaxin (Bennett et al., 1992), in addition to SNAP-25 (Oyler et al., 1989). Studies involving clostridial neurotoxins (proteases that cleave SNARE proteins), first demonstrated the

requirement of syntaxin, synaptobrevin, and SNAP-25 in vesicle fusion (reviewed in Schiavo et al., 2000). Additionally, genetic disruption (involving temperature sensitive and null mutants) of syntaxin, synaptobrevin, and SNAP-25 demonstrate that these proteins are essential for vesicle fusion in evoked synaptic transmission (Broadie et al., 1995; Schulze et al., 1995; Sweeney et al., 1995; Deitcher et al., 1998; Rao et al., 2001; Schoch et al., 2001; Vilinsky et al., 2002). One model of fusion pore activity within the SNARE complex suggests that the trans-SNARE complex directly executes fusion. In this model, the fusion pore is considered to be a transient lipid-based intermediate, resulting from the dissipation of a hemi-fusion intermediate (Jahn and Sudhof, 1999; Jahn et al., 2003; Sudhof, 2004; Sudhof, 2008). Additionally, the fusion pore is represented by a "junction-like," proteinaceous pore formed by the 5-8 syntaxin transmembrane segments (Han et al., 2004; Han and Jackson, 2005; Sorenson, 2005).

b. Disassembly of the SNARE Complex

The disassembly of the SNARE complex is essential for maintained synaptic vesicle trafficking in vivo (Sudhof, 2008; Wickner, 2010; Xu et al., 2010). Though experimental analysis has not yet definitively resolved if SNARE disassembly is required for vesicle recruitment to active zones or for vesicle docking, priming, and fusion, recruitment of the ATPase N-ethylmaleimide-sensitive fusion (NSF) protein to the SNARE complex via SNAP adaptors stimulates the disassembly of the complex (reviewed in Sudhof, 2004; Sudhof, 2008). It has also been that this process takes place after vesicle fusion (Littleton et al., 2001), and before endocytosis (Littleton et al., 2001).

c. Calcium Sensors at the Synapse

In all synapses, Ca^{2+} triggers SV fusion to drive neurotransmitter release (Baker et al., 1971; Heuser et al., 1971; Sudhof, 2001; Sudhof, 2004; Sudhof, 2008). Though the SNARE complex has been demonstrated to provide the essential SV fusion machinery, it is still unclear exactly how Ca^{2+} influx triggers vesicle fusion. Synaptotagmin has been proposed to be the major Ca^{2+} sensor that mediates fusion, though its precise mechanism of fusogenic action is largely still unknown (reviewed in: Sudhof, 2001; Sudhof, 2004; Sudhof, 2008). Synaptotagmin I (henceforth now referred to as synaptotagmin), is the most abundant Ca^{2+} binding protein present in the synaptic vesicle, and accounts for ~10% of the total vesicle protein content (Perin et al., 1990; Chapman and Jahn, 1994). Synaptotagmin contains two well-characterized Ca^{2+} and phospholipid binding motifs known as C2 domains. This common motif is present in over 100 proteins (Chapman et al., 1995, 1996; Davis et al., 1999; Schiavo et al., 1997). Synaptotagmin binds the SNARE complex and individual t-SNARES (syntaxin and SNAP-25) in a Ca^{2+} stimulated manner (Chapman et al., 1995, 1996; Davis et al., 1999; Schiavo et al., 1997; Sudhof, 2001; Sudhof, 2004; Sudhof, 2008). Additionally, Synaptotagmin has been shown to undergo homo-oligomerization via Ca^{2+} dependent activation of its C2B domain (Chapman et al., 1996; Osborne et al., 1999; Littleton et al., 1999; Sudhof, 2001; Sudhof, 2004; Sudhof, 2008). In *Drosophila*, a mutant that deletes the entire gene function disrupts synaptotagmin-dependent SV endocytosis (Littleton et al., 1999), but a single point mutation within the C2B domain selectively inhibited Ca^{2+}-dependent exocytosis after the vesicle had docked (Littleton et al., 1999). Analyses of the mutant containing the C2B point mutation showed that Ca^{2+} dependent synaptotagmin oligomerization and SNARE complex assembly were both disrupted (Littleton et al., 2001). These data suggest a model in which Ca^{2+} dependent conformational changes in the

C2B domain cause synaptotagmin oligomerization and trigger fusion via the clustering of SNARE complexes.

D. Identification of Putative Neuronal Ca^{2+} Sensors

i. Unc-13

Unc-13 contains potential Ca^{2+} - binding C2 domains, and the unc-13 mutant phenotype indicates a specialized role for unc-13 in neural-specific synaptic vesicle exocytosis. Moreover, *C. elegans* unc-13 associates with components of the core fusion complex, and the *dunc-13/unc-13 /munc 13-1* null mutations result in a neural-specific block in SV fusion equivalent to the disruption of this complex (Richmond and Broadie, 2002; Junge et al., 2004; Sudhof, 2008). Thus, unc-13 may mediate the calcium dependence of synaptic vesicle fusion. However, it remains to be determined if the putative Ca^{2+}-sensing ability of unc-13 proteins are required for the Ca^{2+} dependence of triggered synaptic vesicle fusion and/or other events downstream of core-complex assembly (Richmond and Broadie, 2002; Junge et al., 2004; Sudhof, 2008). Future work is needed to discern the molecular interactions of unc-13 governing the exocytotic process in vivo (Aravamudan et al., 1999; Richmond and Broadie, 2002; Junge et al., 2004).

ii. Frequenin

Frequenin belongs to the EF-hand family of Ca^{2+} binding proteins (Burgoyne and Weiss, 2001; Burgoyne et al., 2004; Blachford et al., 2009), which includes recoverin, calmodulin, neurocalcin, visinin-like proteins (VILIPs), and hippocalcin. Although the functional roles of these Ca^{2+} - binding proteins are highly diverse, accumulating evidence suggests that many of these proteins modulate ion channels, and other proteins, often bestowing Ca^{2+} sensitivity to the function of interacting partners (Burgoyne and Weiss, 2001; Burgoyne et al., 2004). The functional role of frequenin (also termed neuronal calcium sensor-1 (NCS-1), is largely unknown. Frequenin appears to be particularly enriched in

synapses, such as the motor nerve NMJ endings. Drosophila that overexpress frequenin upon heat shock, exhibit an extraordinarily enhanced, frequency-dependent facilitation of neurotransmitter release (Amici et al., 2009; Blachford et al., 2009; Sanchez-Garcia et al., 2010). Early reports suggest an involvement in exocytosis, because overexpression of frequenin results in enhanced neurotransmission in neurons and exocytosis in neuroendocrine cells (Burgoyne and Weiss, 2001; Burgoyne et al., 2004). This occurs through the modulation of Kv4 channels, which slows neuronal inactivation in a Ca^{2+} dependent manner (Amici et al., 2009; Blachford et al., 2009; Sanchez-Garcia et al., 2010), and accelerates recovery from inactivation (Burgoyne et al., 2004; Amici et al., 2009; Blachford et al., 2009; Sanchez-Garcia et al., 2010). These data suggest that frequenin is involved in the exocytotic fusion process at the NMJ.

iv. Calcium Activated Protein for Secretion (CAPS)

CAPS was discovered as a neuron/endocrine-specific 150 KDa protein that reconstitutes Ca^{2+} - triggered DCV exocytosis in permeable neuroendocrine cells (Walent et al., 1992; Hay and Martin, 1992; Rendon et al., 2001). It is currently known as CAPS-1 because of the highly homolgous and more ubiquitously expressed CAPS-2 protein in higher vertebrates (Speidel et al., 2003). Null mutants in the single CAPS gene in *C.elegans* (Avery et al., 1993) and *Drosophila* (Renden et al., 2001) exhibit loss of secretion of a subset of transmitters. CAPs is proposed to act as a Ca^{2+} binding protein within the fusion complex (Walent et al., 1992). Additionally, CAPS has a pleckstrin homology domain that has a preference for binding to PtdIns(4,5)P2 (Speidel et al., 2003), and a C-terminal region with homology to that of Munc-13, potentially indicating a role in vesicle trafficking. The presence of Ca^{2+} appears to change the phospholipid specificity of CAPS: it binds to PtdIns(4,5)P2 in the absence of Ca^{2+}, but in the range of 10-100 μM Ca^{2+}, it exhibits a preference for phosphatidylcholine/ phosphatidylethanolamine - containing liposomes

(Loyet et al., 1998). Ca^{2+} influx may therefore trigger the fusion process at least in part by changing the phospholipid-binding properties of CAPS, potentially allowing for the stabilization of the secretory vesicle or exocytotic compartment of the nerve terminal (Sudhof, 2008; James et al., 2009), though the function of CAPS in vesicle fusion still requires extensive investigation.

E. Endocytosis/Local Recycling

Vesicle recycling is essential for sustained synaptic transmission. Three pathways have been proposed to function during endocytosis; “kiss and stay,” “kiss and run,” and clathrin-mediated endocytosis (CME) pathways (Figure 1.2). The first two pathways are fast (<1s), involving the transient opening and closure of the fusion pore, where SVs either remain at the active zone, and are refilled with neurotransmitter (“kiss and stay”) or are recycled locally, independent of clathrin (“kiss and run”). These pathways are thought to preferentially recycle SVs into the readily releasable pool under low frequency stimulation. In contrast, CME is relatively slow (30-40s) and may be employed preferentially at higher stimulation frequencies (Koenig and Ikeda, 1996; Pyle et al., 2000; Richards et al; 2000; Sudhof, 2004).

It is still generally accepted that CME represents the major pathway for the retrieval of synaptic vesicle membranes following their complete fusion with the presynatic membrane (Dittman and Ryan, 2009). This process occurs in the periactive zone (the region surrounding the synaptic active zone) and is divided into three major steps: 1) clathrin coat assembly, 2) invagination and fission, and 3) clathrin uncoating (Cremona and DeCamilli, 1997; Slepnev and DeCamilli, 2000; Cremona and DeCamilli, 2001). Recruitment of adaptor proteins (APs) including the AP2 complex and AP180, involves interactions with phosphoinositides, synaptotagmin, and many accessory proteins (Jung and Haucke, 2007; Wenk and DiCamilli, 2004). This mechanism recruits a clathrin lattice to

the plasma membrane. Clathrin accessory proteins are recruited to facilitate invagination of the coated pit, by changing membrane curvature and recruiting other endocytic proteins. Amphysin and endophilin are two well characterized clathrin accessory proteins (Slepnev and DeCamilli, 2000). At vesicle fission, dynamin (which composes the core of the fission complex (Pucadyll and Schmid, 2009)) is recruited to the stalk of the deeply invaginated coated pit to mediate the fission of the clathrin-coated vesicle from the presynaptic membrane. Dynamin is a GTPase with a pleckstrin homology domain (PH domain), GTPase enhancing domain (GED domain), and a proline-rich domain in its C-terminus. In *Drosophila*, the shibire locus encodes dynamin. Shibire was discovered based on a temperature sensitive phenotype that results in paralysis at non-permissive temperature that is reversed upon lowering to permissive temperature (Poodry and Edgar, 1979; Kosaka and Ikeda, 1983; van der Bliek and Meyerowitz, 1991; Kasuya et al., 2009). In shibire mutants, vesicle recycling is arrested at a very specific stage of membrane retrieval from presynaptic plasma membrane (Poodry and Edgar, 1979; Kosaka and Ikeda, 1983, van der Bliek and Meyerowitz, 1991; Kasuya et al., 2009). At this “collared pit” stage, nascent endocytic vesicles are attracted to plasma membrane via a narrow neck bearing an electron dense collar (van der Bliek and Meyerowitz, 1991; Kasuya et al., 2009). Observation of clathrin-coated pit dynamics using total internal reflection microscopy indicates that, during fission, dynamin recruitment to coated pits is rapidly followed by the recruitment of actin, suggesting a role for actin and dynamin interacting accessory proteins in promoting constriction of the vesicle neck (Merrifield et al., 2005; Ferguson et al., 2009). Following vesicle budding, the clathrin coat is rapidly removed. This reaction has been shown to require ATP, synaptojanin I, and auxilin (Wenk and DiCamilli, 2004; Dittman and Ryan, 2009). Most of the newly formed vesicles are transported from the periactive zone directly back to the site of release, whereas a smaller fraction fuse with a primary endosomal

compartment for additional sorting or degradation (Heuser and Reese, 1973; Miller and Heuser, 1984; Jahn and Sudhof, 2006; Dittman and Ryan, 2009).

Characterization of Novel Genes Regulating the *Drosophila* SV cycle

To identify further essential components of the SV cycle, a *Drosophila* forward genetic screen approach was exploited, which formed the basis of this thesis. The *Drosophila* genome was mutated using ethyl methane sulfonate (EMS), and screened for synaptic transmission mutants using electroretinogram (ERG) physiological recordings in the adult visual system (Pak et al., 1967). In this project, I originally targeted eight genetic loci identified in this screen by Dr. William Pak's laboratory at Purdue University. The particular mutant class specifically lacks the lights "on/off transient" component of the ERG. These transients represent responses by the photoreceptor cell to the initiation and cessation of light, involving synaptic transmission events between photoreceptor cells and their laminar targets (Pak et al., 1969). Experiments with many different visual system mutants indicate that the impairment of synaptic transmission in the eye results in a loss of these ERG transients (Pak et al., 1969; Pak et al., 1970; Leung et al., 2000; Gengs et al., 2002). Axonal pathfinding and synaptic morphology appeared unaffected in the visual system of the eight mutants, and therefore, they were identified as genes specifically required for synaptic transmission.

The *Drosophila* visual system is a difficult place to assay synaptic function directly: photoreceptor synapses are poorly accessible and intractable to most functional synaptic assays (Atwood et al., 1993**;** Kurdyak et al., 1994; Li et al., 2002; Sudhof, 2004, Sudhof 2008). In

Figure 1.3: Electron Micrograph of the *Drosophila* NMJ. The *Drosophila* NMJ makes an ideal synapse for experimental study due in part to an ease in experimental accessibility and distinct morphological structures. This image shows the clear separation that exists between the pre and post synaptic compartments of the NMJ, in addition to active zones and a synaptic cleft which can be easily visualized. Black arrow points to a synaptic vesicle in the readily releasable pool; white arrow points to vesicle fusion at the active zone. Image taken from Long et al., 2008, Journal of Neuroscience.

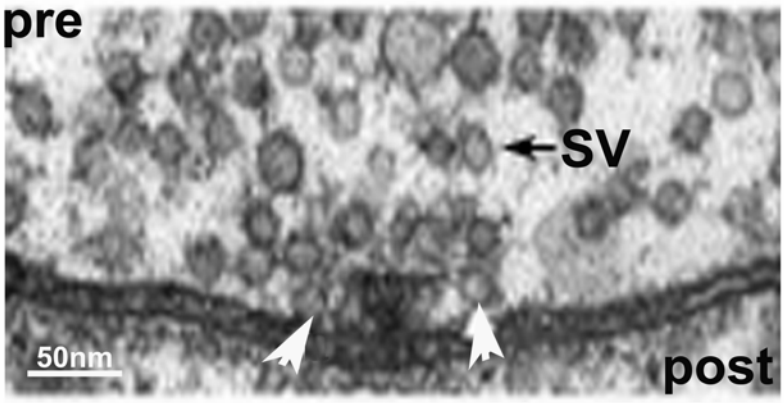
pre
SV
50nm
post

contrast, the *Drosophila* NMJ (Fig.1.3) is well - characterized and easily accessible, with the molecular mechanisms of its SV cycle routinely studied (Fig. 1.2). *Drosophila* NMJ synapses have been extensively defined at the cellular, ultrastructural and electrophysiological levels, making them attractive sites for synaptic cell biological assays (Atwood et al., 1993**;** Kurdyak et al., 1994; Li et al., 2002; Sudhof, 2004, Sudhof 2008). Using this synapse to characterize new vesicle cycle proteins, two complementation groups were selected for detailed analysis: Fuseless (Fusl), and No-on-and-no-off transient C (NonC).

Fuseless as a novel regulator of presynaptic calcium channels

Fuseless (Fusl) is shown here to be a novel presynaptic integral membrane protein with a proposed critical function in regulating active zone voltage-gated Ca^{2+} channels. Thus the Ca^{2+} trigger driving SV fusion. Protein supplied with an acute (12 hour) pulse of expression targeted only to the presynaptic side, indicates a dynamic function in neurotransmitter release. Presynaptic active zones are disrupted in the absence of Fuseless, with around half the normal NC82/Bruchpilot (ELKS/CAST/ERC homolog) active zone domains (Wagh et al., 2006; Kittel et al., 2006). Presynaptic functional defects in null *fuseless* mutants are similar to those found in the Ca^{2+} channel mutant *cacophony* (e.g. reduced Ca^{2+}-dependent basal transmission and Ca^{2+}-dependent facilitation; Xing et al., 2005; Kawasaki et al., 2000). Other mechanistic defects also suggest a disrupted Ca^{2+}-trigger for exocytosis, including reduced FM1-43 and SV cycling indicating a specific exocytosis defect. Consistently, the Fuseless protein regulates Cacophony Ca^{2+} channel expression and localization to presynaptic active zones. Mutant synapses exhibit elevated resting [Ca^{2+}] and a profound reduction in Ca^{2+} influx during depolarization, demonstrating a role for Fuseless in regulating the Ca^{2+} dynamics driving neurotransmission. Mutants do not exhibit postsynaptic upregulation in glutamate receptor expression or function,

consistent with the hypothesis that the retrograde pathway driving these compensations requires functional presynaptic Ca^{2+} channels (Frank et al., 2006). Additionally, presynaptic function in null *fuseless* mutants is enormously enhanced simply by introducing an exogenous Ca^{2+} influx trigger, showing that regulation of active zone Ca^{2+} channel domains is the primary role of Fuseless in controlling neurotransmission strength.

No on and no off transient – C (NonC)

The *no-on-and-no-off transient C* (nonC) gene encodes the phosphatidylinositol 3-kinase-like kinase (PIKK) Smg1, a regulatory kinase of the nonsense-mediated decay (NMD) pathway. NMD is an mRNA surveillance system critical to the maintenance of transcript integrity. The Smg complex (Smg1-7) degrades mRNA transcripts containing nonsense mutations that would produce truncated proteins with potentially deleterious activities. This study reveals that the NMD pathway regulatory kinase Smg1, as well as two other pathway components (Upf2/Smg3 and Smg6), function to protect the development of synaptic morphological architecture and maintain high fidelity neurotransmission function, especially under conditions of heightened activity. NMD activity is required in two very distinct synaptic classes, retinal photoreceptor synapses and the NMJ, suggesting that a NMD-mediated protective mechanism is broadly important in synapses throughout the nervous system. At the *Drosophila* NMJ synapse, an extended allelic series of Smg1 mutants show impaired structural architecture, with decreased terminal arbor size, branching and synaptic bouton number. Functionally, loss of Smg1 results in a ~50% reduction in basal neurotransmission strength, progressive transmission fatigue and greatly impaired synaptic vesicle recycling especially during high-frequency stimulation. Mutation of two other NMD pathways genes (Upf2/Smg3 and Smg6) similarly impairs neurotransmission and synaptic vesicle cycling. These findings suggest that the NMD pathway acts to regulate mRNA integrity in order to

safeguard synapse morphology and maintain synaptic functional efficacy. We have proposed a model in which is that *S*mg mutants are unable to prevent translation of damaged transcripts, and thus “toxic proteins” result in smaller, less developed and functionally compromised synapses. Where and when the NMD machinery performs this essential activity is uncertain; it could be wholly in the neuronal soma, or locally at synapses for transcripts that may undergo local translation. Mutant defects in *S*mg mutants appear largely restricted to the presynaptic domain of the NMJ; postsynaptic scaffolding and glutamate receptor expression is not detectably altered in mutants, and there is no detectable change in postsynaptic physiological function.

Taken together, the functional and morphological characterizations presented herein on the Fuseless and No-on-and-no-off-transients C proteins contribute to the body of knowledge on novel regulators of the synaptic vesicle cycle and bring new insights into the mechanism of Ca^{2+} triggered synaptic vesicle fusion, and replenishment of the readily releasable pool through regulated endocytosis.

CHAPTER II

Presynaptic Calcium Channel Localization and Calcium Dependent Synaptic Vesicle Exocytosis Regulated by the Fuseless Protein

This paper has been published under the same title in the *Journal of Neuroscience*, 2008.

A. Ashleigh Long[1], Eunju Kim[2], Hung-Tat Leung[2], Elvin Woodruff III[1], Lingling An[3], R. W. Doerge[3], William L. Pak[2] and Kendal Broadie[1]

[1]Department of Biological Sciences, Kennedy Center for Research on Human Development, Vanderbilt University, Nashville TN 37235-1634 USA

[2]Department of Biological Sciences and [3]Department of Statistics, Purdue University, West Lafayette, IN 47907 USA

Abstract

A systematic forward genetic Drosophila screen for electroretinogram mutants lacking synaptic transients identified the fuseless (fusl) gene, which encodes a predicted 8-pass transmembrane protein in the presynaptic membrane. Null fusl mutants display >75% reduction in evoked synaptic transmission but, conversely, a ~3-fold increase in the frequency and amplitude of spontaneous synaptic vesicle fusion events. These neurotransmission defects are rescued by a wildtype fusl transgene targeted only to the presynaptic cell, demonstrating a strictly presynaptic requirement for Fusl function. Defects in FM dye turnover at the synapse show a severely impaired exo-endo synaptic vesicle cycling pool. Consistently, ultrastructural analyses reveal accumulated vesicles arrested in clustered and docked pools at presynaptic active zones. In the absence of Fusl, calcium-dependent neurotransmitter release is dramatically compromised and there is little enhancement of synaptic efficacy with elevated external Ca^{2+} concentrations. These defects are causally linked with severe loss of the Cacophony voltage-gated Ca^{2+} channels, which fail

to localize normally at presynaptic active zone domains in the absence of Fusl. These data indicate that Fusl regulates assembly of the presynaptic active zone Ca^{2+} channel domains required for efficient coupling of the Ca^{2+} influx and synaptic vesicle exocytosis during neurotransmission.

Introduction

The calcium influx triggering neurotransmission occurs via voltage-gated calcium channels clustered at presynaptic active zones. Vesicular exocytosis is driven by the rapid (<1 ms) elevation of calcium concentration (>1000 fold) within the presynaptic bouton (Dodge and Rahamimoff, 1967). High [Ca^{2+}] microdomains are generated by the opening of calcium channels directly tethered to docked synaptic vesicles, poised to fuse with the presynaptic membrane (Delcastillo and Katz, 1954a; Katz and Miledi, 1965a, Llinas et al., 1992; Horrigan and Bookman, 1994; Becherer et al., 2003; Demuro and Parker, 2006). Any disruption of these localized Ca^{2+} spikes significantly impairs vesicle exocytosis to interfere with the efficacy of basal synaptic transmission as well as Ca^{2+}-dependent modulation.

Biochemical and genetic approaches have led to the identification of presynaptic proteins linking Ca^{2+} dynamics with the synaptic vesicle (SV) cycle (Chen et al., 2001; Farsad and De Camilli, 2002; Rizo and Sudhof, 2002; Khvotchev et al., 2003; Takamori et al., 2006). *Drosophila* genetic screens have made important contributions to our understanding of this Ca^{2+}-driven machinery. A screen for defective courtship identified mutations in *cacophony* (*cac*), encoding a Ca^{2+} channel $\alpha 1$ subunit, which exhibit reduced synaptic efficacy (Von Schilcher, 1976; Kawasaki et al., 2000; Kawasaki et al., 2004; Xing et al., 2005). A screen for defective locomotion identified mutations in *frequenin* (*freq*; NCS-1), encoding an EF-hand Ca^{2+} sensor, which exhibits reduced Ca^{2+}-dependent exocytosis and facilitation (Pongs et al., 1993; Bourne et al., 2001; Wang et al., 2001; Pan et al., 2002; Tisujimoto et al., 2002; Sippy et al., 2003). *Drosophila* mutants of *synaptotagmin I*, an integral SV Ca^{2+}-binding protein, display >75% reduced

evoked neurotransmitter release and elevated spontaneous SV fusion, which helped establish the hypothesis that Synaptotagmin acts as a Ca^{2+} sensor synchronizing fast exocytosis (Littleton et al., 1993; Broadie et al., 1994; DiAntonio and Schwarz, 1994; Geppert et al., 1994; Yoshihara and Littleton, 2002). Mutants in *Drosophila unc-13*, a protein with C2 and C1 domains, display blocked SV fusion and arrested docked SVs at active zones, which helped establish the hypothesis that UNC-13 regulates SV priming (Aravamudan et al., 1999; Aravamudan and Broadie, 2003; Speese et al., 2003).

To identify new synaptic components, we performed *Drosophila* screens isolating synaptic mutants in the visual system utilizing electroretinogram recordings (Pak 1975; Burg et al., 1993). Since photoreceptor synapses are intractable for functional assays, detailed analyses were performed at the accessible neuromuscular junction (NMJ). The *fuseless* (*fusl*) mutants display dramatically impaired transmission at both photoreceptor and NMJ synapses. Neurotransmission defects are rescued by targeted presynaptic expression of a *fusl* transgene, confirming gene identity and specific presynaptic requirement. The fuseless gene encodes a predicted 8-pass transmembrane protein of the presynaptic membrane, which regulates the localization of Cacophony Ca^{2+} channels to presynaptic active zones. Consistent with the loss of the Ca^{2+} trigger for SV exocytosis, *fusl* mutants show a severe reduction in SV cycling, as measured via lipophilic dye imaging, and a great elevation in the number of SVs clustered around active zones and docked with the presynaptic membrane poised for fusion, as shown by ultrastructural analyses. These data demonstrate that Fusl functions in the presynaptic membrane to facilitate localized expression of Ca^{2+} channels in active zone domains, and that this activity is required for efficient synaptic vesicle exocytosis.

Materials and Methods

Second Chromosome Mutagenesis Scheme

The second chromosome mutagenesis was done with an Oregon-R (OR) wild-type stock isogenized for the second chromosome and a dominant temperature sensitive lethal mutation on the second chromosome, *DTS-2* (Suzuki and Procunier, 1969). Wild-type males were fed 25 mM ethyl methane sulfonate (EMS) in 1% sucrose for 18 hrs (Ohnishi, 1977) and mated to virgin females carrying the *DTS-2* second chromosome over the second chromosome balancer, *SM5*, marked with *Curly* (*Cy*) (Lindsley and Zimm, 1992) (Fig. 1A). From the offspring of this cross, males carrying the mutagenized second chromosome over *DTS-2* were selected and single-male mated to virgin females of the *DTS-2/SM5 Cy* stock. Raising the temperature to 29^{o}C killed *DTS-2*-carrying offspring of this cross (F2 in Fig. 1A), and the only surviving offspring were those carrying the mutagenized second chromosome over the *SM5* balancer. Mating flies *inter se* generated offspring that are either homozygous or heterozygous for the mutagenized second chromosome (F3 in Fig. 1A). These flies were tested directly for mutant phenotypes by ERG recording (Fig. 1B). For recessive mutations, heterozygotes, which could be distinguished from homozygotes from the presence of *Cy* in the balancer chromosome, served as internal wild-type controls. Each line resulting from separate single-male mating in the P2 cross was considered a potential independent mutagenesis event. Lines that displayed mutant phenotypes for at least three generations were made homozygous and kept as mutant alleles.

Microarray Analysis: RNA Isolation, Gene Chip Hybridization and Statistics

Three independent replicate RNA samples (>5 µg) were prepared from isolated heads of each of the three *fusl* alleles and wild-type controls. Total RNA was extracted with the RNeasy mini Kit (Qiagen). Each RNA sample was checked for quality and concentration by 1% agarose-

formaldehyde gel separation and a spectral scan in the 210-230 nm region. The Affymetrix *Drosophila* genome array (Affymetrix GeneChip) version 2.0 was used in this work based on *Drosophila* Genome Annotation release 3.1 (released in 2003, Flybase; each chip contains 18,800 probe sets). The Purdue Genomics Core Facility processed the samples according to the Affymetrix protocol: (http://www.affymetrix.com/Auth/support/download/manuals/expression_s2_manual.pdf). Briefly; from total RNA, mRNA was reverse transcribed to cDNA, and the resulting cDNA used to generate amplified biotin-labeled cRNA. cRNA was fragmented by heating and hybridized to the chip. An analysis of variance (ANOVA) was used to statistically test for differences in mRNA steady-state levels between mutants and the control using normalized data (Craig et al., 2003). It is necessary to adjust the type I error rate to accommodate multiple testing issues, using both the false discovery rate (FDR) approach (Benjamini and Hochberg, 1995) and Holm's sequential Bonferroni correction procedure (Holm, 1979). The significance level was chosen as 0.05. Genes falling within the mapped chromosomal limits of *fusI* were first identified. Statistical analysis of the microarray data provided the log-fold change in expression along with standard deviations and the P-value detected by probe sets corresponding to each gene. Candidate genes were identified as those with the largest log-fold changes (in absolute value) and with the lowest P values. For sequencing candidate genes, primers were designed for several overlapping fragments encompassing the entire mRNA. RT-PCR reactions were done with the Qiagen Onestep RT-PCR kit and PCR fragments were electrophoresed on a 1% agarose gel and purified using the QIA-quick Gel Extraction Kit (Qiagen). Each purified PCR fragment was paired with its own primers in separate sequencing reactions to determine both forward and reverse cDNA sequences.

Validation of Gene Identification: RNAi

Double-stranded RNA was used to knock down the *CG14021* gene by direct injection into the embryo (Lam and Thummel, 2000). Non-homologous regions of *CG14021* were identified; one such region being nucleotide #1227 to 1748 (Acc # NM164640). First-strand cDNA was synthesized using Superscript III (Invitrogen) with oligo (dT) primer. The template DNA for transcription reaction was amplified by PCR and used for the transcription reaction to synthesize the desired double-stranded RNA fragments (T7 RNA polymerase reaction kit, Ambion). The synthesized RNA fragments were precipitated, washed with 70% EtOH, and, after briefly air-drying, dissolved into injection buffer (5 mM KCl, 0.1 mM Na_2PO_4, pH 6.8) at 5 μM concentration for injection.

Validation of Gene Identification: cDNA and Genomic Rescue

The cDNA rescue construct utilized the GAL4-pUAST modular expression system (Brand and Perrimon, 1993). The eGFP coding sequence was fused to the *CG14021* sequence in the construct for ready visualization of the gene product. *CG14021* cDNA was generated using Superscript III reverse transciptase (Invitrogen) from total wild-type RNA. The *CG14021* coding sequence (Acc #: NM164640; 857..2215) was amplified using PFU DNA polymerase (Stratagene). The PCR product was subcloned into T-easy vector (Promega) and cloned into the *pP{UAST}* vector at the *EcoR* I cloning site. The eGFP coding sequence was amplified by PCR using pIRES2-EGFP plasmid DNA as template, and the eGFP tag was fused in frame at the C-terminus of the CG14021 coding sequence utilizing the *Bgl* II and *Kpn* I sites. Transgenic flies carrying the *pP{UAST}* vector were generated by injection of the vector into w^{1118}; $fusl^{1}$ mutant embryos. To activate the target sequence, these flies were crossed to those expressing GAL4 driven by either the *Rh1* promoter for photoreceptor-specific expression or the *elav* promoter for neuron-specific expression. *CG14021-eGFP* fusion genes were used in genomic rescue constructs to enable localization of the CG14021 protein in

transformants. The *CG14021* gene encodes two transcripts RA and RB, generated by alternative splicing of the first intron (Fig. 2B). The coding sequence is the same but the non-coding first exons are located at two different locations several kb upstream of the coding sequence. Therefore, two different genomic constructs were generated corresponding to the two different transcripts. Immediately upstream of the smaller RA transcript is a 2 kb promoter region containing the TATA box, the insect transcription initiation site, and the 11-bp conserved sequence for photoreceptor cell expression. For the larger RB transcript, the promoter was taken to be the ~1 kb region between the *CG14021* gene and the neighboring up-stream gene *CG12512*. The sequences used were, in Flybase nucleotide coordinate units, 2L:5,330,871..5,338,053 for the smaller transcript and 2L:5,330,871..5,339,224 for the larger transcript (Fig. 2B). Each of these sequences, from which the stop codons and 3' untranslated regions had already been removed, was amplified in several fragments by PCR, linearized and cloned into the *Pst* I and *Not* I sites of a modified *pP{UAST}* vector. The *pP{UAST}* vector was modified by removing the UAS promoter and cloning the eGFP coding sequence into its *Kpn* I and *Xba* I cloning sites. Each of the two *CG14021* genomic sequences was cloned into the modified vector to generate a vector containing in-frame fusion of eGFP coding sequence at the C-terminal end of the *CG14021* genomic sequence. The two vectors along with *fusl* mutants were sent out to Rainbows Transgenic Flies, Inc. for generation of transgenic flies.

Fuseless Antibody Generation

A synthetic peptide corresponding to amino acid residues AMASFLIGGLGHFFF was used for immunization, and injected into two rabbits, following standard immunization protocols (Open Biosystems, Huntsville, AL). For epitope preservation, these antibodies work best with brief Bouin's (picric acid) Fixative (15 mins). The antibodies were used at a dilution of 1:100 in PBS-TX-BSA, where the concentration of TX-100 was 1%, and BSA was 2%. Antibodies were incubated overnight (12 hrs) at 4^{o}C. The secondary antibody Alexa Fluor 546 goat anti-rabbit

(Invitrogen, Eugene, Oregon) was used at a dilution of 1:200 for 2 hrs at room temperature.

Frozen Cryosectioning of the Visual System

The sectioning of *Drosophila* heads was done as described (Melzig et al., 1998). Heads from young adults were fixed for 2.5 hrs in an ice-cold solution containing 4% 1-ethyl-3,3-dimethylamino- propyl carbodi-imide (Sigma) in 67 mM phosphate buffer, pH 7.4, and then washed overnight in 22.5% sucrose in PBS (130 mM NaCl, 7 mM Na_2HPO_4, and 3 mM NaH_2PO_4 , pH 7.4). The heads were then embedded on small cryostat chucks with 18% carboxymethyl-cellulose, shock frozen in melting nitrogen, and sectioned at 10µm thickness on a cryostat microtome. The sections were blocked for 30 mins in PBST (phosphate buffered saline, 0.05% Triton X-100/4% BSA) and incubated in anti-fusl antiserum in PBS (diluted 1:100) containing 4% BSA overnight at 4°C. After 3x PBST washes, specimens were incubated for 2 hrs at room temperature in goat anti-rabbit IgG labeled with Alexa Fluor 488 (Invitrogen) diluted 1:200 with PBS containing 4% BSA. Specimens were washed 3x in PBST, mounted with ProLong Gold Antifade Reagents (Molecular Probes), and viewed on a Bio-Rad MRC1024 confocal microscope (Nikon 60x, 1.4NA lens) using the Bio-Rad LaserSharp software. Acquired images were processed with image J and Photoshop 7.0.

Immunohistochemistry at the Neuromuscular Junction

Wandering 3rd instar larvae were dissected in standard *Drosophila* saline, fixed for 15 mins in Bouin's Fixative, washed for 30 mins in PBS-TX and stained with the primary antibodies for 4 hrs at RT. Presynaptic NMJ terminals were visualized with Texas Red-conjugated anti-Horse Radish Peroxidase (anti-HRP; 1:200; Molecular Probes, Eugene, OR), which recognizes a neuronal membrane epitope. Staining of synaptic vesicles was done with Synaptotagmin I antibody (anti-rabbit, 1:500; gift from Dr. Hugo

Bellen, Baylor College of Medicine, Houston, TX). Postsynaptic glutamate receptors were visualized using GluRIIA antibody (8B4D2, anti-mouse; 1:10; University of Iowa Developmental Studies Hybridoma Bank). Secondary antibodies were Alexa 488 and Alexa 633 (1:200; Molecular Probes, Eugene, OR) incubated for 2 hrs at RT. All images were taken on an upright Zeiss 510-Meta confocal microscope.

Electrophysiology: Electroretinogram (ERG) and Intracellular Recordings

ERGs were recorded as previously described (e.g. Larrivee et al., 1981). A 300 W Halogen lamp (OSRAM) was used to generate light stimuli which were delivered to the eye using a light guide (Fig. 1B). Orange stimuli were generated by interposing a Corning CS2-73 filter in the light path. The stimulus intensity was attenuated in log-unit steps using Kodak neutral density filters. Orange stimuli were used because they generate larger on-/off-transients than white light stimuli. The unattenuated intensity at the level of the eye was 830 $\mu W/cm^2$. Both the recording and ground electrodes were filled with Hoyle's solution. The ground electrode was inserted into the head and the recording electrode was inserted through the cornea into the photoreceptor layer. The fly was dark-adapted for 2 mins before each stimulus, and all recordings were carried out at 25^oC. Intracellular recordings were performed essentially as described by Johnson and Pak (1986). Briefly; a small cut was made on the head so as to cover a portion of the cornea and a part of the head. The cut was immediately sealed with vacuum grease to prevent fluid loss. Both the recording and ground electrodes were inserted through the cut with the recording electrode tip placed within the photoreceptor layer and the ground electrode tip very close to the photoreceptor layer. The recording electrode, filled with 2M KCl, had a resistance of 25-50 Ω. The light source and the filters were the same as in ERG recordings. Signals were sampled at 2 kHz with an analog-to-

digital converter, and the data were acquired and analyzed with Axoscope software (Axon Instruments).

Electrophysiology: Two Electrode Voltage Clamp (TEVC) Recordings

Electrophysiology at the wandering 3rd instar NMJ was done using standard TEVC techniques as described previously (Rohrbough et al., 1999). In brief; larvae were raised at 25°C and dissected dorsally in modified *Drosophila* saline containing additional sucrose (34 mM) and 5 mM trehalose to prevent muscle vacuolization and to mimic conditions of the natural haemolymph as described (Stewart et al., 1994). Saline contained (in mM): 128 NaCl, 2 KCl, 4 $MgCl_2$, 5 Trehalose, 70 Sucrose, and 5 Hepes, and received appropriate volumes of 100mM Ca_2Cl stock solution to make the $[Ca^{2+}]$ indicated. Larvae were secured on sylgard-coated coverslips using surgical glue (Liquid Suture, Allentown, Pa.). Evoked EJCs were stimulated with a glass suction electrode on the appropriate segmental nerve at a suprathreshold voltage level. Glutamate iontophoresis was performed as previously described (Featherstone et al., 2005). Briefly; glutamate (100 mM; pH=9) was pressure ejected from a small diameter (10 μm) glass pipette and glutamate-gated currents recorded in TEVC. All current recordings were done in voltage clamped muscle (V_{hold} = -60mV) on muscle 6 (segment A3) with Axoclamp 200B (Axon Instruments) and analyzed with Clampex 7.0 software.

FM-143 Dye Imaging

Dye imaging studies were performed as described previously (Trotta et al., 2004). Briefly; wandering 3rd instar animals were dissected in 1.8 mM Ca^{2+} standard saline. Preparations were incubated with FM1-43 (10 μM; Molecular Probes) for 2 mins in high $[K^+]$ saline (90 mM [NaCl] reduced to 50mM) at RT. Preparations were then washed in buffered 0 mM Ca^{2+} saline for 2 mins. Images were acquired on a Zeiss 510-Meta confocal microscope. The mean pixel fluorescence at individual NMJ boutons was

determined using ImageQuant software (Molecular Dynamics). The mean pixel intensity of at least five single boutons was averaged for each NMJ and two NMJs per animal were then averaged to generate a single data point. The vesicle cycle was stimulated again using the high [K^+], as above but without FM1-43, for 2 mins to unload FM1-43 dye from the NMJ boutons and provide a measure of exocytosis efficacy. The degree of unloading was quantified in the same manner as that of the loading procedure. FM1-43 dye loading was also assayed using electrical motor nerve stimulation as previously described (Dermaut et al., 2005). In brief; the nerve was stimulated with a glass suction electrode at 30 Hz for 5 mins with 10 μM FM1-43 in the bath. Preparations were then washed in buffered 0 mM Ca^{2+} saline for 2 mins. Loading was quantified using average mean pixel intensity per bouton as above.

Electron Microscopy: Ultrastructural Analysis

Mutant (*fusl*^{1};*fusl*^{1} and *fusl*^{1}/Df) and control (wild-type OR-R and +/Df) wandering 3rd instar larvae were fixed, sectioned and visualized in parallel using standard TEM techniques, as reported previously (Featherstone et al., 2001). Briefly; animals were dissected in 0.05M PBS and placed in 2.0% glutaraldehyde for 15 mins; replaced with fresh 2.0% glutaraldehyde for 1 hr. Preparations were washed in PBS (3X), transferred to 1% O_sO_4 in dH_2O for 2 hrs, and washed in dH_2O (3X). Preparations were stained *en bloc* in 1% aqueous uranyl acetate for 1 hr, washed in dH_2O (3X), dehydrated through an EtoH series (30%-100%), passed through propylene oxide, transferred to a 1:1 araldite:propylene oxide mixture, and embedded in araldite media. Ultra-thin serial sections (50-60nm) were obtained on a Leica UCT Ultracut microtome and transferred to formvar-coated grids. Grids were examined on a Phillips CM10 TEM equipped with an AMT 2 mega pixel camera. Four animals from each genotype were processed. NMJs were sectioned, and profiles for each identified type I synaptic bouton were quantified in a section containing only a single

prominent electron-dense active zone (AZ) T-bar. Synaptic vesicles in the "clustered" pool were defined as those <250 nm of the AZ T-bar. Docked vesicles were defined as those <0.5 vesicle diameter (<20 nm) of the electron-dense plasma membrane at the AZ. Quantified measurements were made using Image J. Bouton and mitochondria area, number of docked, clustered and total vesicles, and vesicle density (corrected for mitochondria area) were scored for each profile. Mean quantified parameters were statistically compared using the Mann-Whitney test, and presentation images were processed in Adobe Photoshop.

Immuno Electron Microscopy

Wandering 3rd instar larvae carrying the *fusl*-GFP transgene in the *fusl*^{1}/*fusl*^{1} null background were dissected and fixed as described above. Preparations were then processed through an anti-GFP immunocytochemical protocol to localize the Fusl fusion protein. Briefly; preparations were rinsed in PBS for 10 mins, then taken through a graded methanol series (50% for 10 mins, 70% for 30 mins) and embedded in LR White (1:1 LR White:fresh absolute ETOH 30 mins, 2:1 LR White:fresh absolute ETOH 30 mins, pure LR White 1hr). Samples were changed to fresh LR White and let stand overnight while agitated. Samples were then embedded in fresh LR White in flat-bottomed capsules (Ted Pella; cat. no. 133-P) with a disk of Aclar plastic (Ted Pella; cat. no. 10501-10) used to make an optically clear surface at the bottom, and a square of Parafilm placed over the top, and sealed with a cap from a BEEM capsule (Kent McDonald, personal communication). Using a staining plate (EMS; cat. no. 71568) grids with 100 nm sections were placed into 40 μl of blocking buffer for 30 mins. Wells from the next row were filled with a commercial anti-GFP antibody (ABCAM) in blocking buffer, and grids were transferred and incubated from 1 hr to overnight in different trials. Grids were then rinsed in PBS-Tween for 2 mins, rinsed in PBS (4X; 2 mins each) and incubated in secondary antibody in blocking buffer for 1-2 hrs. Grids were poststained

with uranyl acetate and lead citrate for 3 mins and then imaged as for regular electron microscopy. NMJ boutons were examined with a Phillips CM10 TEM equipped with an AMT 2 mega pixel camera, and images processed in Adobe Photoshop.

Elav; UAS-Cac-GFP Imaging and Electrophysiology

To quantitatively assess voltage-gated calcium channels at the NMJ, the UAS-Cac-GFP transgenic line (kindly provided by Dr. Richard Ordway, Pennsylvania State University, PA) was crossed into control and *fuseless* null mutant backgrounds. The UAS-Cac-GFP transgene was then driven specifically in the motor neuron presynaptic terminal by crossing in the pan-neuronal *elav* GAL4 driver (Andrews et al., 2002; Trotta et al., 2004). Wandering 3rd instars were dissected in modified *Drosophila* saline, as above. A NMJ was identified and type I boutons examined by confocal microscopy. TEVC was carried out on controls (*elav*-GAL4;UAS-Cac-GFP in a wild type background) and mutants ($fusl^{1}/fusl^{1}$; *elav*-GAL4;UAS-Cac-GFP) as described above.

Results

Isolation of Synaptic Mutants by Electroretinogram Recording

An ethyl methyl sulfonate (EMS) chemical mutagenesis for synaptic mutants was performed targeting the second chromosome, which contains ~36% of the *Drosophila* genome (Fig. 2.1A). Males carrying an EMS-mutagenized second chromosome were singly mated in a second generation cross to isolate different strains. The dominant temperature sensitive 2 (DTS2) mutation was used to select for the mutagenized second chromosome over balancer chromosome among F2 offspring (Fig. 2.1A). Crossing *inter se* produced F3 generation homozygous second chromosome mutants that were screened as adults for defects in synaptic transmission in the visual system.

The mutant screen was performed by direct electroretinogram (ERG) recording as diagramed in Figure 2.1B. The ERG is a light-evoked,

extracellularly recorded mass response of the eye consisting of contributions from several different types of cells. During light stimulation, lights-on and lights-off ERG transients represent synaptic transmission in the visual system. From our screen, 16 mutant complementation groups on the second chromosome were identified based on grossly abnormal ERG responses. The majority of these mutants impact the phototransduction pathway directly (reviews: Pak, 1975, 1995; Pak and Leung, 2003). However, a 'transientless' ERG phenotype characterized 6 mutant complementation groups, indicating a specific impairment in synaptic transmission. The fuseless (fusl) complementation group was one of these six, with two mutant alleles identified in the ERG screen and an additional allele obtained from John Merriam's group at UCLA (Markow and Merriam, 1977).

Fuseless is Required for Synaptic Transmission in the Visual System

The ERG consists of a corneal-negative (downward), sustained component and two transient components at lights-on and lights-off (Fig. 2.1C). The sustained component reflects the summed phototransduction responses of photoreceptors. The on- and off-transients arise from the lamina to which the majority class of photoreceptors (R1-6) synapse (reviews: Buchner, 1991; Pak, 1995). The on-transient, in particular, corresponds directly to the responses of transients represent synaptic transmission in the visual system. From our screen, 16 mutant complementation groups on the second chromosome were identified based on grossly abnormal ERG responses.

Figure 2.1: Phototransduction mutagenesis identifies a novel mutant specifically defective in synaptic transmission. A) Second chromosome mutagenesis scheme. EMS mutagenized males were single-mated in a second generation cross to track each mutant line independently. The dominant temperature-sensitive (DTS-2) mutation allowed only animals carrying the mutagenized second chromosome over balancer to survive among F2 offspring. Crossing *inter se* produced offspring (F3) that are either homozygous or heterozygous for the mutagenized second chromosome. These animals were screened by electroretinogram (ERG) recording. **B)** Cartoon of ERG recording. The fly was mounted in low-melting point wax, with a recording electrode in the cornea and a reference electrode in head. The light stimulus (300W Halogen lamp) was led to eye using an optical light guide. **C)** The *fusl* mutants show a specific loss of ERG synaptic transients. Representative ERG traces (left) elicited from wildtype (WT) and *fusl* using 2 sec orange light stimuli. Responses at three different light intensities are shown superimposed. Synaptic on- and off-transients are absent in *fusl* mutants. Right panel: Peak ERG and synaptic on-transient amplitudes (as defined in the left panel) plotted against stimulus intensity for WT (N=8) and *fusl* (N=9). **D)** Representative photoreceptor intracellular recordings from WT and *fusl*, shown superimposed. The receptor potentials have indistinguishable amplitudes (WT: 23.8 ± 2.7 mV; *fusl*: 22.5 ± 2.1 mV) and time (N=7). However, the *fusl* response is slowly decaying: WT has completely returned to baseline [9.8 ± 0.9 sec (N=7) after stimulus termination], while the mutant response still displays a 2.0 ± 0.8 mV (N=7) depolarization (arrow).

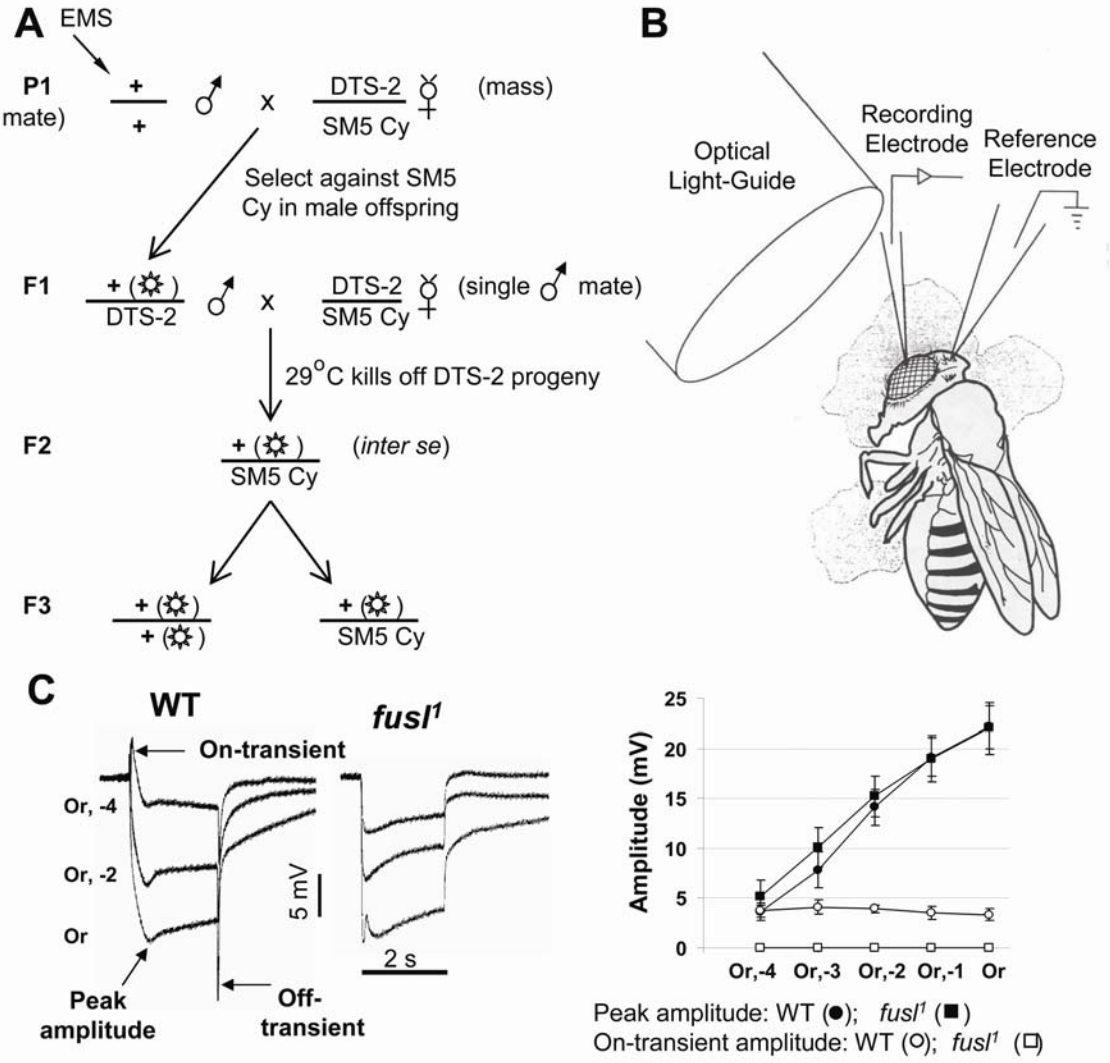
A
EMS
P1
mate)
+
+
x
DTS-2
SM5 Cy
(mass)
Select against SM5
Cy in male offspring
F1
+ (☼)
DTS-2
x
DTS-2
SM5 Cy
(single ♂ mate)
29°C kills off DTS-2 progeny
F2
+ (☼)
SM5 Cy
(inter se)
F3
+ (☼)
+ (☼)
+ (☼)
SM5 Cy
B
Optical
Light-Guide
Recording
Electrode
Reference
Electrode
C
WT
fusl1
On-transient
Or, -4
Or, -2
Or
5 mV
2 s
Peak
amplitude
Off-
transient
Amplitude (mV)
25
20
15
10
5
0
Or,-4
Or,-3
Or,-2
Or,-1
Or
Peak amplitude: WT (●); fusl1 (■)
On-transient amplitude: WT (○); fusl1 (□)
D
WT
fusl1
5 mV
2 s Or

The majority of these mutants impact the phototransduction pathway directly (reviews: Pak, 1975, 1995; Pak and Leung, 2003). However, a 'transientless' ERG phenotype characterized 6 mutant complementation groups, indicating a specific impairment in synaptic transmission. The fuseless (fusl) complementation group was one of these six, with two mutant alleles identified in the ERG screen and an additional allele obtained from John Merriam's group at UCLA (Markow and Merriam, 1977).

Fuseless is Required for Synaptic Transmission in the Visual System

The ERG consists of a corneal-negative (downward), sustained component and two transient components at lights-on and lights-off (Fig. 2.1C). The sustained component reflects the summed phototransduction responses of photoreceptors. The on- and off-transients arise from the lamina to which the majority class of photoreceptors (R1-6) synapse (reviews: Buchner, 1991; Pak, 1995). The on-transient, in particular, corresponds directly to the responses of laminar neurons to input from photoreceptors R1-6. As shown in Fig. 2.1C, the sustained photoreceptor component of *fusl* mutants is normal in both amplitude and duration, but the synaptic on-/off-transients present in the wild-type control are absent in *fusl* mutants. The peak amplitude of the phototransduction component and the synaptic on-transient were quantified and plotted as a function of the stimulus intensity (Fig. 2.1C, right). The *fusl* mutants display normal amplitude phototransduction responses at all stimulus intensities, but lack any detectable synaptic responses over the entire intensity range. Intracellular recordings from photoreceptors confirmed the normal amplitude and duration of photoreceptor potentials (Fig. 2.1D). However, the photoreceptor potential in *fusl* mutants displayed an aberrant, slowly-decaying component (Fig. 2.1D). This depolarizing tail phenotype was specific to *fusl* mutants since a similar slowly decaying tail was not observed in other transientless synaptic mutant complementation groups. However,

the slowly decaying tail does not detectably affect the amplitude and waveform of the photoreceptor potential during the period of light stimulus.

Genomic and Microarray Analyses Identify the fuseless Gene

Deficiency mapping showed that *fusl* is uncovered by deficiency *Df(2L)Exel6012* and is covered (complemented) by deficiency *Df(2L)cl7*, localizing the *fusl* gene between the left breakpoint of *Exel6012* and the left breakpoint of cl7 (Fig. 2.2A). *Exel6012* breakpoints were defined at the molecular level, and the molecular coordinate of its left breakpoint is 2L:5,303,145. The left breakpoint of deficiency *cl7* is defined by the location of the *nompC* gene, which is either deleted or disrupted by *c17.* According to Affymetrix *Drosophila* microarray annotation, there are nine genes within the interval defined by these two breakpoints.

To identify the candidate *fusl* gene in the mapped interval, microarray analyses were performed on *fusl* mutants to screen for genes with altered mRNA interval, the *CG14021* gene displayed the most significant changes in mRNA levels for all three *fusl* mutant alleles. Specifically, the probe set for *CG14021* detected log-fold changes of -0.593 (p-value = 0), -0.895 (p-value = 0), and -0.559 (p-value = $3.8x10^{-15}$) in the three *fusl* alleles. Another gene in this interval, *cype*, also had low p-values even though log-fold changes were only moderate. The log-fold changes and p values for this gene were: -0.352 (p-value = 0, -0.459 (p-value = 0), and +0.208 (p-value = 0). levels. Microarrays were performed on the three alleles of *fusl* along with appropriate wild-type controls (data not shown). Of the nine genes in the mapped A third gene, *vri*, also had a fairly high log-fold change with a p-value of zero, but only in a single *fusl* allele (-0.680, p value = 0). Log-fold changes were low (0.26 and -0.28) and p-values were high ($3x10^{-13}$ and $1.5x10^{-6}$) in the other two *fusl* alleles. The microarray analyses therefore revealed two candidate *fusl* genes; *CG14021* and *cype*.

Figure 2.2: Maps of the *fusl* genomic region, gene and gene product. A) The mutant genomic region. The *fusl* mutation is uncovered by the *Df(2L)Exel6012* deficiency (top line), but complemented by *Df(2L)cl7* (second line). The third line indicates cytogenetic boundaries and the fourth line shows the nucleotide coordinates. **B)** The *CG14021* gene and its gene products. The gene generates two transcripts (RA, RB) by alternative splicing that differ in the location of the non-coding first exon but contain identical coding sequence. Untranslated regions are shown in gray. The predicted protein is 453 amino acids and contains eight predicted transmembrane domains. Mutations found in the coding regions of CG14021 in three characterized *fusl* alleles are shown at the bottom. **C)** Related proteins from multiple species were used to construct the phylogenetic tree. Protein sequences are identified from top to bottom by species, protein name, function (if known) and accession numbers, as follows: *Apis: Apis mellifera* (XM_623675.2); *Tribolium: Tribolium castaneum* (XM_968828.1); *Anoph: Anopheles gambiae* (XM_317156.2); *D. mel.: Drosophila melanogaster* CG14021 (NM_135079.4); *D. pseudo: Drosophila pseudoobscura* (XM_001356784.1); Cym G: *Klebsiella oxytoca*, cyclodextrin transport (Q48397); Wzx: *Escherichia coli*, transbilayer movement of a trisaccharide-lipid intermediate (P27834); Shi A, *Escherichia coli*, shikimate transporter (P76350); YF62: *Methanococcus jannaschii*, putative membrane protein (Q58957); Sialin, *Homo sapiens*, transport of sialic acid in lysosomes (Q9UGH0).

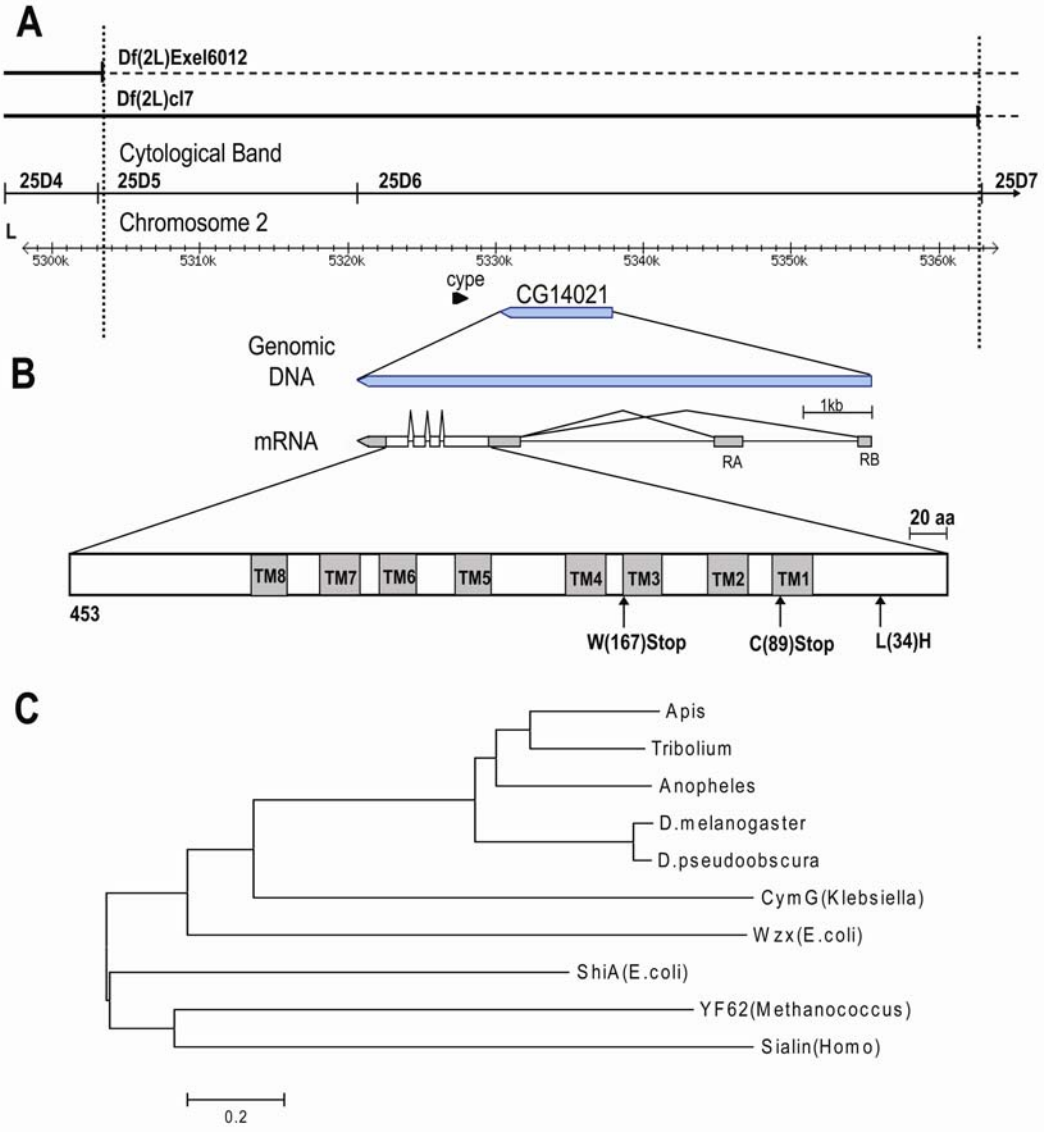
A
Df(2L)Exel6012
Df(2L)cl7
Cytological Band
25D4
25D5
25D6
25D7
L
Chromosome 2
5300k
5310k
5320k
5330k
5340k
5350k
5360k
cype
CG14021
B
Genomic
DNA
mRNA
1kb
RA
RB
20 aa
TM8
TM7
TM6
TM5
TM4
TM3
TM2
TM1
453
W(167)Stop
C(89)Stop
L(34)H
C
Apis
Tribolium
Anopheles
D.melanogaster
D.pseudoobscura
CymG(Klebsiella)
Wzx(E.coli)
ShiA(E.coli)
YF62(Methanococcus)
Sialin(Homo)
0.2

To distinguish between these two candidate genes, we sequenced both in all three *fusl* alleles. Sequencing revealed no mutations in the *cype* gene in any of the three mutant alleles. The *CG14021* gene, on the other hand, was found to carry stop codons in all three alleles (Fig. 2.2B). Two of the allelic mutants turned out to be identical with a nonsense mutation (TGT->TGA) that terminates the protein at Cys(89). This allele is now designated $fusl^{1}$. The other allele ($fusl^{2}$) also carries a nonsense mutation (TGG->TAG) that truncates the protein at Trp(167). In addition, it carried a missense mutation (CTC->CAC), which results in a Leu(34)His change. Identification of these mutations strongly indicated that *CG14021* is the fuseless gene and that these mutations are responsible for the mutant phenotypes. Subsequent RNAi and transgenic rescue experiments (see below) confirmed that *CG14021* is the fuseless gene.

Fuseless is a Predicted 8-Pass Transmembrane Transporter

The fuseless *(CG14021)* gene encodes two transcripts, RA and RB, which differ in the first non-coding exons (and promoters) located at two different locations (Fig. 2.2B). Upstream of the RA transcript is a ca. 2 kb promoter region containing the TATA box, transcription initiation site, and the consensus 11-bp conserved sequence for photoreceptor expression, suggesting that the RA isoform is expressed in photoreceptors. The coding sequences of the two *fusl* transcripts are identical and encode a protein of 453 amino acids, with eight predicted transmembrane regions, characteristic of a transporter (Fig. 2.2B). This is a novel protein derived from annotated genome sequences, and its function is not known. The most salient feature of the predicted protein is the presence of eight transmembrane domains (Fig. 2.2B). BLAST searches reveal that proteins most closely related to Fusl have been identified in several insect species (*Apis mellifera, Anopheles gambiae, Drosophila pseudoobscura, Tribolium castaneum*; Fig. 2.2C). These proteins share 36% (*Anopheles*) to 81% (*D. pseudoobscura*) amino acid identity (51 to 87% similarity) with the Fusl protein. Moreover, all

four proteins share with Fusl the eight transmembrane domains at conserved locations. The *Anopheles* protein differs from the others slightly by having a ninth transmembrane domain at its C-terminus. All of these proteins are novel and their function is unknown. The phylogenetic relationship between these proteins is shown in Figure 2.2C. Other proteins identified in BLAST searches shared with fuseless $\leq$ 21% and $\leq$ 39% amino acid identity and similarity, respectively. Among these, the five proteins with the highest amino acid identity, and of comparable size to Fusl, are included in the phylogeny tree in Figure 2.2C. All of these proteins for which functions are known act as transmembrane transporters for various substrates. Indeed, four of the five proteins included in the phylogeny tree are known transporters, whereas the function is not known for the fifth protein (Fig. 2.2C). Thus, the eight transmembrane domains and the known transporter function of related proteins both suggest that the Fusl protein likely functions as a transmembrane transporter.

Fuseless is a Presynaptic Plasma Membrane Protein in Visual System and NMJ

The above evidence suggests that Fusl in a multipass transmembrane protein required in the visual system for photoreceptor synaptic transmission. To test the predicted cellular distribution of the Fusl protein in the visual system, we generated a specific anti-Fusl peptide antibody (see Methods). In whole mount preparations (Fig. 2.3A), anti-Fusl immunoreactivity labels the retinal photoreceptors, revealed with co-labeling with the neuronal membrane epitope marker anti-HRP. To assay Fusl localization more precisely, frozen sections were made of the visual system. Staining with the Fusl antibody reveals expression in the retina, lamina and medulla (Fig. 2.3B). Photoreceptor labeling is consistent with plasma membrane localization, with Fusl co-localizing with the membrane anti-HRP epitope. In the lamina and medulla, Fusl has a highly punctate expression pattern, consistent with synaptic localization (Fig. 2.3C). These

Figure 2.3: Fusl protein expression in the visual system. A) Whole mount of *Drosophila* eye showing expression of Fuseless (green) and HRP (red). **B)** Cryo-section of the visual system, showing Fusl expression in retina, lamina, and medulla (green), costained with actin (red). **C)** Cross section of the visual system using a costain Fusl (green) and actin (red).

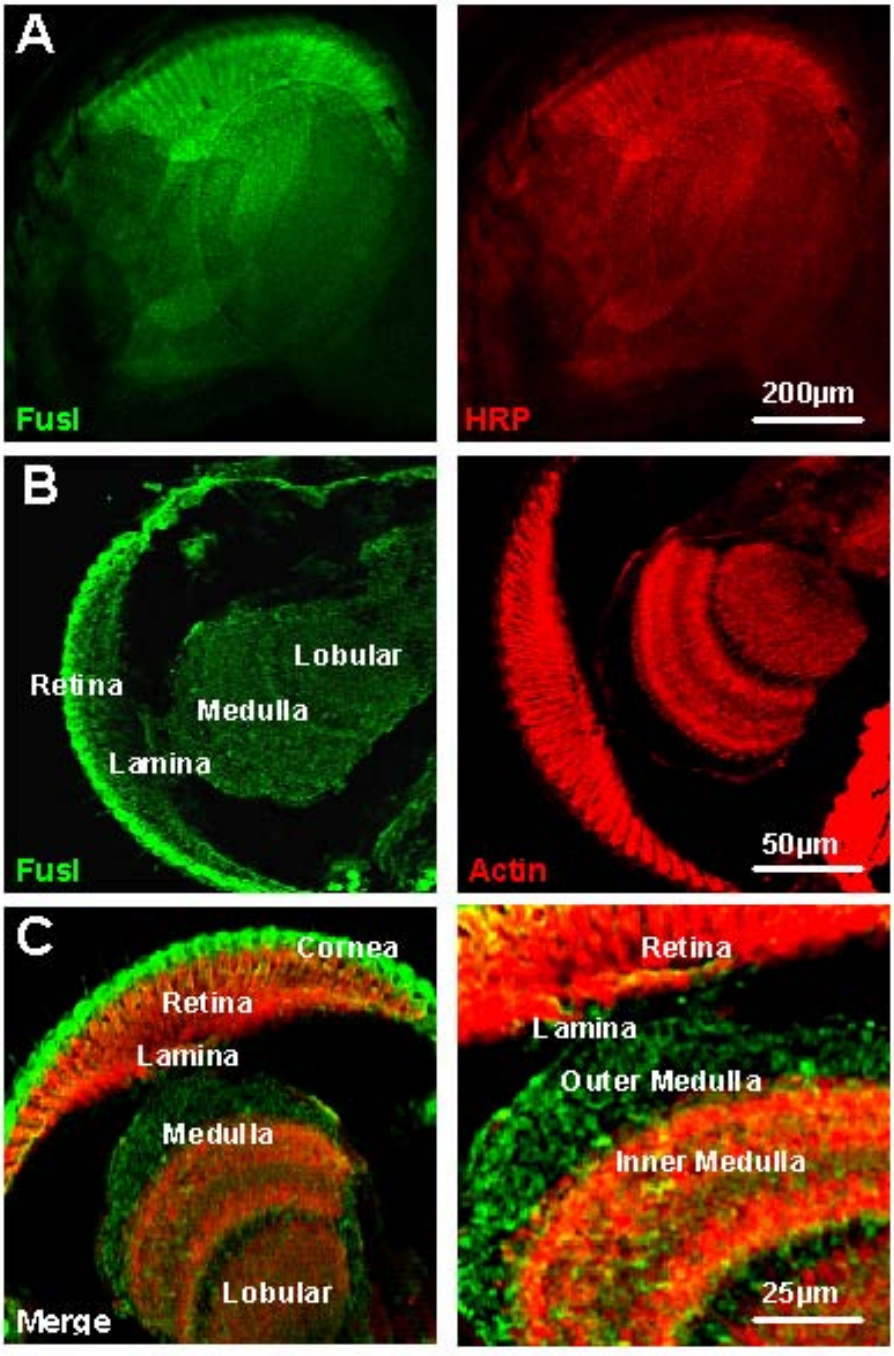
A
Fusl
HRP
200µm
B
Retina
Lobular
Medulla
Lamina
Fusl
Actin
50µm
C
Cornea
Retina
Lamina
Medulla
Lobular
Merge
Retina
Lamina
Outer Medulla
Inner Medulla
25µm

results suggest that Fusl is an integral protein of the plasma membrane and may be enriched in synaptic termini.The larval neuromuscular synaptic system has the best-characterized structure and molecular architecture in *Drosophila*, and was therefore used to study and synaptic expression and function of the Fusl protein in further detail. Fusl expression was assayed at three levels; 1) with anti-Fusl antibody, 2) with a fusl-GFP transgene that rescues fusl mutant phenotypes (see below) and 3) at ultrastructural resolution with immunogold electron microscopy. Confocal imaging was employed to examine the expression of antibodies raised against the native Fusl protein (Fig. 2.4A-C). Anti-Fusl immunoreactivity is detectable only in the nervous system, without expression in other tissues, suggesting that Fusl is a neural-specific protein (Fig. 2.4A). This expression is lost in the $fusl^{1}$ mutant, confirming that this allele is a protein null and demonstrating the specificity of the antibody (Fig. 2.4B). Fusl is highly expressed within both the presynaptic nerve and in the plasma membrane surrounding boutons at the NMJ (Fig. 2.4A,B). The protein is very weakly or undetectably expressed in neuronal soma or proximal processes within the CNS (data not shown). Within the nerve and presynaptic NMJ arbors, Fusl co-localizes nearly identically with the presynaptic plasma membrane marker anti-HRP (Fig. 2.4B,C). In high magnification images of synaptic boutons, Fusl appears clearly membrane-associated and restricted to the outermost periphery of the bouton. Indeed, Fusl appears to localize more tightly with the plasma membrane than the classic membrane marker anti-HRP (Fig. 2.4C), consistent with it being an integral plasma membrane protein. The distribution of EGFP-tagged-fuseless shows an identical pattern, with the protein concentrated in NMJ synaptic boutons and highly enriched at the plasma membrane of the bouton periphery (Fig. 2.4D).

Figure 2.4: Fusl protein localizes in the presynaptic plasma membrane. A) Very low magnification image of the neuromusculature. Anti-Fusl immunoreactivity observed only in presynaptic nerve and NMJ synapses. Scale bar: 200 μm. **B)** Low magnification images of Fusl staining within a single NMJ synaptic arbor. Neuronal membranes labeled with anti-HRP (green) compared to anti-Fusl (red). The wild-type (WT) control is show on top, and the *fusl*^{1}*; fusl*^{1} mutant on the bottom. Scale bar: 20 μm. **C)** High magnification images of individual NMJ synaptic boutons in control (left) and mutant (right). Fusl is restricted to the plasma membrane. Scale bar: 2 μm. **D)** The transgenic Fusl-GFP fusion protein co-localizes with anti-HRP in synaptic boutons, revealing a peripheral, plasma membrane associated localization. Scale bar: 2 μm. **E)** Fusl-GFP distribution by immunoEM. Anti-GFP with an electron-dense gold (15 nm immunogold) label visualized by TEM. Gold label (arrows) observed in and immediately adjacent to the presynaptic plasma membrane (PM) in the NMJ bouton. Scale: 50 nm.

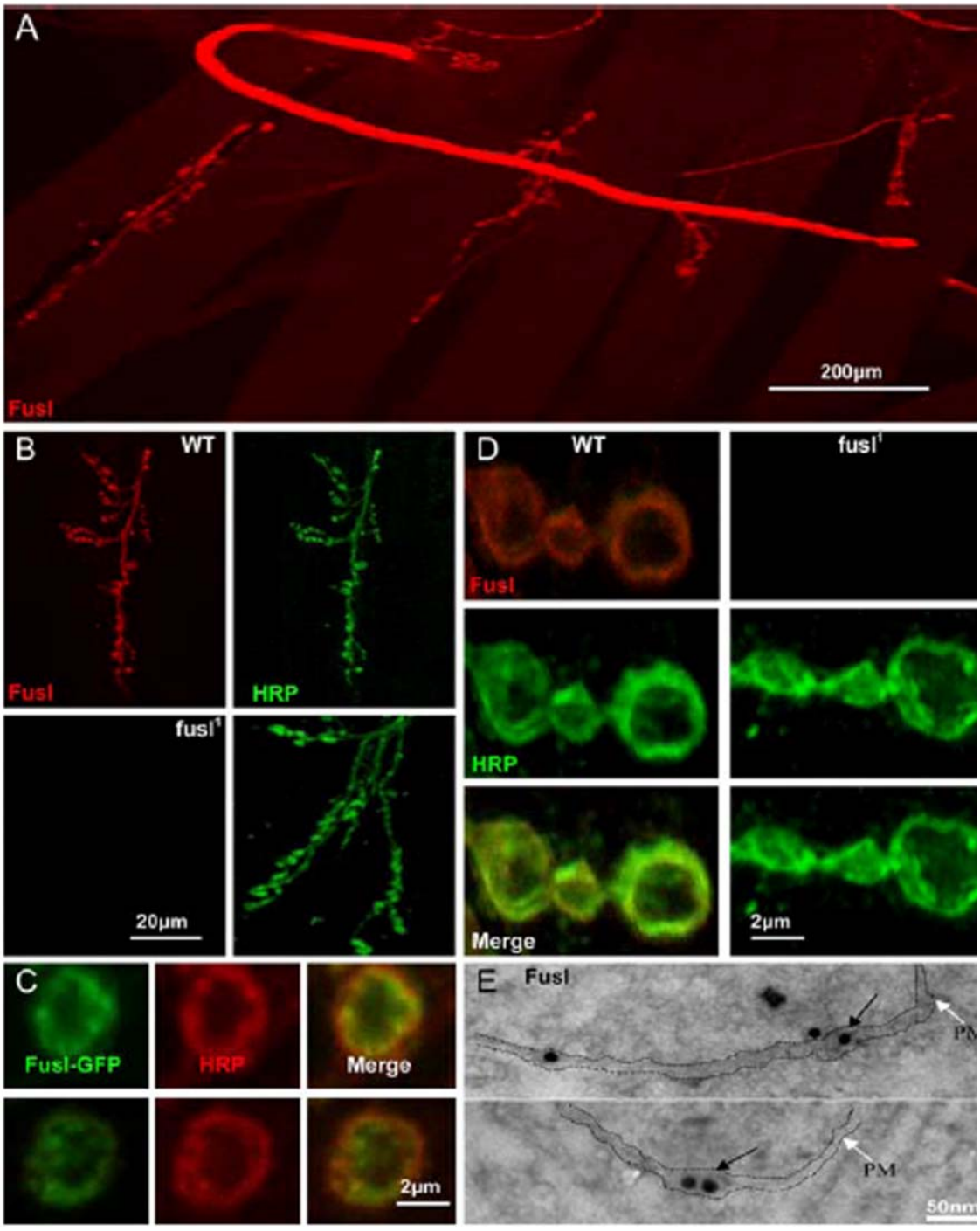
A
Fusl
200μm
B
WT
Fusl
HRP
fusl¹
20μm
D
WT
fusl¹
Fusl
HRP
Merge
2μm
C
Fusl-GFP
HRP
Merge
2μm
E
Fusl
PM
PM
50nm

Both techniques show that Fusl is not restricted to active zones, or to any type of localized membrane domain, but rather shows a general presynaptic neuronal membrane localization. To examine Fusl localization as precisely as possible, immunoelectron microscopy was next used to image the EGFP-tagged-fuseless protein (Fig. 2.4E). Ultrastructurally, the Fusl protein was found to be restricted to the extreme periphery of synaptic boutons and to be membrane associated, consistent with confocal imaging and protein predictions. The gold label was observed within and immediately adjacent to the presynaptic plasma membrane (Fig. 2.4E, arrows) but was also observed associated with vesicle membranes within <250 nm of the plasma membrane (Fig. 2.4E, top). The Fusl protein was observed in close association with presynaptic active zones, but it was not restricted to active zones and showed a general presynaptic membrane distribution. This imaging is consistent with a plasma membrane localized protein (Lnenicka et al., 2006) and also consistent with the 8-pass transmembrane structure of the Fusl protein (Fig. 2.2B).

Impaired presynaptic function may arise from many causes, including defects in the architectural or molecular differentiation of the presynaptic terminal. To test these possibilities, NMJ structure and molecular composition were systematically compared between *fusl* null mutants and controls (Fig. 2.4 and data not shown). The fusl mutant does not show any detectable defects in the gross architecture of the neuromusculature, with normal motor nerve trajectories, normal muscle anatomy and normally placed and differentiated NMJs. NMJ structure was examined using anti-HRP labeling to reveal the presynaptic neuronal membrane. No defects were observed in NMJ placement, size, branching or synaptic bouton formation (Fig. 2.4B). No detectable differences were observed in *fusl* null mutants in the localization, area or mean fluorescence intensities of presynaptic markers, such as the integral synaptic vesicle protein Synaptotagmin 1, or postsynaptic glutamate receptors (data not shown). These data show that Fusl is not required for synaptic

morphogenesis or the gross molecular differentiation of pre- and postsynaptic compartments.

Fuseless Regulates Glutamatergic Synapse Function

The larval glutamatergic NMJ synapse is by far the best-defined model synapse in the *Drosophila* system, and was therefore employed to systematically characterize the role of Fusl in synaptic mechanisms. Any significant impairment in larval NMJ function should first be revealed by compromised coordination and/or locomotion. Two larval behavioral assays were conducted to assess coordination (eating pharyngeal movements) and locomotion (body wall contractions) (Fig. 2.5A). All *fusl* mutant alleles showed a clear and obvious impairment in both of these behaviors compared to controls. The homozygous $fusl^{1}$ and $fusl^{2}$ mutants, and the heterozygous $fusl^{1}$/Df mutants, all exhibit a highly significant reduction in pharyngeal movements and locomotor body wall contractions ($P<0.001$, N=10 animals for each genotype), compared to both wild-type (WT) and +/Df controls (Fig. 2.5A). Similar behavioral defects have been described as defining a synaptic impairment (Xing et al., 2005).

To directly assess synaptic function of the larval NMJ, basal neurotransmission assays were done on *fuseless* mutants and controls, with both evoked excitatory junctional currents (EJCs) and spontaneous miniature EJCs (mEJCs) measured in the two electrode voltage clamp (TEVC) configuration (Figs. 2.5B,C). Evoked transmission assays were done in 0.5 mM extracellular [Ca^{2+}], to reveal changes in basal synaptic function most clearly (Rohrbough et al., 1999; Zhang et al., 2001; Trotta et al., 2004). At a stimulation frequency of 0.5 Hz, control animals exhibited a mean EJC amplitude of 69.5 ± 4.9 nA, whereas all *fusl* mutants showed a similar, highly significant decrease in EJC amplitude; 19.1 ± 3.5 nA ($fusl^{1}$), 21.3 ± 3.9 nA ($fusl^{2}$), and 18.2 ± 4.0 nA ($fusl^{1}$/Df) ($P<0.001$, N=12 for all genotypes; Fig. 2.5B). These results show that Fusl plays an important facilatory function in synaptic transmission.

Figure 2.5: Loss of Fusl critical impairs movement and NMJ synaptic function. **A)** Defective larval movement in *fusl* mutants. Movements were quantified over a 1 min period for both pharynx contraction (left) and body wall peristalsis (right). All *fusl* mutants (open bars) display significantly reduced movements compared to both controls (hatched bars). $P<0.001$, N=10 animals for all genotypes shown. **B)** Impaired NMJ synaptic transmission in *fusl* mutants. Representative traces of excitatory junctional currents (EJCs; left), evoked by 0.5 Hz motor nerve stimulation in control and *fusl* mutant. Current recordings were made in two-electrode voltage-clamp (TEVC) mode at -60 mV from muscle 6 (segment 3). Right; Quantified mean EJC amplitude for controls (hatched bars) and mutants (open bars). $P<0.001$, N=10 animals for each genotype. **C)** Mutants display increased spontaneous neurotransmission events. Representative miniature excitatory junctional currents (mEJCs; left) traces in control (top), mutant (middle) and mutant with 1 copy of wild-type *fusl* transgene (bottom). The *fusl* mutant displays a higher frequency of mEJCs with obviously elevated amplitudes. Quantification of mEJCs reveals a 3-fold increase in mean mEJC amplitude (left) and >2-fold increase in mean mEJC frequency (right). $P<0.001$, N=10 animals for all genotypes. **D)** RNAi knockdown of CG14021 mimics the *fusl* mutant transmission defect, and targeted presynaptic expression of a wildtype CG14021 transgene rescues the *fusl* mutant transmission defect. Representative EJC traces (left) from WT control, dsRNAi injected animal and presynaptic transgenic rescue of *fusl* mutant (elav-GAL4; UAS-CG14021 in the $fusl^{1}/fusl^{1}$ background). Right; Quantification of mean EJC amplitude in controls (hatched bars), mock and dsRNAi injected animals, *fusl* mutant alone and with transgenic CG14021 rescue. Sample size of 10 animals for all genotypes represented ($P<0.001$).

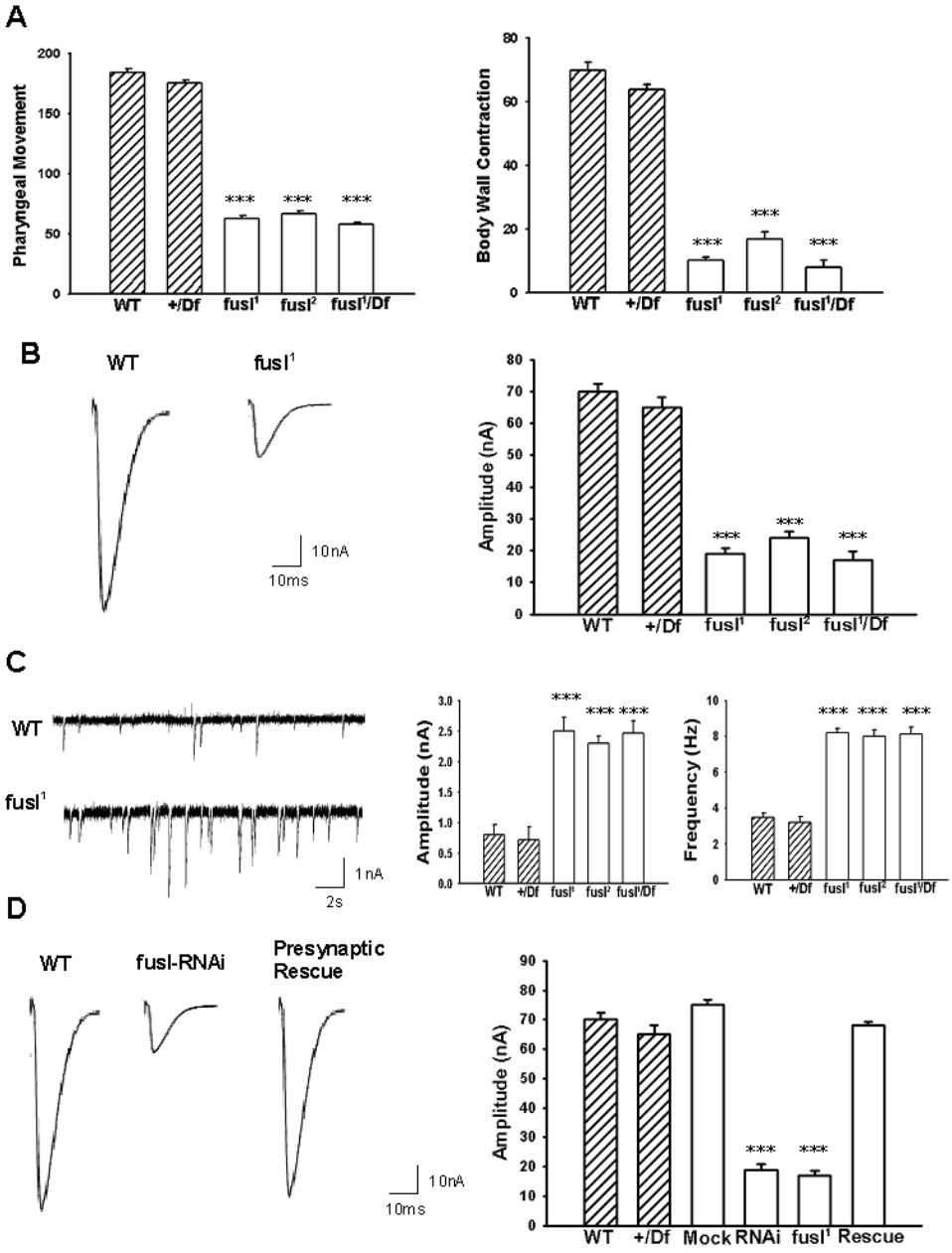
A
Pharyngeal Movement
200
150
100
50
0
***
***
***
WT
+/Df
fusl1
fusl2
fusl1/Df
Body Wall Contraction
80
60
40
20
0
***
***
***
WT
+/Df
fusl1
fusl2
fusl1/Df
B
WT
fusl1
10nA
10ms
Amplitude (nA)
80
70
60
50
40
30
20
10
0
***
***
***
WT
+/Df
fusl1
fusl2
fusl1/Df
C
WT
fusl1
1nA
2s
Amplitude (nA)
3.0
2.5
2.0
1.5
1.0
0.5
0.0
***
*** ***
WT
+/Df
fusl1
fusl2
fusl1/Df
Frequency (Hz)
10
8
6
4
2
0
*** *** ***
WT
+/Df
fusl1
fusl2
fusl1/Df
D
WT
fusl-RNAi
Presynaptic Rescue
10nA
10ms
Amplitude (nA)
90
80
70
60
50
40
30
20
10
0
***
***
WT
+/Df
Mock RNAi
fusl1 Rescue

In order to assay spontaneous vesicle fusion in the absence of evoked synaptic transmission, mEJCs were recorded in the presence of TTX in the same 0.5 mM [Ca^{2+}]. Surprisingly, all *fusl* mutants showed a significant increase in both the amplitude and frequency of mEJC fusion events (Fig. 2.5C, sample traces at left). The mEJC amplitude was elevated nearly 3-fold in the absence of *fusl* function; in controls, mEJC amplitude was 0.7 ± 0.4 nA (WT) and 0.6 ± 0.2 nA (+/Df), whereas in mutants mEJC amplitude was 2.5 ± 0.4 nA (*fusl*^{1}), 2.3 ± 0.3 nA (*fusl*^{2}) and 2.46 ± 0.21 (*fusl*^{1}/Df) (P<0.001, N=10 animals for all genotypes; Fig. 2.5C, middle). The mEJC frequency was more than doubled in the absence of *fusl* function; in controls, mEJC frequency was 3.6 ± 0.5 Hz (WT) and 3.2 ± 0.6 Hz (+/Df), whereas in mutants mEJC frequency was 8.2 ± 0.23 (*fusl*^{1}), 7.9 ± 0.36 (*fusl*^{2}) and 8.0 ± 0.43 (*fusl*^{1}/Df) (P<0.001, N=10 animals for all genotypes; Fig. 2.5C, right). These data show that loss of *fusl* function dramatically reduces evoked neurotransmission efficacy, while increasing the size and rate of spontaneous synaptic vesicle fusion events.

The similarity in *fusl*^{1}, *fusl*^{2} and *fusl*^{1}/Df quantified phenotypes suggest that both *fusl*^{1} and *fusl*^{2} represent the null mutant condition, consistent with the sequenced stop mutations in *CG14021* (Fig. 2.2B). RNA interference (RNAi) against *CG14021* and transgenic expression of the wild-type *CG14021* gene were additionally employed to confirm the *fusl* gene identity (Fig. 2.5D). When EJC amplitudes were measured, as above, *CG14021* RNAi injected animals had a similar phenotype to *fusl*^{1} mutants: 17.4 ± 1.57 nA (*fusl*^{1}) compared to 19.2 ± 1.89 nA (RNAi) (P<0.001 to WT, N=10 animals for both genotypes). As a control, mock-injected animals had robust EJCs, indistinguishable from WT (Fig. 2.5D, right). A wild-type copy of UAS-*CG14021* driven by the neuronal GAL4-elav in the *fusl*^{1} homozygous null mutant background completely rescued the synaptic transmission defect (Fig. 2.5D, “rescue” sample trace on the left). The transgenic rescue animals showed average EJC amplitudes of 66.1 ± 1.0 nA, comparable to the controls (Fig. 2.5D, right). The elevated mEJC

amplitude and frequency were similarly rescued upon presynaptic expression of the wildtype *fusl* transgene (Fig. 2.5C, bottom trace). Controls showed average mEJC amplitude of 0.62 ± 0.3 nA and frequency of 3.4 ± 0.7 Hz, and *fusl* mutants with one copy of the wild-type gene expressed presynaptically displayed a similar 0.7 ± 0.4 nA amplitude and 3.9 ± 0.9 Hz amplitude ($P>0.05$; N=10 animals for both genotypes). Note that full rescue of evoked and spontaneous transmission is achieved by driving the *fusl* gene only in the presynaptic cell. Thus, these data confirm the *fusl* gene identity and also demonstrate a specific presynaptic requirement for the Fusl protein.

Fuseless Regulates the Synaptic Vesicle Cycle and Vesicle Exocytosis

Fuseless in the presynaptic membrane regulates neurotransmission efficacy, predicting defective neurotransmitter release. To investigate the size and cycling dynamics of the endo-exo synaptic vesicle (SV) pool, the lipophilic fluorescent dye FM1-43 was used to image endocytosis and exocytosis (Fig. 2.6; Kuromi and Kidokoro, 2000; Fergestad and Broadie, 2001; Trotta et al., 2004). Larval NMJ preparations were exposed to FM1-43 in the presence of 90 mM [K^+] saline, which depolarizes the nerve terminal and induces rapid vesicular cycling. Preparations were then washed and imaged in buffered 0 mM [Ca^{2+}] saline to halt SV cycling. A second high [K^+] depolarization was used in the absence of FM1-43 to assess dye unloading by SV exocytosis. Representative images of loaded and unloaded NMJ arbors are shown in Figure 2.5A. Mean fluorescent intensities were quantified following both FM1-43 loading and unloading. After loading, control boutons displayed mean fluorescent values of 172.1 ± 5.9 (WT) and 165.3 ± 5.3 (+/Df), whereas *fusl* mutants showed significantly reduced loading; 122 ± 5.2 (*fusl*^{1}), 112.1 ± 4.8 (*fusl*^{2}) and 115.0 ± 5.7 (*fusl*^{1}/Df) ($P<0.01$, N=10 animals for each genotype; Fig. 2.6B, left “load”). This phenotype indicates a decrease in the cycling rate or size of the exo-endo SV pool, consistent with

presynaptic impairment of neurotransmission (Kuromi and Kidokoro, 2000). Following unloading, controls displayed a reduction of FM1-43 fluorescence of >90%, whereas the *fusl* mutants showed a high FM1-43 dye retention and a specifically compromised ability to unload (Fig. 2.6A). The mean values following unloading for the controls was 15.4 ± 4.6 (WT) and 19.3 ± 5.7 (+/Df), while the mutants showed >5-fold higher values of 114.0 ± 5.6 (*fusl*^{1}), 103.1 ± 4.7 (*fusl*^{2}) and 109.2 ± 5.7 (*fusl*^{1}/Df) (P<0.001, N=10 animals for all genotypes; Fig. 2.6B, right "unload"). These data indicate that SV cycling is impaired in *fusl* mutants, with a particularly severe defect in SV exocytosis.

To examine synaptic vesicles directly, we used electron microscopy to quantify SV number and distribution within presynaptic boutons (Fig. 2.7). The overall synaptic ultrastructure appeared normal in *fusl* null mutants (Fig. 2.7A). Presynaptic boutons were of normal size, contained the expected array of organelles and displayed well-differentiated presynaptic and postsynaptic membrane profiles. Controls had bouton areas of 4.9 ± 0.6 (WT) and 3.7 ± 0.4 (+/Df), while mutants had areas of 3.9 ± 0.4 (*fusl*^{1}) and 4.7 ± 0.5 (*fusl*^{1}/Df) (P>0.4; N=4 animals, >20 boutons for each genotype). Likewise, presynaptic active zones appeared well differentiated, with a normal ultrastructural appearance (Fig. 2.7B). Synaptic vesicles appeared the same size in mutant and controls. In contrast, loss of Fusl results in striking differences from control in SV populations, with a dramatic elevation of vesicle number throughout the bouton (Fig. 2.7A) and specifically clustered around presynaptic active zones (Fig. 2.7B). In *fusl* mutants, the SV number was more than doubled as quantified by counting the number of total vesicles in each NMJ profile; the SV number in controls was 199 ± 19.0 (WT; N=21) and 184.5 ± 27.1 (+/Df; N=20), whereas the SV number in mutants was 422 ± 53.4 (*fusl*^{1}; N=17) and 475 ± 69.4 (*fusl*^{1}/Df; N=16) (P<0.001; Fig. 2.6C). In terms of vesicle density (μm^2) the numbers were

Figure 2.6: Lipophilic dye imaging of the synaptic vesicle cycle reveals a significant impairment in the endo-exo cycling pool in *fusI* mutants. A) Representative images of the NMJ synapse following FM1-43 loading and unloading. Preparations were incubated for 2 mins in 90 mM [K^+] saline to depolarize the synapse in the presence of FM1-43, washed in Ca^{2+}-free saline to arrest SV cycling and then imaged for the endocytosed dye (load). Synapses were then again depolarized for 2 mins in 90 mM [K^+] saline in the absence of FM1-43, washed in Ca^{2+}-free saline and then imaged for the loss of dye via exocytosis (unload). Scale bar: 20 μm. B) Quantification of FM1-43 fluorescence intensity in NMJ boutons following dye loading and unloading. Null *fusI* mutants display a significant impairment of endo-exo cycling ($P<0.01$), with a dramatic reduction in dye exocytosis ($P<0.001$). Sample size 10 animals, 20 NMJs per genotype.

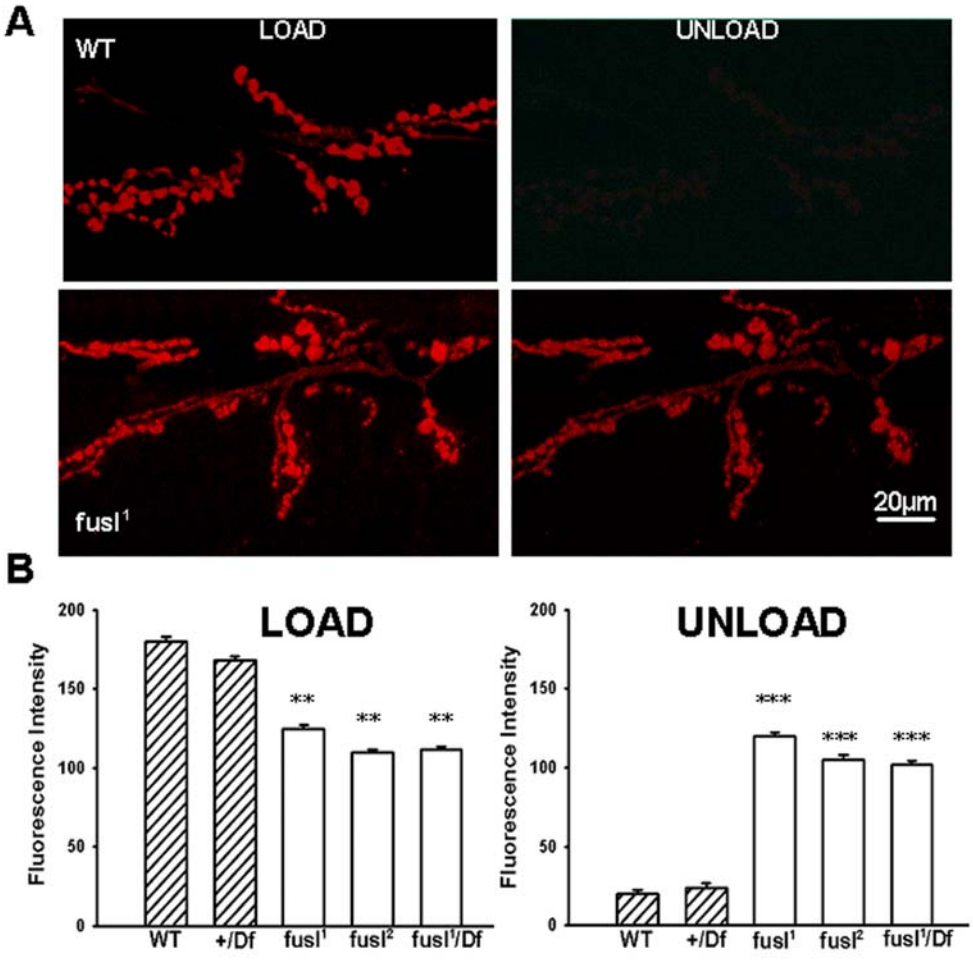
A
LOAD
UNLOAD
WT
fusl1
20µm
B
LOAD
UNLOAD
Fluorescence Intensity
200
150
100
50
0
**
***
WT
+/Df
fusl1
fusl2
fusl1/Df

Figure 2.7: Ultrastructural analyses reveal accumulation of clustered and docked synaptic vesicles at presynaptic active zones in *fusl* mutant. A) Representative TEM images of WT control (left) and *fusl* mutant (right) NMJ boutons. The mutant has normal bouton size, morphology and postsynaptic subsynaptic reticulum (SSR). Normal active zones (AZ) are visible in both panels as electron-dense synaptic membranes and T-bars. Null *fusl* mutant synapses display an obvious increase of synaptic vesicles throughout the terminal. Scale: 250 nm. **B)** High magnification images of active zones. In control animals (left) the clustered area (250 nm radius from T-bar center) has ~15 vesicles localized around the T-bar and ~2 docked vesicles (white arrowheads) contacting the presynaptic plasma membrane adjacent to the T-bar. In *fusl* mutants (right) there is a dense aggregation of clustered vesicles and clear increase in the number of docked vesicles. Scale: 50 nm. **C)** Quantitative analysis of ultrastructural phenotypes, including total vesicle number, clustered vesicle number (<250 nm from T-bar), vesicle density and docked vesicle number (<20 nm from AZ). White bars represent control animals and black bars represent mutant animals. The bouton profile sample size is >17 for each parameter; 4 animals were assayed for each genotype. Significance indicated as *** denotes P<0.001.

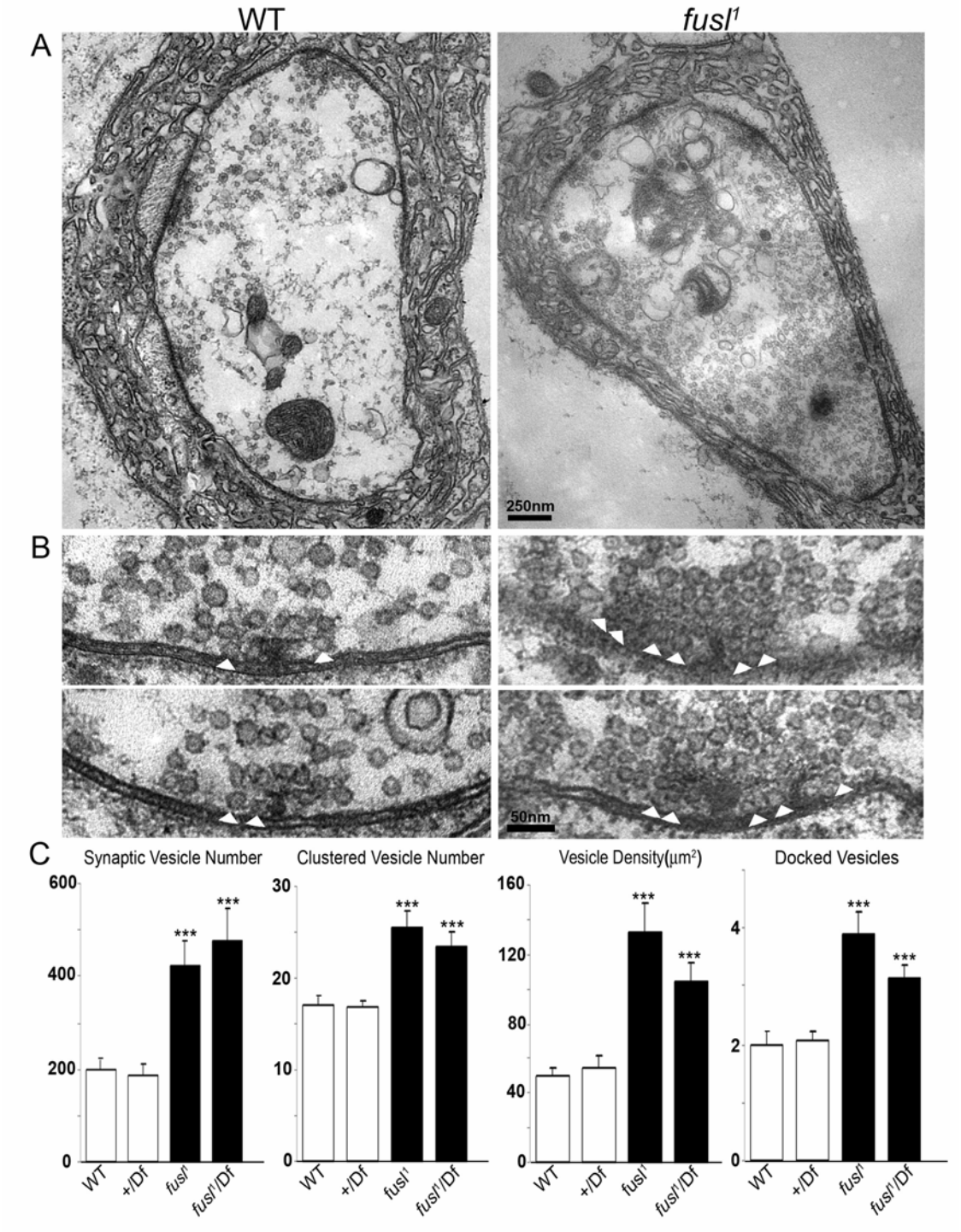
WT
fusl1
A
250nm
B
50nm
C
Synaptic Vesicle Number
Clustered Vesicle Number
Vesicle Density(μm2)
Docked Vesicles
600
400
200
0
30
20
10
160
120
80
40
4
2
***
WT
+/Df
fusl1
fusl1/Df

49.6 ± 4.5 (WT) and 54.9 ± 6.9 (+/Df) for controls, and more than doubled density in mutants at 132 ± 16.9 (*fusl*^{1}) and 103 ± 10.8 (*fusl*^{1}/Df). There was a parallel increase in the number of synaptic vesicles clustered (<250 nm) around individual active zones; in controls the clustered SV number was 17.0 ± 0.9 (WT; N=21) and 16.8 ± 0.8 (+/Df; N=20), whereas in mutants it was 25.5 ± 1.6 (*fusl*^{1}; N=17) and 23.4 ± 1.4 (*fusl*^{1}/Df; N=20) (P<0.001; Fig. 2.7C). Likewise, the number of SVs physically docked at the presynaptic active zone densities was very significantly increased in *fusl* mutants. In controls, the number of docked vesicles was 2.0 ± 0.2 (WT; N=21) and 2.0 ± 0.1 (+/Df; N=20), and it increased in mutants to 3.8 ± 0.4 (*fusl*^{1}; N=17) and 3.1 ± 0.2 (*fusl*^{1}/Df; N=20). These defects are characteristic in known SV fusion mutants (Richmond and Broadie, 2002; Kidokoro, 2003; Huang et al. 2006) and indicative of an impairment in SV exocytosis.

Loss of Fusl Causes [Ca^{2+}] Insensitivity During Neurotransmission

To further examine the cause of Ca^{2+}-dependent transmission impairments in the absence of fuseless, we assayed the effect of external [Ca^{2+}] on transmission amplitude (Fig. 2.8). Stimulation-evoked EJCs were compared over a range of [Ca^{2+}] from 0.2 mM to 1.8 mM. Figure 7A shows sample traces of wild-type controls and *fusl*^{1} mutants at 0.2, 0.4 and 1.0 mM [Ca^{2+}]. At the low end of this range (0.2 mM [Ca^{2+}]), *fusl* mutants display a mean EJC amplitude of 7.2 ± 5.4 nA compared to control amplitude of 11.1 ± 4.6 nA (Fig. 8A). At the higher end (1.0 mM [Ca^{2+}]) *fusl* mutants had a mean EJC amplitude of 18.7 ± 4.2 nA (*fusl*^{1}) compared to 110 ± 4.9 nA in control (Fig. 2.8A). Thus, over this [Ca^{2+}] range, the amplitude of the control EJC increased 10-fold, whereas the mutant increased only 2-fold. These data suggest an impairment in the Ca^{2+} influx trigger driving synaptic vesicle exocytosis.

EJC amplitudes are graphed as a function of external [Ca^{2+}] in Figure 2.8B. In lower external calcium (<1.0 mM), [Ca^{2+}] primarily limits EJC

Figure 2.8: Loss of the Ca^{2+} sensitivity of neurotransmission. A) Representative EJC records from *fusl* mutants (top row) and WT controls (bottom panel) in a range of external [Ca^{2+}]; 0.2mM (left), 0.5mM (center), 1.0mM (right). Null *fusl* mutants display insensitivity to increasing [Ca^{2+}], with only small increases in EJC amplitude. **B)** Quantification of EJC amplitude as a function of [Ca^{2+}]. Mean EJC amplitudes are shown for 0.2, 0.4, 1.0, and 1.8 mM [Ca^{2+}] for two controls (WT, Df/+) and two mutants (*fusl*^{1}, *fusl*^{1}/Df). Sample size 10 animals per genotype for each data point.

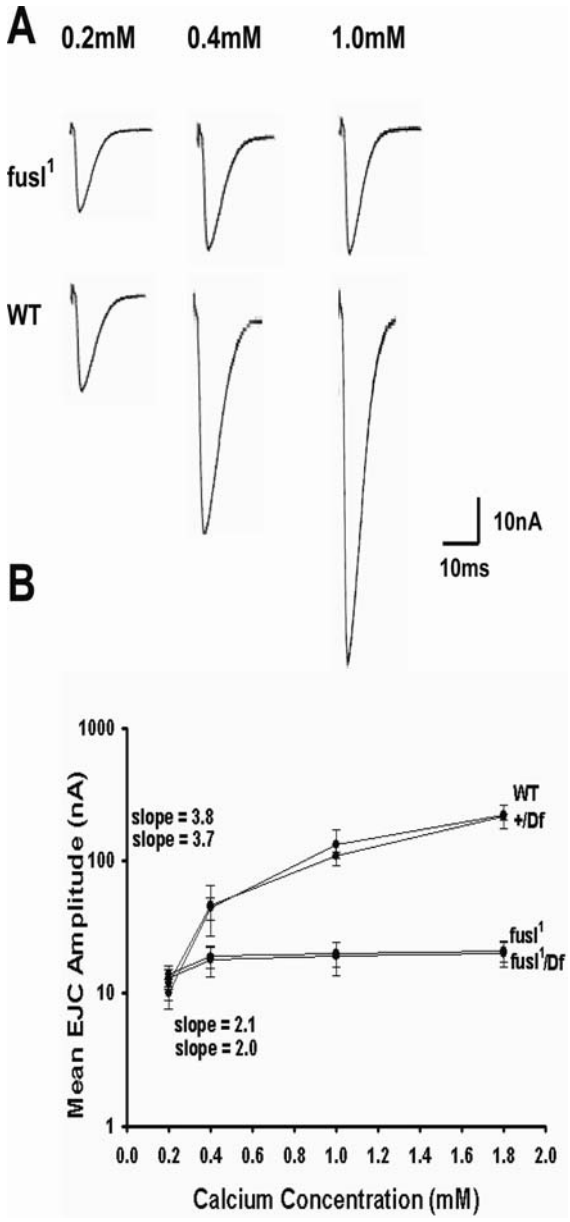
A
0.2mM
0.4mM
1.0mM
fusl1
WT
10nA
10ms
B
1000
100
10
1
Mean EJC Amplitude (nA)
slope = 3.8
slope = 3.7
slope = 2.1
slope = 2.0
WT
+/Df
fusl1
fusl1/Df
0.0
0.2
0.4
0.6
0.8
1.0
1.2
1.4
1.6
1.8
2.0
Calcium Concentration (mM)

transmission and a sharp rise in EJC amplitudes occurs in the control compared to *fusl* mutants. At higher [Ca^{2+}] (>1.0 mM), transmission strength is no longer solely limited by [Ca^{2+}], but mean EJC amplitude in controls continues to increase with increasing [Ca^{2+}] (Fig. 2.8B). In contrast, in *fusl* mutants there is very little Ca^{2+}-dependent increase in EJC amplitude as a function of increasing external [Ca^{2+}] (Fig. 2.8B). These data indicate a remarkable reduction in the sensitivity of basal neurotransmission strength to external [Ca^{2+}] in the absence of Fusl function. Given the presynaptic membrane localization of the Fusl protein, these functional defects are most consistent with impaired Ca^{2+} influx.

Presynaptic Calcium Channel Localization Depends on Fuseless

One explanation for the functional defects in *fusl* mutants could be loss or functional misregulation of presynaptic Ca^{2+} channels**.** The *Drosophila* NMJ contains a single, well-characterized voltage-gated Ca^{2+} channel, with the pore-forming α1 subunit encoded by *cacophony* (*cac*; Von Schilcher, 1976; Kawasaki et al., 2000; Kawasaki et al., 2004; Xing et al., 2005). To examine these calcium channels, we used a UAS-Cac-GFP fusion protein driven with presynaptic *elav*-GAL4, which has previously been used to document the tight, punctate localization of Cacophony Ca^{2+} channels at presynaptic active zones (Kawasaki et al., 2004). This transgenic reporter was crossed into the control and $fusl^{1}$ null backgrounds, with Cac-GFP expression analyzed using confocal microscopy (Fig. 2.9).

In agreement with previous reports, we found that Cac-GFP localizes to a number of discrete punctate active zone domains in presynaptic NMJ boutons (Fig. 2.9A). In striking contrast, Cac-GFP is dramatically reduced in *fusl* mutants; the overall expression level is much lower and the punctate Cac-GFP domains are only barely distinguishable (Fig. 2.9A, right). These Ca^{2+} channels were quantified by counting the number of Cac-GFP puncta per bouton and by calculating the mean density (Fig. 2.9B, left), as well as by measuring the fluorescence intensity

throughout synaptic boutons and calculating the mean intensity per unit area (Fig. 2.9B, right). The number of Cac-GFP puncta in *fusl* mutants is very significantly (P<0.0001, N=10 animals, 20 NMJs and 100 boutons per genotype) reduced compared to control (control; 4.9 ± 2.4, *fusl*^{1}; 0.3 ± 0.1, Fig 2.9B). In most boutons within a mutant NMJ arbor, there were no detectable Ca^{2+} channel domains and those observed were very faint. As this assay method is somewhat subjective, the mean fluorescence intensity of Cac-GFP was next assessed by outlining synaptic boutons and measuring the average density of the fluorescent signal in controls and mutants. Control synaptic terminals had a mean Cac-GFP density of 10.4 ± 3.4, whereas *fusl* null terminals had a 10-fold lower density of 1.7 ± 0.9 (*fusl*^{1}; Fig. 2.9B, right) (P>0.0001, N=10 animals, 20 NMJs and 100 boutons per genotype). These results show that Fusl plays a critical role in the localized expression of the Cacophony voltage-gated Ca^{2+} channels in presynaptic boutons and specifically in the formation of active zone domains. Driving UAS-Cac-GFP in neurons represents an over-expression condition, with terminals containing the native Cacophony voltage-gated Ca^{2+} channels as well as the introduced fusion protein, which is known to be functional (Kawasaki et al., 2004). Since *fusl* mutants show a defect in Ca^{2+} channel expression (Fig. 2.8A), this over-expression condition could provide some rescue of the neurotransmission phenotype. To test this possibility, electrophysiology was used to compare basal EJC amplitudes in the control and experimental lines. Representative traces (left) and the quantified mean EJC amplitudes (right) are shown in Figure 2.9C. Overexpression of the Cacophony Ca^{2+} channel was unable to detectably rescue the *fuseless* evoked transmission defect (control; 62.1 ± 4.2 nA, *fusl*^{1}; 18.6 ± 3.2 nA, *fusl*^{1}, Cac-GFP; 20.2 ± 3.9 nA, Fig. 2.9C) (P<0.0001 between mutants and control, N=10 animals per genotype). These data show that Fusl is required for presynaptic localization of voltage-gated Ca^{2+} channels.

Figure 2.9: Presynaptic voltage-gated Ca^{2+} channels lost in *fusl* mutants. A transgenic line of the Cacophony α-1 pore subunit of the presynaptic voltage-gated Ca^{2+} channel fused to GFP (UAS-Cac-GFP) driven by the *elav*-GAL4 neural driver in the presynaptic NMJ terminal in the control or $fusl^{1}$ null backgrounds. **A)** Representative images of control (left) and $fusl^{1}$ mutant (right) expressing Cac-GFP. Low magnification images of the NMJ (top panels: scale bar, 20 μm) and high magnification images of synaptic boutons (bottom panels: scale bar, 2 μm. **B)** Quantitation of the number of Cac-GFP puncta (left) and the Cac-GFP fluorescent intensity density (right). Control and mutant are very highly significantly different (***, $P<0.0001$). **C)** Representative EJC traces of *elav*-GAL4; UAS-Cac-GFP in a wildtype background (control), a $fusl^{1}$ homozygous background ($fusl^{1}$, Cac-GFP) and the $fusl^{1}$ mutant alone ($fusl^{1}$). Right panel: Quantification of mean EJC amplitudes. There was no significant difference between $fusl^{1}$, Cac-GFP and $fusl^{1}$ mutants, but there was a significant $P<0.0001$ difference between mutants and control. N=10 animals for each genotype.

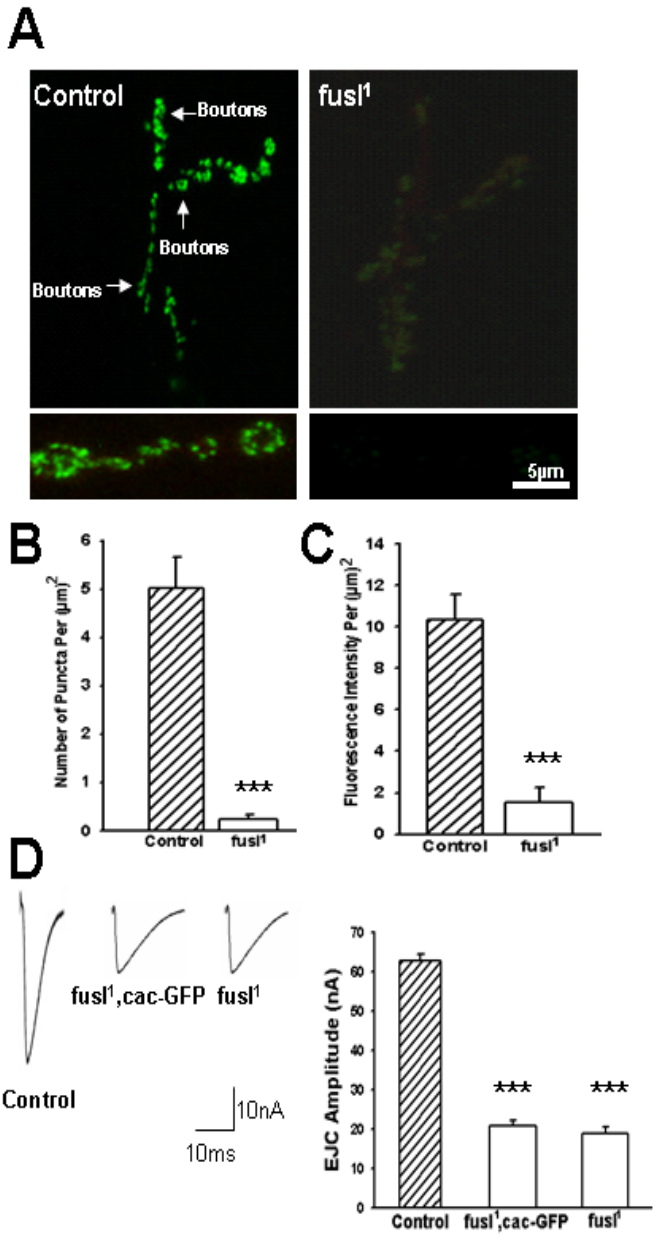
A
Control
Boutons
Boutons
Boutons
fusl1
5μm
B
Number of Puncta Per (μm)2
***
Control
fusl1
C
Fluorescence Intensity Per (μm)2
***
Control
fusl1
D
fusl1,cac-GFP
fusl1
Control
10nA
10ms
EJC Amplitude (nA)
***
***
Control
fusl1,cac-GFP
fusl1

Discussion

Using an unbiased, forward genetic screen for synaptic dysfunction mutants in the *Drosophila* visual system, we have identified a new presynaptic integral membrane protein with a critical function in regulating active zone voltage-gated Ca^{2+} channels and thus the Ca^{2+} trigger driving the synaptic vesicle fusion underlying neurotransmission. The Fuseless protein is a predicted 8-pass transmembrane protein whose closest known human homolog is the transmembrane protein Sialin, a transporter belonging to a group of anion/cation symporters (Yarovaya et al., 2005; Wreden et al., 2005). The monosaccharide sialic acid cleaved from sialoglycoconguates is exported across membranes by the Sialin transporter (Morin et al., 2004). Two inherited diseases occur when the *sialin* gene is mutated: Infantile Sialic Acid Storage Disease (ISSD) and Salla Disease (SD), which are characterized by severe CNS defects including mental retardation (Morin et al., 2004; Verheijen et al., 1999).The modification of cell surface proteins by addition of sialic acid is known to regulate critical neuronal processes including intercellular adhesion and signaling (Kiss and Rougon, 1997). In *Drosophila*, *fuseless* mutations profoundly disrupt synaptic transmission, both at central, histaminergic photoreceptor synapses and at peripheral, glutamatergic NMJ synapses, indicating a conserved, critical function in multiple classes of chemical synapse. The requirement for the Fusl protein can be supplied with expression targeted only to the presynaptic side, indicating a function in transmitter release. Functional defects in *fusl* mutants are similar to those found in the Ca^{2+} channel mutant *cacophony* (Xing et al., 2005; Kawasaki et al., 2000). Other mechanistic defects also suggest a disrupted Ca^{2+}-trigger for exocytosis, including reduced FM1-43 and SV cycling. Consistently, the Fusl protein strongly regulates Cacophony Ca^{2+} channel localization to presynaptic active zones. Together, these results indicate that formation of

active zone Ca^{2+} channel domains is the primary role of Fuseless in controlling neurotransmission strength.

Fuseless Regulates Neurotransmitter Release to Control Transmission Strength

Loss of Fuseless protein results in a range of synaptic dysfunction phenotypes that appear to be mechanistically linked to disruption of presynaptic Ca^{2+} dynamics. Mutant synapses display a strong reduction in evoked neurotransmitter release over a wide range of external calcium concentrations. In low [Ca^{2+}], normal synapses display a log-linear dependence of transmitter release on [Ca^{2+}] (Dodge and Ramimoff, 1967), but *fusl* null synapses display only a small increase in transmission amplitude even with large changes in external [Ca^{2+}], indicating a fundamental defect in Ca^{2+} influx dependent secretion (Zucker et al., 1993; Zucker et al., 1996). In contrast, *fusl* mutants exhibit elevated spontaneous vesicle fusion frequency and amplitude, which are both rescued by targeted presynaptic expression of the wild-type *fusl* gene, indicating elevated secretion under non-stimulated conditions (Deitcher et al., 1998; Yoshihara et al., 2000; Trotta et al., 2004). The increased mEJC amplitude may reflect an increased incidence of synchronous spontaneous fusion events, although summation events are evident in only a small subset of currents. It appears unlikely that either increased SV glutamate content (Daniels et al., 2004) or compensatory upregulation in postsynaptic glutamate receptor density (DiAntonio et al., 1999) are involved, as vesicle size appears normal in ultrastructural studies and glutamate receptor expression/function are not detectably altered in *fusl* null mutants. The increased incidence of spontaneous vesicle fusion events is consistent the elevated number of vesicles docked at presynaptic active zones. It is widely believed that fusion probability is a function, in part, of the number of docked, fusion-competent vesicles.

Fuseless Regulates Presynaptic Active Zone Calcium Channel Domains

The calcium concentration in the nerve terminal at rest is astoundingly low, providing the necessary canvas for the action potential-driven spike of calcium influx to drive rapid vesicle exocytosis (Katz and Miledi, 1968; Katz and Miledi, 1970; Llinas et al., 1976). The Fuseless protein plays a critical role in the presynaptic localization of voltage-gated Ca^{2+} channels, as revealed by assaying the *cacophony*-encoded α1 pore subunit, which directly mediates Ca^{2+} influx (Smith et al., 1996; Eberle et al., 1998). In mammals, the binding of the tSNARE Syntaxin to presynaptic Ca^{2+} channels led to the identification of the SYNPRINT interaction domain within P/Q and N type channel subunits (Sheng et al., 1998). The SYNPRINT domain is thought to physically tether the Ca^{2+} channel to Syntaxin to help mediate the localized, rapid coupling of Ca^{2+} influx to vesicle fusion (Mochida et al., 1996; Sheng et al., 1998), and also bidirectionally regulate the activity of the channels (Wu et al., 1999). In *Drosophila*, the *cacophony* Ca^{2+} channel triggers similar fast neurotransmitter release (Kawasaki et al., 2000), but no sequence homologous to SYNPRINT has been identified (Wu et al., 1999; Littleton and Ganetzky, 2000), suggesting another mechanism for coupling Ca^{2+} influx to the fusion of docked vesicles (Kawasaki et al., 2002). In vertebrates, the calcium channel α1 subunit has been demonstrated to regulate channel dynamics including activation/inactivation rates, and also directly interacts with Synaptotagmin and other proteins involved in Ca^{2+}-dependent vesicle fusion (Hille, 2001). Interestingly, the α1 subunit has also been demonstrated to bind extracellular laminins, and facilitate the organization of presynaptic active zones (Nishimune et al., 2004). It follows, then, that significant loss of the α1 subunit predicts underdeveloped active zones and significant reduction in transmitter exocytosis (Wagh et al., 2006; Kittel et al., 2006).

In all characterized synapses, calcium channels cluster at presynaptic active zones, where they form a tight spatial association with synaptic vesicles docked and ready for fusion (Mochida et al., 1996; Sheng et al., 1998; Wu et al., 1999; Nishimune et al., 2004) In the absence of Fusl protein, ultrastructurally normal active zones form, but fail to cluster Ca^{2+} channels. It has been recently reported that reduction in Ca^{2+} channel density or function can contribute to disorganized active zones (Nishimune et al., 2004; Wagh et al., 2006; Kittel et al., 2006) and a reduction in active zone formation (Wagh et al., 2006; Kittel et al., 2006). In particular, it has been proposed that the *Drosophila* Bruchpilot protein stabilizes the formation of active zones by triggering the integration of active zone components and specifically Cacophony Ca^{2+} channels. The *bruchpilot* mutants show reduced Ca^{2+} channel clustering, density and localization, and reduced vesicular release probability (Wagh et al., 2006; Kittel et al., 2006). Likewise, in *fuseless* mutants, loss of Ca^{2+} channels, and Ca^{2+} channel local function, is proposed to be the primary defect in coupling Ca^{2+} influx to vesicle exocytosis, leading to the observed disruption in vesicle release probability.

Null *fuseless* mutants have an increased number of vesicles clustered and docked at the presynaptic density. These phenotypes are consistent with direct disruption of Ca^{2+}-triggered vesicle exocytosis. Similar vesicle accumulation characterizes *syntaxin1A*, *dunc-13*, *comatose* and *rolling blackout* mutants, for example, each of which has a specific exocytosis deficit (Broadie et al., 1995; Kawasaki et al., 1998; Littleton et al., 1998; Aravamudan et al., 1999; Kidokoro, 2003; Huang et al., 2006).It has been shown that a specific block in SV exocytosis leads to a secondary accumulation of vesicles in pools upstream of the presynaptic membrane. FM dye studies complement the ultrastructural analyses. As is expected for any defect in the SV cycle, there is a decrease in the overall rate of endo-exo cycling in *fusl* mutants. In addition, there is a particularly severe defect in acute FM dye release in the absence of Fusl function, consistent with a

specific defect in SV exocytosis. We attribute these *fusI* mutant defects wholly to the loss of the appropriate Ca^{2+} influx trigger to signal release of otherwise fusion-competent vesicles.

CHAPTER III

The nonsense-mediated decay pathway maintains synapse architecture and synaptic vesicle cycle efficacy

This paper has been accepted for publication under the same title in the *Journal of Cell Science*, 2010.

A. Ashleigh Long[1], Cecon T. Mahapatra[2,5], E. A. Woodruff III[1], Jeff Rohrbough[1], Hung-Tat Leung[2,6], S. Shino[2], L. An[3,7], R. W. Doerge[3], Mark M. Metzstein[4], William L. Pak[2] and Kendal Broadie[1]

[1]Department of Biological Sciences, Department of Cell and Developmental Biology, Vanderbilt Brain Institute, Kennedy Center for Research on Human Development, Vanderbilt University, Nashville TN 37235-1634 USA

[2]Department of Biological Sciences and [3]Department of Statistics, Purdue University, West Lafayette, IN 47907 USA

[4]Eccles Institute of Human Genetics, University of Utah Medical School, Salt Lake City, Utah 84112 USA

[5]Present address: Department of Anatomy and Neurobiology, University of Vermont, Burlington, VT 05402 USA

[6]Present address: Department of Biological Sciences, Grambling State University, Grambling, LA 71245 USA

[7]Present address: Department of Agricultural and Biosystems Engineering, University of Arizona, Tucson, AZ 85721 USA

Abstract

A systematic *Drosophila* forward genetic screen for photoreceptor synaptic transmission mutants identified no-on-and-no-off transient C (nonC) based on loss of retinal synaptic responses to light stimulation. The cloned gene encodes phosphatidylinositol 3-kinase-like kinase (PIKK) Smg1, a regulatory kinase of the nonsense-mediated decay (NMD) pathway. The Smg proteins act in an mRNA quality control surveillance

mechanism to selectively degrade transcripts containing premature stop codons, thereby preventing the translation of truncated proteins with dominant negative or deleterious gain of function activities. At the neuromuscular junction (NMJ) synapse, an extended allelic series of Smg1 mutants show impaired structural architecture, with decreased terminal arbor size, branching and synaptic bouton number. Functionally, loss of Smg1 results in a ~50% reduction in basal neurotransmission strength, as well as progressive transmission fatigue and greatly impaired synaptic vesicle recycling during high-frequency stimulation. Mutation of other NMD pathways genes (Upf2/Smg3 and Smg6) similarly impairs neurotransmission and synaptic vesicle cycling. These findings suggest that the NMD pathway acts to regulate proper mRNA translation to safeguard synapse morphology and maintain synaptic functional efficacy.

Introduction

Post-transcriptional regulation of gene expression playss a critical role in the development, maintenance and plasticity of neuronal synapses. At the mRNA level, translation control in soma as well as remotely in dendrites and axonal growth cones (Bassell and Warren, 2008; Dictenberg et al., 2008; Giorgi et al., 2007; Lin and Holt, 2007; Piper and Holt, 2004) regulates pathfinding, synaptogenesis and synaptic function (Hu et al., 2002; Schacher and Wu, 2002; Sebeo et al., 2009; Sherff and Carew, 1999; Sherff and Carew, 2002; Yan et al., 2009). Neuronal mRNA transport and translation is often mediated by interaction between the 3' untranslated region (3' UTR) "zipcode" and mRNA-binding proteins such as zip-code binding protein (ZBP) and cytoplasmic polyadenylation element binding protein (CPEB) (Brittis et al., 2002; Lin and Holt, 2008). Other mRNA-binding proteins, such as fragile X mental retardation protein (FMRP), similarly play critical roles in the regulation of synaptic mRNA stability, trafficking and translation (Gatto and Broadie, 2008; Pan and Broadie, 2007; Pan et al., 2004; Pan et al., 2008; Repicky and Broadie,

2009; Tessier and Broadie, 2008; Zhang et al., 2001; Zhang et al. 2005). On the other hand, local protein degradation via the ubiquitin proteasome system (UPS) has also recently been established as a key mechanism shaping synaptic structural development, neurotransmission strength and synaptic plasticity (Haas and Broadie, 2008; Haas et al. 2007; Speese et al., 2003).

The *C. elegans* and *Drosophila* genetic systems have provided vital insights into the mechanisms of post-transcriptional regulation in sculpting synaptic properties. *Drosophila* FMRP (dFMRP) is involved in mRNA trafficking and stability (Pan and Broadie, 2007; Pan et al., 2008; Pan et al., 2004; Tessier and Broadie, 2008; Zhang et al., 2001; Zhang et al. 2005), and the activity-dependent regulation of mRNA translation (Gatto and Broadie, 2008; Tessier and Broadie, 2008). At the synapse, dFMRP has multiple functions in controlling axonal and dendritic arbor size, bouton number and distribution, transmission strength, postsynaptic glutamate receptor trafficking and the regulation of presynaptic vesicle pools (Gatto and Broadie, 2008; Pan and Broadie, 2007; Pan et al., 2008; Pan et al., 2004; Repicky and Broadie, 2009; Tessier and Broadie, 2008; Zhang et al., 2001; Zhang et al. 2005). In balance with translation regulation, UPS-mediated degradation has dynamic functions controlling synapse architecture, neurotransmission strength and synaptic protein abundance, including postsynaptic glutamate receptors (Haas and Broadie, 2008; Haas et al. 2007; Speese et al., 2003). The ubiquitin ligase *highwire* acts to restrict synaptic overgrowth by down-regulating the MAPKKK Wallenda pathway, with mutants exhibiting increased NMJ branch and bouton numbers (Wan et al., 2000; Wu et al., 2007). Loss of *C. elegans rpm-1* similarly causes disruption of synapse architecture and function (Nakata et al., 2005). RPM-1 negatively regulates the MAP kinase pathway of MAPKKK DLK-1, MAPKK MKK-4 and p38 MAPK PMK-3. Recently, this pathway was shown to regulate trafficking of the AMPA-type glutamate receptor GLR-1 (Park et al., 2009). Destabilization of enhancer

binding protein CEBP-1 mRNA has also recently been shown to alter local translation of MAPKKK components in distal axons to disrupt axon morphology and synapse formation in *C. elegans* (Yan et al., 2009). Other recent work has shown the importance of microRNA pathways (Cheever and Ceman, 2009a; Cheever and Ceman, 2009b; Kiebler et al., 2006; Xu et al., 2008;) and processing bodies (P-bodies) (Barbee et al., 2006; Gibbings et al., 2009; Miyoshi et al., 2009; Pillai et al., 2005).

Nonsense-mediated decay (NMD), an mRNA surveillance system that ensures message integrity by degrading transcripts containing nonsense mutations (Bramham et al., 2008; Giorgi et al., 2007), represents a relatively unexplored mechanism for regulating mRNA stability in neurons. Importantly, NMD is also proposed to regulate normal transcript expression, and so provide an alternative mechanism of control. Seven NMD pathway "suppressor with morphogenetic effect on genitalia" (*Smg)* genes were originally identified in *C. elegans* (Hodgkin et al., 1989), with six gene homologs subsequently identified in *Drosophila* (Gatfield and Izaurralde, 2004; Metzstein and Krasnow, 2006). It was recently demonstrated that eIF4AIII, a core exon junction complex (EJC) component, is associated with neuronal mRNA granules (Barbee et al., 2006; Giorgi et al., 2007; Shibuya et al., 2004; Shibuya et al., 2006). In mammals, the EJC is thought to play a critical role in directing transcripts to the NMD pathway. This system controls glutamate receptor expression and long-term potentiation at the synapse via regulation of Arc protein expression (Bramham et al., 2008; Giorgi et al., 2007; Waung et al., 2008). Predicted NMD pathway targets include a number of synaptic genes, however the functional requirement of NMD in maintaining the synapse has not before been directly tested *in vivo*.

Classical *Drosophila* forward genetic screens to generate mutants with defective adult eye electroretinograms resulted in isolation of a pool of mutants with profoundly disrupted photoreceptor synaptic transmission. These genes were targeted to identify novel mechanisms required for

synapse formation and function. Cloning and genomic rescue of the *no-on-and-off transient C* (*nonC*) mutant from this pool showed it to be the phosphatidylinositol 3-kinase-like kinase (PIKK) *S*mg*1* gene, the regulative kinase of the NMD pathway. Detailed analyses at the well-characterized NMJ synapse pursued with an extended series of *Smg1* alleles showed defects in morphological architecture and impaired synaptic function owing to disrupted synaptic vesicle cycling. Similarly, mutation of other key NMD pathway components, including *Upf2* (*Smg3*) and *Smg6* mutants that abrogate NMD and cause accumulation of PTC-containing transcripts (Metzstein and Krasnow, 2006), comparably impairs presynaptic function. These results demonstrate that NMD mRNA regulation is critical for the proper development of synaptic architecture and for the maintenance of synaptic transmission efficacy.

Materials and Methods

Genetic Stocks

The first nonC mutant ($nonC^{P37}$) was isolated by ethyl methanesulfonate (EMS) mutagenesis of Oregon R (OR) base stock (Pak et al., 1969). The $nonC^{MC45}$ and $nonC^{MC47}$ mutants were generated independently by P-element hybrid dysgenesis (Engels, 1989). The method of microarray-based identification of genes with mutations responsible for ERG defects has been described previously (Leung et al., 2008; Long et al., 2008). The $Smg1^{rst2}$ allele is a premature stop (AAA to TAA) at amino acid 704 (Chen et al., 2005). The $Smg1^{32AP}$ allele is a genetic null isolated in a mosaic screen of EMS-induced X-chromosome mutations (Metzstein and Krasnow, 2006). The $Smg6^{292}$ mutant, isolated in a screen using an NMD-sensitive reporter construct, is a point mutation (GT to AT) disrupting the sixth intron splice site, truncating Smg6 at amino acid 558 to generate a null condition (K. Frizzell, S. Rynearson, and M.M. Metzstein, unpublished data). The $Upf2^{25G}$ (*Smg3*) mutant was isolated in a genetic mosaic screen for EMS–induced X chromosome mutations,

resulting in near complete loss of NMD activity (Metzstein and Krasnow, 2006). The Smg1 genomic rescue construct was generated from BAC clone RP98-5L2 containing the Smg1 gene (X:6718671 to 6732283; 13612 bp) and 5'-flanking region (X:6715452 to 6718670; 3218 bp) by recombineering (Groth et al., 2004; Venken et al., 2006). The rescue construct lines were confirmed by PCR in the null mutant backgrounds.

Immunohistochemistry and Fluorescence Quantification

Wandering third instars were dissected and fixed in Bouin's fixative (10 mins) or ice-cold methanol (5 mins), washed in PBS–TX-100 (30 mins) and then incubated with primary antibodies at RT (4 hrs). Presynaptic NMJ terminals were visualized with anti-horseradish peroxidase (HRP) (Texas Red Conjugated 1:200 (Invitrogen), or anti-rabbit 1:250; Sigma). Presynaptic active zones were visualized using anti-bruchpilot (NC82; anti-mouse; 1:100; University of Iowa Developmental Studies Hybridoma Bank (DSHB)). The postsynaptic domain was visualized with anti-Discs Large (DLG; anti-mouse; 1:100; DSHB) and anti-GluRIIA (8B4D2; anti-mouse; 1:10; DSHB). Secondary antibodies were Alexa 488 (1:200; anti-mouse; Invitrogen) and Alexa 546 (1:200; anti-rabbit; Invitrogen) incubated at RT (2 hrs). Imaging was done on a Zeiss 510-Meta confocal microscope (Jena, Germany). Branch and bouton number were quantified from HRP-labeled NMJs, with branches and boutons averaged between A3 hemisegments in each animal for each n=1. Fluorescence intensities were measured in entire NMJs or individual boutons using Metamorph software (MDS Analytical Technologies, USA).

Electrophysiology

Electroretinogram (ERG) recordings were made as previously described (Long et al. 2008). In brief, with recording electrode through the cornea in the photoreceptor layer and ground electrode in the head, animals were dark-adapted (2 mins) and then a 300 W halogen lamp used to generate

light stimuli (CS2-73 filter) via a light guide. Light intensity was attenuated in log-unit steps using neutral density filters from an unattenuated intensity of 830 μW/cm^2. Signals were sampled at 2 kHz with an analog-to-digital converter, and data analyzed with Axoscope software (Molecular Devices, Sunnyvale, CA). Two-electrode voltage-clamp (TEVC) recordings were made at the wandering third instar NMJ as previously described (Long et al. 2008; Rohrbough et al., 1999). In brief, muscle 6 in segment A3 was voltage-clamped (V_{hold} = -60 mV) with current recordings made on an Axoclamp 200B amplifier (Molecular Devices) and analyzed with Clampex 7.0 software (Axon Instruments). Recording saline contained (in mM): 128 NaCl, 2 KCl, 4 $MgCl_2$, 0.5 Ca_2Cl, 5 trehalose, 70 sucrose, 5 HEPES. Miniature excitatory junctional currents (mEJCs) were recorded continuously in gap-free recording mode (n=1 represents 120 secs) in a low pass setting (500Hz). For evoked EJCs, cut motor nerves were stimulated with glass suction electrodes at suprathreshold voltage (0.5 msec). Currents were filtered at 1000Hz and analyzed with PClamp 7.0 software.

Electron Microscopy

NMJ ultrastructural analyses were performed as reported previously (Long et al. 2008; Vijayakrishnan et al., 2009). In brief, two approaches were used: 1) dissected third instars were immediately fixed (resting condition), or 2) the cut segmental nerve (segment A3) was stimulated with a glass suction electrode at 20 Hz for 1 min immediately followed by fixation (stimulated condition). Preparations were fixed in 2% glutaraldehyde (1 hr), washed in PBS (10 mins) and then transferred into 1% O_sO_4 in PBS (2 hrs). Segment A3 muscle 6/7 was dissected free for all further processing. Preparations were stained en bloc in 1% aqueous uranyl acetate (1 hr), dehydrated in an ethanol series then propylene oxide (30 mins) and embedded in araldite. Ultrathin (<60nm) sections were cut (Leica Ultracut UCT 54 ultramicrotome) and transferred to

formvar-coated slot grids on synaptiek grid-sticks for post-staining with lead nitrate and uranyl acetate. Sections were imaged using a Phillips CM10 Transmission Electron Microscope at 80kV, with Images collected on a 2-megapixel AMT CCD camera.

Lipophilic Dye Imaging

NMJ FM1-43 dye loading using electrical motor nerve stimulation was done as previously described (Dermaut et al., 2005). In brief, 20 Hz suprathreshold motor nerve stimulation was applied for 60 secs in 0.5 mM Ca^{2+} saline containing 10 µM FM1-43. Preparations were immediately washed in 0 mM Ca^{2+} saline for 5 mins, and fluorescent images of NMJ 6/7 terminals acquired on a Zeiss confocal microscope. Fluorescence intensities were determined using Metamorph software (MDS Analytical Technologies, USA) using the hand-select line drawing tool to trace around each bouton. The fluorescent signal was also photoconverted to an electron-dense signal for ultrastructural analyses as previously described (Vijayakrishnan et al., 2009). In brief, FM1-43 loaded preparations were fixed in 1.6% paraformaldehyde/2% glutaraldehyde (5 mins), washed in Tris-buffered saline (TBS, pH 7.5; 20 mins), and then incubated in 0.15% 3,3'-diaminobenzidine (DAB, DEKO; 5 mins). The DAB solution was refreshed and samples illuminated using a 100 watt mercury lamp, a 63x0.95W objective and a standard FITC filter for 20 mins. Photoconverted preparations (see Fig. 7B) were post-fixed overnight in 2% glutaraldehyde at 4^{o}C, placed in 1% osmium (O_sO_4) at RT (1 hr) and then placed in uranyl acetate at RT (1 hr). Samples were then processed for electron microscopy using the standard protocol, as described above.

Statistics

ANOVA parametric statistics with Dunnett's analyses were employed to determine statistical differences between matched mutants and controls in all studies.

Results

Visual system screen for synaptic transmission mutants identifies *nonC*

The ERG consists of a corneal-negative (downward) sustained component of summed photoreceptor phototransduction, and two transient components at lights-on and lights-off arising from neurotransmission in the lamina (Fig. 3.1A). The on-transient, in particular, corresponds directly to responses of laminar neurons to synaptic input from photoreceptors R1–6 (for review, see Pak, 1995). In wildtype animals, the peak amplitude of the sustained component increases with the strength of the light stimulus in a semilog dependent manner over a 3 log unit range of stimulus intensity (Fig. 3.1A). Synaptic transient amplitudes are lower only at the weakest light stimulus intensity, and then increase to a constant level over the next three orders of light intensity magnitude increments (Fig. 3.1A). The peak amplitude of the phototransduction component and the synaptic on- and off-transient amplitudes were quantified and plotted as a function of the stimulus intensity (Fig. 3.1B). In the *nonC* mutant isolated in the screen ($nonC^{P37}$), robust phototransduction persists but the synaptic transients are not detectable (Fig. 3.1A). Neither on-transients (Fig. 1Ba) nor off-transients (Fig. 3.1Bc) of any significant amplitude could be elicited from the $nonC^{P37}$ mutant at any of the four light intensities tested. An independently isolated *nonC* mutant allele, $nonC^{MC45}$, showed a similar, selective synaptic impairment (Fig. 3.1A). This mutant also had no detectable photoreceptor synaptic on-transients (Fig. 3.1Ba), and displayed off-transients of reduced amplitude (Fig. 3.1Bc). The peak phototransduction responses of photoreceptors were slightly depressed in $nonC^{P37}$ and comparable to wildtype in $nonC^{MC45}$ (Fig. 3.1Bb). The loss of photoreceptor synaptic transmission in both *nonC* mutant alleles was totally rescued by introduction of the wildtype candidate gene (Fig. 3.1A, right; Fig. 3.1B),

demonstrating that the synaptic defect is due solely to the loss of this single gene function (see below).

Identification of *nonC* candidate genes

Candidates for the *nonC* gene were identified by a microarray-based approach screening for statistically significant alterations in mRNA levels of genes within the chromosomally mapped mutant interval (Fig. 3.2) (Leung *et al*., 2008; Long *et al*., 2008). Deficiency mapping placed *nonC* between the right breakpoint of deficiency *Df(1)ED6849* (X:6698829) and right breakpoint of duplication *Dp(1,Y)dx49* (6D8) (Fig. 3.2A). To accommodate possible mismatch between reported chromosomal breakpoints and gene locations, microarray data were examined in a wider region than that defined by mapping; namely 6C13-6E2, the 120 kb region between coordinates X:6660000 and X:6780000, which contains 17 genes. Microarray data showed that four genes showed statistically significant changes in mRNA levels in *nonC* mutants: *shf*, *Smg1*, *CG4557*, and *CG4558* (Fig. 3.2A). Thus, these genes were identified as candidates. All genes were fully sequenced in three different *nonC* mutants; $nonC^{P37}$, $nonC^{MC45}$ and $nonC^{MC47}$. No mutations were found in the *shf, CG4557 or CG4558* genes in any *nonC* mutants. In contrast, the *S*mg*1* gene carried a T to C transition in nucleotide 2552, resulting in the isoleucine to threonine change in aa 851 in both $nonC^{MC45}$ and $nonC^{MC47}$ (Fig. 3.1B). Four other genes in the *S*mg*1* vicinity (6D4-7 region; Fig. 3.2A) and two genes in the 6E4 region were also sequenced. No mutations were detected in any of these genes in $nonC^{P37}$, $nonC^{MC45}$ or $nonC^{MC47}$. The genes sequenced included *CG12796*, which resides within the 4th intron of *S*mg*1*. These results suggested that *S*mg*1* was the most likely candidate for the *nonC* gene. Following this identification, previously described *Smg1* alleles were obtained, including $Smg1^{rst2}$, a premature stop codon resulting at amino acid 704 AAA to TAA (Chen et al., 2005), and $Smg1^{32AP}$, a genetic null

Figure 3.1. **Genetic screen identifies *nonC* retinal synaptic transmission mutants.** Electroretinogram (ERG) synaptic on- and off-transients are lost in *nonC* mutants and restored by *S*mg*1* genomic rescue. **A)** Orange light stimuli (4s) at four intensities (log unit intervals; indicated by uppermost traces) was used to elicit ERG responses from wildtype and *nonC* mutant alleles ($nonC^{P37}$ and $nonC^{MC45}$; left panel) and mutants carrying a wildtype *S*mg*1* genomic rescue construct ($nonC^{P37}$ rescue and $nonC^{MC45}$ rescue; right panel). **B)** Quantification of ERG response amplitudes for on-transients (a), peak phototransduction response (b) and off-transients (c). All genotypes were white-eyed; mutants were marked with *cn;bw*, and wildtype was derived from Oregon R and marked with *w*. Rescued flies contained a mini-*w*+ marker in the transgene. Sample size n=10 animals for each genotype in stimulus every condition.

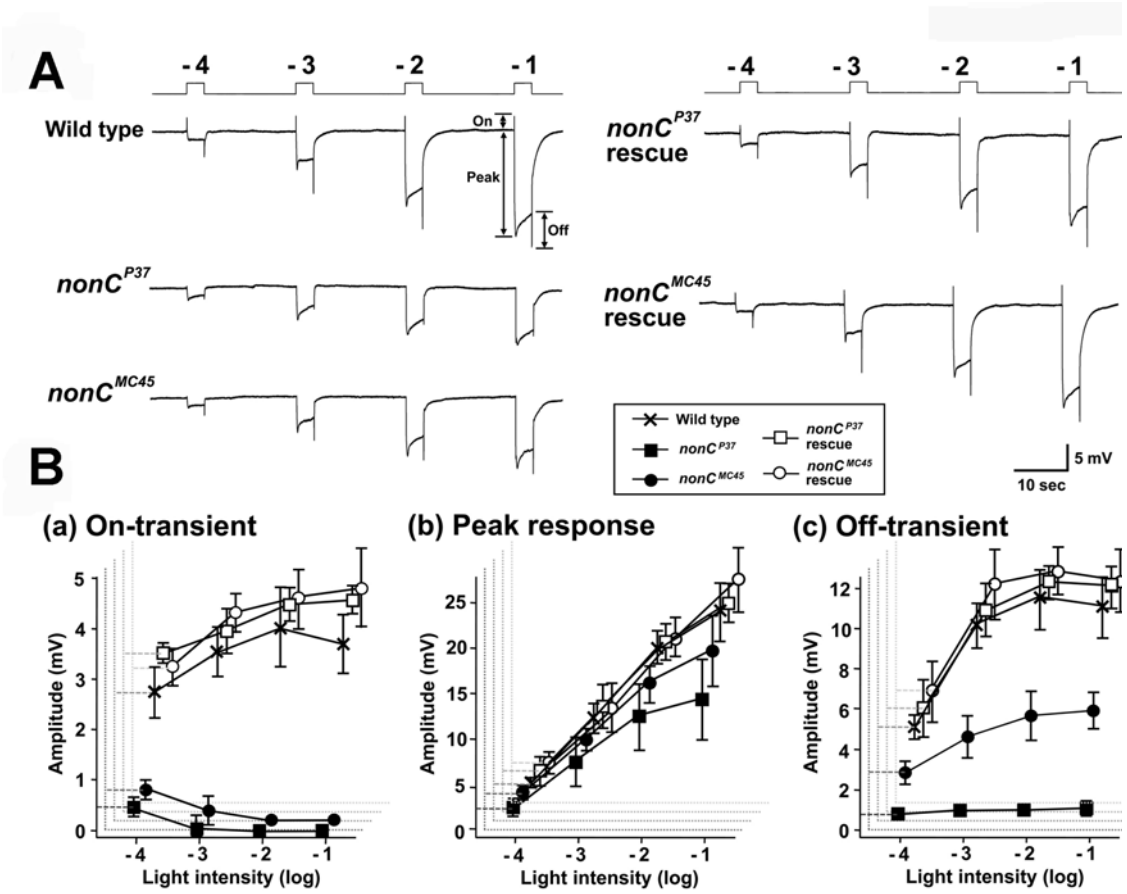
A
-4
-3
-2
-1
Wild type
On
Peak
Off
nonC^P37
rescue
nonC^P37
nonC^MC45
rescue
nonC^MC45
Wild type
nonC^P37
nonC^MC45
nonC^P37 rescue
nonC^MC45 rescue
5 mV
10 sec
B
(a) On-transient
(b) Peak response
(c) Off-transient
Amplitude (mV)
Light intensity (log)

Figure 3.2. Maps of the *S*mg*1* genomic region, *Smg1* gene, and gene products. A) The genomic region. The *nonC* mutations are covered by duplication *Dp(1;Y)dx49* (double line; top) and complemented by deficiency *Df(1)ED6849* (dotted; second line). The *Df(1)ED6849* right breakpoint is defined at X:6698829, and *Dp(1;Y)dx49* right breakpoint localized to 6D8. **B)** The *Smg1* gene and products. The 13.6 kb gene generates one mRNA encoding a 3218 amino acid protein with HEAT (huntington, elongation factor 3, alpha regulatory subunit of protein phosphatase 2A, and the yeast PI3-kinase TORI), kinase and FATC (FRAP, ATM, TRRAP, C-terminal) domains characteristic of phosphatidylinositol 3-kinase (PI3-K) related protein kinases. The site of 3 mutations shown on the Smg1 protein map. **C)** Phylogenetic tree constructed from *Smg1* orthologs. Scale bar indicates 0.1 fractional difference in alignment. Proteins by species, name/function, accession number, and % amino acid identity with *Drosophila* Smg1, as follows: *Homo sapiens (Hs)*, PI3-K related kinase (NP_055907.3), 34.1%; *Canis familiaris (Cf)*, PI3-K related kinase, (XP_851552.1), 33.8%; *Mus musculus (Mm)*, RIKEN cDNA 2610207I05 (NP_001026984.1), 34.0%; *Rattus norvegicus (Rn)*, PI3-K related kinase (XP_001078729.1), 34.1%; *Gallus gallus (Gg)*, PI3-K related kinase (XP_414907.2), 34.2%; *Danio rerio (Dr)*, PI3-K related kinase (NP_001073513.1), 24.8%; *Drosophila melanogaster (Dm)*, Smg1/CG32743 (NP_727132.1); *Caenorhabditis elegans (Ce)*, Smg1 (XP_001078729.1), 36.2%.

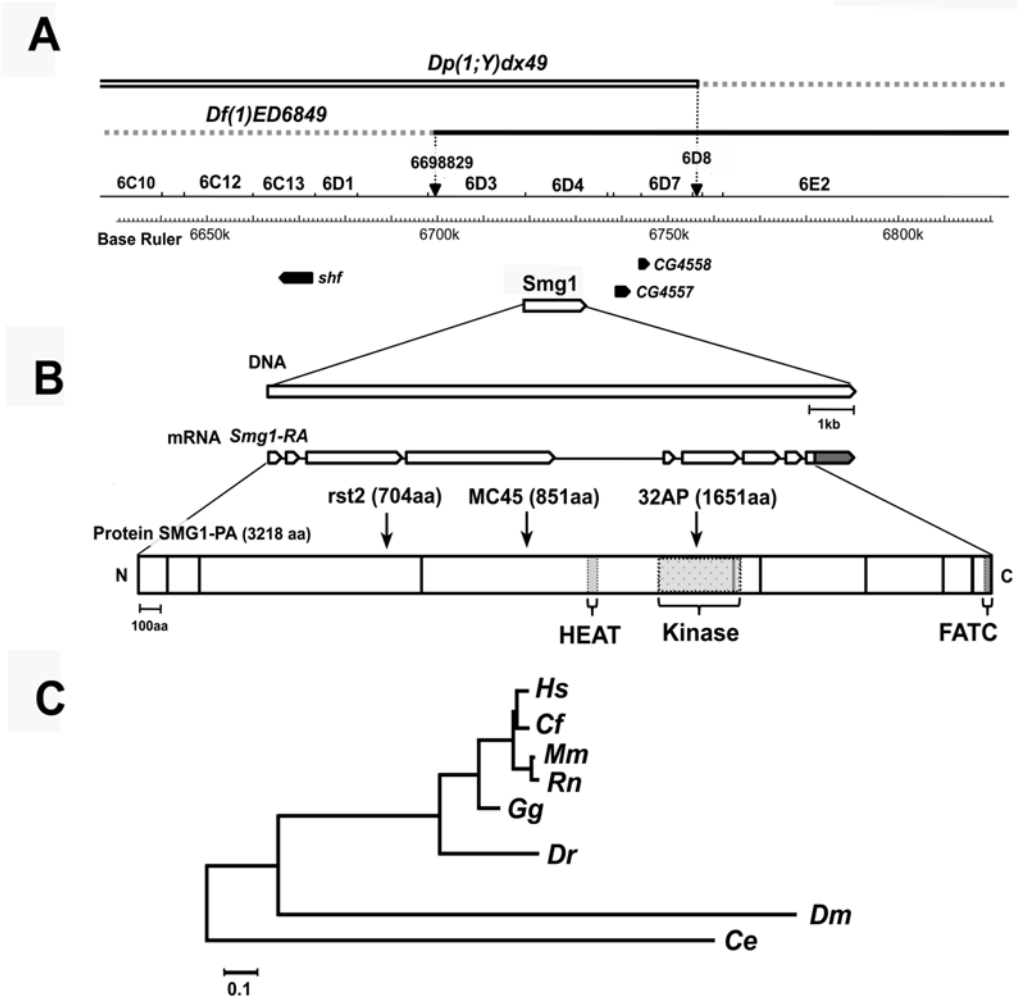
A
Dp(1;Y)dx49
Df(1)ED6849
6698829
6D8
6C10
6C12
6C13
6D1
6D3
6D4
6D7
6E2
Base Ruler
6650k
6700k
6750k
6800k
B
shf
Smg1
CG4558
CG4557
DNA
1kb
mRNA Smg1-RA
rst2 (704aa)
MC45 (851aa)
32AP (1651aa)
Protein SMG1-PA (3218 aa)
N
C
100aa
HEAT
Kinase
FATC
C
Hs
Cf
Mm
Rn
Gg
Dr
Dm
Ce
0.1

due to a point mutation in the *Smg1* kinase domain at amino acid 1651 (Metzstein and Krasnow, 2006) (Fig. 3.2B).

Validation of *Smg1* gene identification

Three approaches were used to test the validity of the *Smg1* gene identification: 1) assay of *Smg1* mRNA levels in *nonC* mutants by quantitativePCR, 2) transient induction of RNA interference (RNAi) by direct injection of double-stranded *Smg1* mRNA fragments, and 3) introduction of a wildtype *Smg1* genomic construct in *nonC* mutants to assess phenotype rescue. Results of quantitative real time PCR showed that the *Smg1* mRNA levels were reduced 20-50%, with greater loss in $nonC^{P37}$ vs. $nonC^{MC45}$. This allele dependence paralleled the relative severity of the ERG phenotype (Fig. 3.1). With the second validation approach, RNAi knockdown of Smg1 expression in wildtype accurately phenocopied *nonC* defects in synaptic transmission (see below). Thus, the first two approaches validate the identification of the Smg1 gene.

The most definitive proof of gene identity is to introduce the candidate wildtype gene into the mutant and assay rescue of mutant phenotype. We used a genomic Smg1 construct driven by the native promoter to ensure proper spatiotemporal expression. The Smg1 gene is ~13.6 kb and the predicted promoter region is ~3.2 kb, generating a sequence of nearly 17 kb and making the use of P-element mediated transformation questionable. We therefore utilized recombineering via the P[acman] vector (Venken *et al*., 2006) and ΦC31-mediated genome integration (Groth *et al*., 2004). Insertion of the genomic construct in multiple Smg1 mutant backgrounds was confirmed by PCR. Two copies of wildtype Smg1 completely rescued the *nonC* synaptic phenotype in adult visual system (Fig. 3.1) and larval neuromuscular junction (see below; Fig. 3.3) in both the $nonC^{P37}$ and $nonC^{MC45}$ mutant alleles. These results taken together strongly support the conclusion that nonC and Smg1 are the same gene. *Drosophila* Smg1 encodes phosphatidylinositol kinase-like

kinase (PIKK), with 34.1% protein sequence identity between CG32743 and human SMG1 (Fig. 3.2C) (Chen et al., 2005).

Smg1 maintains glutamatergic synapse function

The NMJ was utilized to systematically characterize Smg1 roles at the synapse. To first assess function, neurotransmission recordings were done on eight genotypes; an allelic series of four independent *Smg1* mutants, two transheterozygous mutant combinations, a wildtype control and a control of mutant containing the wildtype Smg1 genomic construct (rescue). Figure 3.3 shows representative EJC responses to single (Fig. 3.3A) and repetitive (Fig. 3.3B) nerve stimulation, and the quantified results on EJC amplitude (Fig. 3.3C) and fidelity (Fig. 3.3D).

With basal stimulation (0.5 Hz), control synapses exhibit robust, high fidelity transmission, whereas all *Smg1* mutants show a similar ~50% decrease in EJC amplitude (Fig. 3.3A), with significant loss of transmission fidelity (Fig. 3.3B). Controls display a mean EJC amplitude of 72.5 ± 4.1 nA and mutants exhibit mean amplitudes of 39.0 ± 7.1 nA ($Smg1^{nonCMC45}$), 41.2 ± 5.0 nA ($Smg1^{nonCP37}$), 38.4 ± 5.7 nA ($Smg1^{rst2}$) and 43.1 ± 4.9 nA ($Smg1^{32AP}$) (Fig. 3.3C). EJC amplitude in all mutants was significantly decreased compared to control ($p<0.003$; $n\geq8$ animals for each genotype), but did not differ significantly between mutant alleles ($p>0.5$). The heteroallelic mutant combination $Smg1^{nonCP37}/Smg1^{rst2}$ showed a similarly decreased EJC amplitude (38.4 ± 6.2 nA) compared to the heteroallelic $Smg1^{nonCP37}/+$ control (74.8 ± 4.5 nA; $p<0.003$). Wildtype Smg1 in the $Smg1^{nonCP37}$ homozygous background (rescue) restored EJC amplitude to slightly above control level (85.1 ± 7.5 nA; Fig. 3.3A-C). These results indicate that loss of Smg1 alone impairs basal synaptic transmission.

Figure 3.3. Loss of Smg1 impairs NMJ synaptic transmission. A) Representative excitatory junction current (EJC) records evoked by 0.5 Hz nerve stimulation in 0.5 mM external Ca^{2+} in wildtype control and *Smg1* mutant genotypes. The rescue condition is a wildtype Smg1 genomic construct in the $Smg1^{nonCP37}$ homozygous mutant background. Arrows indicate time of stimulation. **B)** Representative EJC trace families evoked by 10 repeated nerve stimuli at 0.5 Hz in control and *Smg1* mutant genotypes. **C)** Quantified mean EJC amplitudes for control, *Smg1* homozygous and transheterozygous mutants, and genomic rescue condition. **D)** Quantification of EJC amplitude variation from mean amplitude, as a measure of transmission fidelity. Significance comparisons between mutants and genomic rescue, and genomic rescue and wildtype control. Significance: p range 0.005 to 0.001 (***), p range 0.01 to 0.005 (**), p range 0.05 to 0.01 (*). Sample size: $n \geq 8$ animals for each genotype. Error bars indicate mean ± SEM.

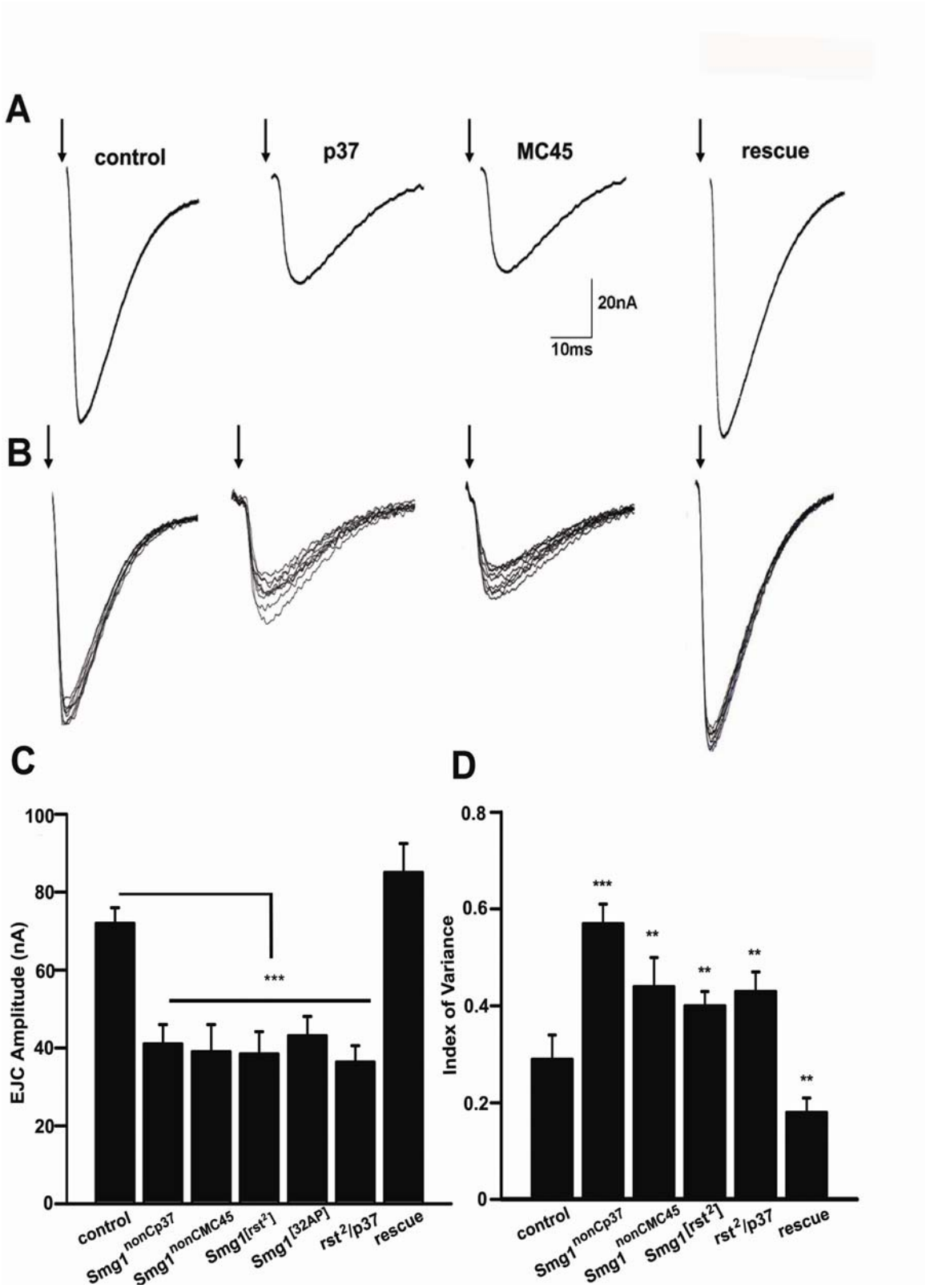
A
control
p37
MC45
rescue
20nA
10ms
B
C
EJC Amplitude (nA)
100
80
60
40
20
0
***
control
Smg1 nonCp37
Smg1 nonCMC45
Smg1[rst2]
Smg1[32AP]
rst2/p37
rescue
D
Index of Variance
0.8
0.6
0.4
0.2
0
***
**
**
**
**
control
Smg1 nonCp37
Smg1 nonCMC45
Smg1[rst2]
rst2/p37
rescue

Presynaptic or postsynaptic defects can impair neurotransmission. One method to differentiate mechanistic defects is to assay spontaneous synaptic vesicle fusion, or miniature EJC (mEJC) events, occurring in the absence of action potentials (Gatto and Broadie, 2008; Long et al. 2008; Trotta et al., 2004). In *Smg1* mutants, there were no detectable changes in mEJC amplitude or frequency compared to controls. The mean mEJC frequencies were: wildtype control, 1.07 ± 0.2 Hz; $Smg1^{nonCP37}$, 1.2 ± 0.3 Hz; $Smg1^{nonCMC45}$, 1.2 ± 0.3 Hz; $Smg1^{rst2}$, 1.1 ± 0.3 Hz; $Smg1^{32AP}$, 1.1 ± 0.3 Hz ($p>0.5$ in all cases; $n\geq8$ animals per genotype). These results suggest no significant alteration in the probability of spontaneous synaptic vesicle fusion at active zones. The mean mEJC amplitudes were: control, 0.7 ± 0.2 nA; $Smg1^{nonCP37}$, 0.8 ± 0.3 nA; $Smg1^{nonCMC45}$, 0.7 ± 0.2 nA; $Smg1^{rst2}$, 0.8 ± 0.3 nA; and $Smg1^{32AP}$, 0.7 ± 0.3 nA ($p>0.5$ in all cases; $n\geq8$ animals per genotype). These results suggest no significant change in glutamate receptor density or channel function at individual postsynaptic sites. Together these data suggest a specific impairment in evoked, Ca^{2+}-influx dependent presynaptic neurotransmitter release.

Consistent with presynaptic dysfunction, *Smg1* mutants display impaired transmission fidelity with repetitive stimulation (Fig. 3.3B). Amplitude variation was calculated by dividing the standard deviation by the mean EJC amplitude for each recording, and then averaging the variation values of animals within the same genotype. For mutants, these values were: $Smg1^{nonCP37}$ 0.57 ± 0.28 ($p<0.004$), $Smg1^{nonCMC45}$ 0.44 ± 0.27 ($p<0.03$) and $Smg1^{rst2}$, 0.41 ± 0.21 ($p<0.04$) compared to the genomic rescue line 0.18 ± 0.08 ($p<0.04$ compared to control; Fig. 3.3D; $n\geq8$ animals for each genotype). The $Smg1^{32AP}$ allele 0.33 ± 0.15 was significantly more variable compared to genomic rescue, but not wildtype ($p=0.4$)**.** For transheterozygote $Smg1^{nonCP37}/Smg1^{rst2}$, variance was calculated at 0.43 ± 0.04 compared to the transheterozygous control at 0.28 ± 0.15 ($p<0.04$). Taken together, these results indicate that loss of

Smg1 function impairs basal synaptic efficacy and reduces the fidelity of neurotransmission.

Smg1 protects morphological synapse development

Defective synapse function may be caused by perturbed development. We assayed NMJ structure using anti-HRP, a presynaptic membrane marker that reveals terminal area, branching pattern and bouton deposition. In parallel, we assayed key molecular components of the synapse, including anti-bruchpilot (NC82) in presynaptic active zones, and anti-discs large (DLG) and glutamate receptor subunit IIA (GluR) in the apposing postsynaptic domains. Two independent mutant alleles *Smg1*^{nonCP37} and *Smg1*^{nonCMC45}, and a third mutant transheterozygous condition, were compared to wildtype and genomic rescue controls at the muscle 6/7 NMJ in segment A3. The summarized results are shown in Figure 3.4.

Loss of Smg1 results in structurally under-elaborated NMJ with reduced terminal area, fewer synaptic branches and boutons, and a synapse generally confined closer to the muscle nerve entry site (Fig. 3.4A-C). Overall, mutant synaptic area was significantly reduced ($p<0.03$; $n\geq8$ animals for each genotype). Wildtype controls had a mean area of 2414 ± 210 μm^2 compared to 1502.8 ± 142 μm^2 in *Smg1*^{nonCP37} and 1607 ± 157 μm^2 in *Smg1*^{nonCMC45} (Fig. 3.4D). This growth defect could be effectively rescued with genomic *Smg1* (2561.0 ± 135.3 μm^2). The transheterozygous mutant *Smg1*^{nonCP37}/*Smg1*^{rst2} exhibited an area of 1524.8 ± 119.0 μm^2 compared to the transheterozygous control *Smg1*^{nonCP37}/+ of 2315.2 ± 172.1 μm^2. In parallel, there was a more highly significant ($p<0.003$; $n\geq8$ animals for each genotype) reduction in the number of synaptic terminal branches in mutants (Fig. 3.4E). A branch was defined as axonal arbor process having 2 or more clearly-defined boutons. Wildtype had an average of 12.2 ± 3.1 branches, approximately

Figure 3.4. Disruption of NMD leads to structurally underdeveloped NMJ synapses. Comparison of wandering 3rd instar NMJ structure and composition in wildtype (WT) control, two independent *Smg1* mutant alleles (*Smg1*^{nonCP37} (P37) and *Smg1*^{nonCMC45} (MC45)), a *Smg1* transheterozygous combination (rst2/p37), and with a wildtype *Smg1* genomic construct in the *Smg1*^{nonCP37} homozygous mutant background (rescue). **A-C)** Representative images of the muscle 6/7 NMJ in abdominal segment A3 probed with different synaptic markers. Higher magnification synaptic bouton images are shown on the right of each panel. **A)** Double labeling with the presynaptic neuronal membrane marker anti-horse radish peroxidase (HRP; red) and the presynaptic active zone protein anti-bruchpilot (NC82; green). **B)** Double labeling with postsynaptic anti-glutamate receptor subunit IIA (GluR; green) and HRP (red). **C)** Double labeling with the membrane associated synaptic scaffold anti-Discs Large (DLG; green) and HRP (red). Quantification of synaptic terminal area **(D)**, number of synaptic branches **(E)** and number of synaptic boutons **(F)**. Significance: p range 0.005 to 0.001 (***), p range 0.01 to 0.005 (**), p range 0.05 to 0.01 (*). Sample size: n≥8 animals for each genotype. Error bars indicate mean ± SEM.

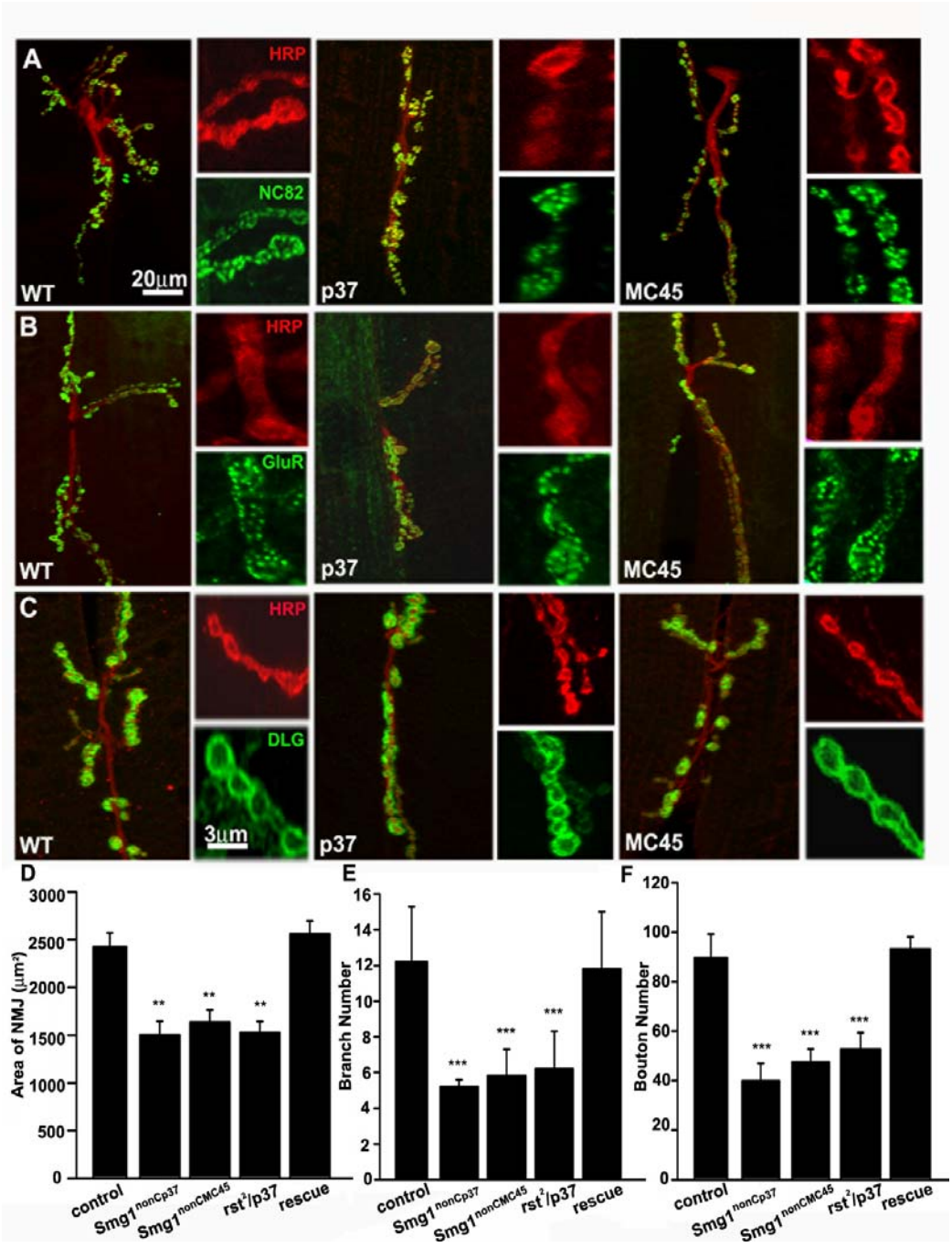
A
HRP
NC82
WT
20μm
p37
MC45
B
HRP
GluR
WT
p37
MC45
C
HRP
DLG
WT
3μm
p37
MC45
D
Area of NMJ (μm²)
3000
2500
2000
1500
1000
500
0
**
**
**
control
Smg1 nonCp37
Smg1 nonCMC45
rst²/p37
rescue
E
Branch Number
16
14
12
10
8
6
4
2
0
***
***
***
control
Smg1 nonCp37
Smg1 nonCMC45
rst²/p37
rescue
F
Bouton Number
120
100
80
60
40
20
0
***
***
***
control
Smg1 nonCp37
Smg1 nonCMC45
rst²/p37
rescue

twice as many compared to *Smg1*^{nonCP37} (5.2 ± 0.4), *Smg1*^{nonCMC45} (5.8 ± 1.5) and *Smg1*$^{rst2/p37}$ (6.2 ± 2.1) This phenotype could also be rescued with wildtype Smg1 (11.8 ± 3.2; Fig. 3.4E). Similarly, the number of synaptic boutons, defined as any clear axonal swelling >1µm in diameter, was significantly reduced in *Smg1* mutants (39.8 ± 7.1, *Smg1*^{nonCP37}; 47.5 ± 6.5, *Smg1*^{nonCMC45}; 52.6 ± 6.8, *Smg1*$^{rst2/p37}$) compared to controls (wildtype, 87.5 ± 11.8; rescue, 93.1 ± 4.9; $p<0.003$, $n\geq8$; Fig. 3.4F). Thus, loss of Smg1 causes impaired synaptic structural development.Synapse molecular components were next examined to determine whether individual synaptic bouton differentiation was compromised by the loss of NMD function. Fluorescence intensity and the number of fluorescent punctae was measured in muscle 6/7 NMJ boutons in both right and left bilateral A3 hemisegments, and then averaged to generate a single datapoint for each larvae. Eight animals were assayed in each of five genotypes. First, the presynaptic active zone protein Bruchpilot, labeled with anti-NC82, was used to examine synaptic vesicle release sites (Fig. 3.4A). Counting the number of anti-NC82 puncta within individual boutons revealed a noticeable but statistically insignificant reduction in *Smg1* mutants (*Smg*1^{nonCp37}, 84.7 ± 8.7; *Smg*1^{nonCMC45}, 79.3 ± 7.8; *Smg1*$^{rst2/p37}$ 89.5 ± 6.7) compared to wildtype (125.2 ± 11.7) and genomic rescue (119.3 ± 10.2) controls. Second, components of the postsynaptic domain were similarly analyzed, including glutamate receptors (GluRIIA; Fig. 3.4B) and membrane scaffold Discs Large (DLG; Fig. 3.4C). No significant changes were evident in either GluRIIA (control, 67.9 ± 1.2; *Smg1*^{nonCp37}, 62.8 ± 1.0; *Smg1*^{nonCMC45}, 58.2 ± 1.2; *Smg1*$^{nonCrst2/p37}$, 65.3 ± 1.3; genomic rescue, 70.5 ± 1.8) or DLG (control, 74.9 ± 5.8; *Smg1*^{nonCp37}, 63.8 ± 4.2; *Smg1*^{nonCMC45}, 71.6 ± 6.1; *Smg1*$^{rst2/p37}$, 59.7± 8.2; genomic rescue, 78.2 ± 9.1) fluorescence intensities (Figs. 3.4B,C). Together, these data show that Smg1 facilitates gross NMJ synaptic morphological development, but

is not detectibly required for maintenance of pre- and postsynaptic molecular specializations in individual boutons.

Smg1 facilitates the synaptic vesicle cycle

Smg1 mutant disruption of NMJ morphology might well be sufficient to explain impaired neurotransmission. The reduction in synaptic bouton number without strong compensation in individual boutons should cause functional impairment. However, synaptic structure and function are not well correlated, and indeed are separately regulated. Therefore, it was possible that other synaptic defects may occur when NMD function is disrupted. To test these possibilities, the NMJ was first examined by transmission electron microscopy. Representative synaptic bouton images and results are shown in Figure 3.5.

Quantified features included synaptic bouton cross-sectional area, mitochondria number/area, synaptic vesicle number/density, active zone number/density, number of clustered vesicles at active zones (<250 nm from t-bar), number of membrane docked vesicles at active zones (<20 nm, from t-bar), and the internal pool of internal synaptic vesicles (>250nm and <500nm from t-bar). Many of these features were indistinguishable between wildtype and *Smg1* mutants, but several changes were found. Bouton size was significantly larger in *Smg1* mutants ($Smg1^{nonCMC45}$ 5.4 ± 0.6 μm^2; $Smg1^{nonCP37}$ 5.3 ± 0.5 μm^2) compared to control (3.1 ± 0.2 μm^2) ($p<0.001$; n=57 control, 50 $Smg1^{nonCMC45}$ and 69 $Smg1^{nonCP37}$ boutons). Consistently, mutants contained significantly ($p=0.01$) more synaptic vesicles ($Smg1^{nonCMC45}$ 317 ± 22 vs. control 257 ± 14), although mean vesicle density was still significantly ($P<0.009$) reduced (e.g. $Smg1^{nonCMC45}$ 82 ± 7 vs. control 104 ± 6), owing to the enlarged bouton area (Fig. 3.5A). In addition, vesicle pool distributions were slightly altered in the absence of Smg1 function. The number of docked vesicles was significantly ($p<0.0001$) elevated in mutants (e.g. $Smg1^{nonCMC45}$, 2.5 ± 0.1) compared to wildtype (1.9 ± 0.1) (Fig. 3.5B, top). The number of active zone clustered

Figure 3.5. Disruption of NMD alters vesicle pool distribution in NMJ boutons. Transmission electron microscopy examination of wandering 3rd instar NMJ synaptic boutons in the wildtype control (WT) and two independent *Smg1* mutant alleles; $Smg1^{nonCP37}$ (P37) and $Smg1^{nonCMC45}$ (MC45). **A)** Representative whole-bouton profiles. Oriented on individual active zone t-bars (arrows), 250 nm and 500 nm semicircles were used to delineate synaptic vesicle (SV) distribution. Also labeled: subsynaptic reticulum (SSR) and mitochondria (M). Scale is 500nm as indicated. **B)** Quantification of SV pools in the three genotypes. Docked vesicles defined as <20 nm from the active zone t-bar. Clustered vesicles defined as <250 nm from the active zone t-bar. SVs between the two semicircles (250-500 nm) were classified as "internal synaptic vesicles". Significance: p range 0.005 to 0.001 (***), p range 0.01 to 0.005 (**), p range 0.05 to 0.01 (*). Sample sizes: n=8 animals, 57 boutons for control; n=7 animals, 69 boutons for $Smg1^{nonCP37}$; n=7 animals, 50 boutons for $Smg1^{nonCMC45}$. Error bars indicate mean ± SEM.

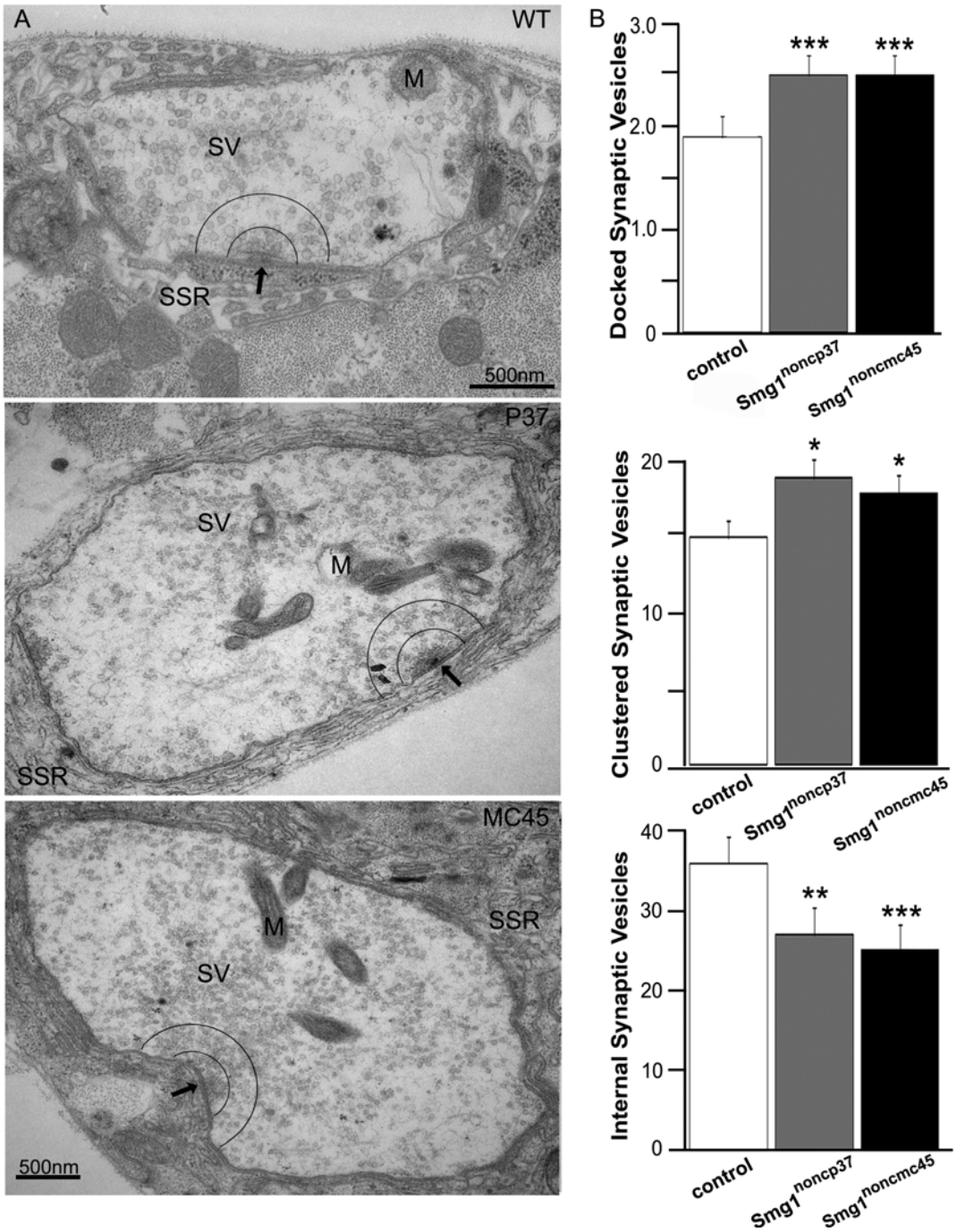
A
WT
M
SV
SSR
500nm
P37
SV
M
SSR
MC45
M
SSR
SV
500nm
B
Docked Synaptic Vesicles
3.0
2.0
1.0
0
***
***
control
Smg1noncp37
Smg1noncmc45
Clustered Synaptic Vesicles
20
10
0
*
*
control
Smg1noncp37
Smg1noncmc45
Internal Synaptic Vesicles
40
30
20
10
0
**
***
control
Smg1noncp37
Smg1noncmc45

vesicles was also significantly increased (P<0.04) in mutants (e.g. *Smg1*^{nonCP37}, 19.0 ± 1.7) compared to control (15.0 ± 1.3) (Fig. 3.5B, middle). In contrast, there was a highly significant (p<0.0001) reduction in the number of internal synaptic vesicles in mutants (e.g. *Smg1*^{nonCMC45}, 25.2 ± 2.0) compared to control (36.0 ± 2.0) (Fig. 3.5B, bottom). Thus, Smg1 is involved in regulating the trafficking underlying synaptic vesicle pools.To investigate synaptic vesicle pool size and cycling dynamics, the lipophilic fluorescent dye FM1-43 was used to image vesicular turnover (Fig. 3.6). Acutely dissected NMJ preparations were exposed to FM1-43 (10 mM) during a 1 minute 20 Hz stimulation of the motor nerve. Preparations were then washed in Ca^{2+}-free saline to halt vesicle cycling and remove external dye, and then imaged to visualize dye uptake (Fig. 3.6A). The *Smg1* mutants were clearly impaired in synaptic vesicle cycling rate compared to controls, with immediately obvious reduced dye incorporation. Mean fluorescent intensities were quantified within individual boutons averaged in n≥8 animals for each genotype (Fig. 3.6B). Wildtype boutons had a mean fluorescent intensity of 130.87 ± 13.6, compared to 45.07 ± 7.8 in *Smg1*^{nonCP37} and 49.9 ± 16.6 in *Smg1*^{nonCMC45}. The transheterozygous mutant *Smg1*^{nonCP37}/*Smg1*^{rst2} exhibited an intensity of 42.5 ± 14.1 compared to the transheterozygous control *Smg1*^{nonCP37}/+ of 118.3 ± 8.7. The mutant decreases were all highly significant (p<0.003) compared to controls. Introduction of wildtype Smg1 resulted in an elevated level of dye loading (145.0 ± 23.2), not significantly different from wildtype (Fig. 3.6B).

The fluorescent FM1-43 signal was photoconverted to an electron-dense signal for EM comparisons (Vijayakrishnan et al., 2009). The converted signal was clearly detected at the light microscopy level to again reveal impaired FM dye loading in *Smg1* mutants (Fig. 7A; compare

Figure 3.6. Loss of Smg1 impairs FM1-43 dye loading in the synaptic vesicle cycle. Confocal lipophyllic FM1-43 dye imaging of the synaptic vesicle cycle at the wandering 3rd instar NMJ in control, two independent *Smg1* mutant alleles (*Smg1*^{nonCP37} (P37) and *Smg1*^{nonCMC45} (MC45)), a transheterozygous mutant combination (rst2/p37), and with a wildtype *Smg1* genomic construct in the *Smg1*^{nonCP37} homozygous mutant background (rescue). **A)** Representative images of NMJ synaptic boutons loaded by a 1 minute, 20 Hz stimulation of the motor nerve. **B)** Quantification of FM1-43 dye loading. Significance: p range 0.005 to 0.001 (***). Sample size: n≥8 animals for each of the 5 indicated genotypes. Error bars indicate mean ± SEM.

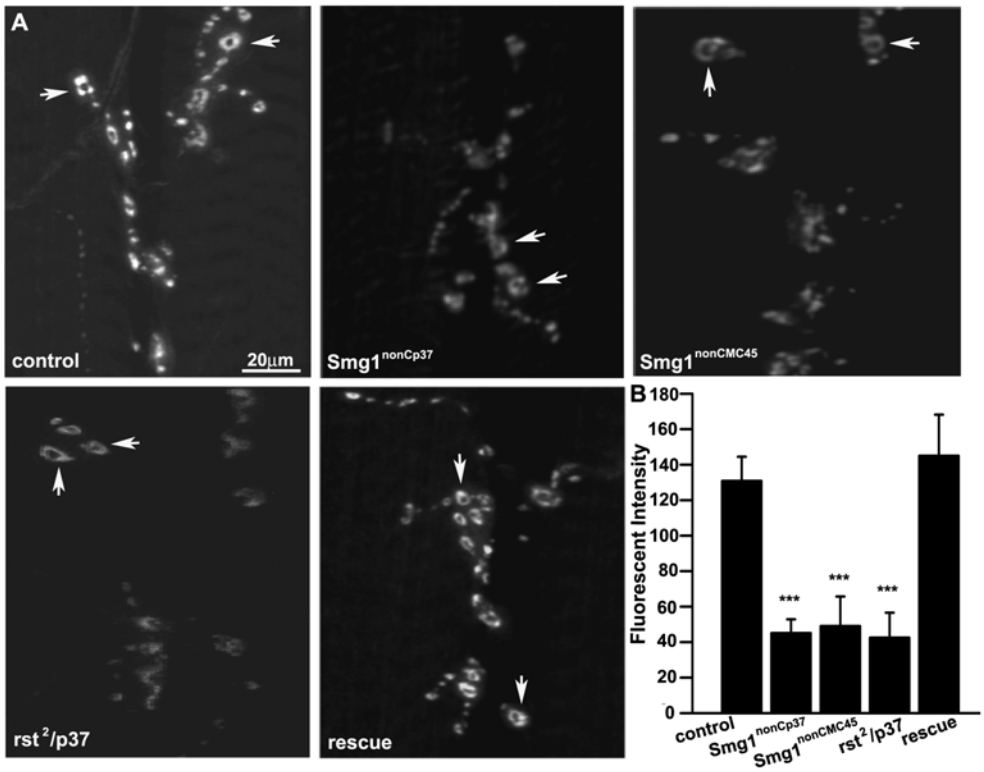
A
control
20μm
Smg1 nonCp37
Smg1 nonCMC45
rst 2/p37
rescue
B
Fluorescent Intensity
180
160
140
120
100
80
60
40
20
0
***
***
***
control
Smg1 nonCp37
Smg1 nonCMC45
rst 2/p37
rescue

to Fig. 3.6A). At EM level, control boutons load dye much more readily within synaptic vesicles, filling the majority of vesicles in any given terminal under these conditions (Fig. 3.7B). In sharp contrast, mutant boutons contained relatively few labeled vesicles. Loading was quantified by counting the number of electron-dense vesicles per bouton cross-section. Controls exhibited an average of 172.0 ± 23.4 loaded vesicles compared to 35.3 ± 3.4 in *Smg1*^{nonCMC45} ($p<0.002$; sample size is 57 boutons for control, and 55 boutons for *Smg1*^{nonCMC45}; Fig. 3.7C). Together, these results show impaired *Smg1* presynaptic function at the level of single synaptic boutons.

Smg1 maintains high frequency transmission

The reduced population of cycling synaptic vesicles in *Smg1* mutants predicts a more severe reduction in mutant synaptic transmission amplitude than documented above (see Fig. 3.3). A likely explanation was that the high frequency stimulation (HFS) required for the FM1-43 dye loading experiments was revealing a greater level of functional impairment under conditions of elevated use. To test this hypothesis, the same 20 Hz HFS paradigm was employed in physiological recordings (Fig. 3.8). Following basal EJC stimulation at 0.2 Hz for 50 seconds (10 stimuli), EJC amplitudes were assessed during a 60 second 20 Hz HFS train (1200 stimuli), followed by a 50 seconds post-HFS recovery at 0.2 Hz stimulation (10 stimuli). Figure 3.8 shows representative EJC responses (Fig. 3.8A) and normalized EJC amplitude results (Fig. 3.8B).

At 0.5 mM external [Ca^{2+}], wildtype NMJs maintain a nearly constant level of transmission, showing no significant tendency to facilitate or fatigue (Fig. 3.8A, top; Fig. 3.8B). Transheterozygote controls (e.g. *Smg1*^{nonCP37}/+) were indistinguishable from wildtype, similarly maintaining normalized values near 1.0 and never decaying below 0.94 of basal

Figure 3.7. FM1-43 photoconversion reveals ultrastructural dye uptake impairment. A) Representative muscle 6/7 NMJ images of the wildtype control and *Smg1*^{nonCMC45} (MC45) mutant embedded *en bloc*, following photoconversion of the fluorescent FM1-43 signal to an electron-dense signal suitable for transmission electron microscopy imaging (see Methods). **B)** Representative transmission electron microscopy images of control (left) and *Smg1*^{nonCMC45} (right) photoconverted boutons. Note the localization of the electron-dense tracer (black) within individual synaptic vesicles**. C)** Quantification of the number of electron-dense, photoconverted synaptic vesicles in bouton cross-sectional profiles. Significance: p range 0.005 to 0.001 (***). Sample size: n=32 boutons (control), n=35 boutons (*Smg1*^{nonCMC45}). Error bars indicate mean ± SEM.

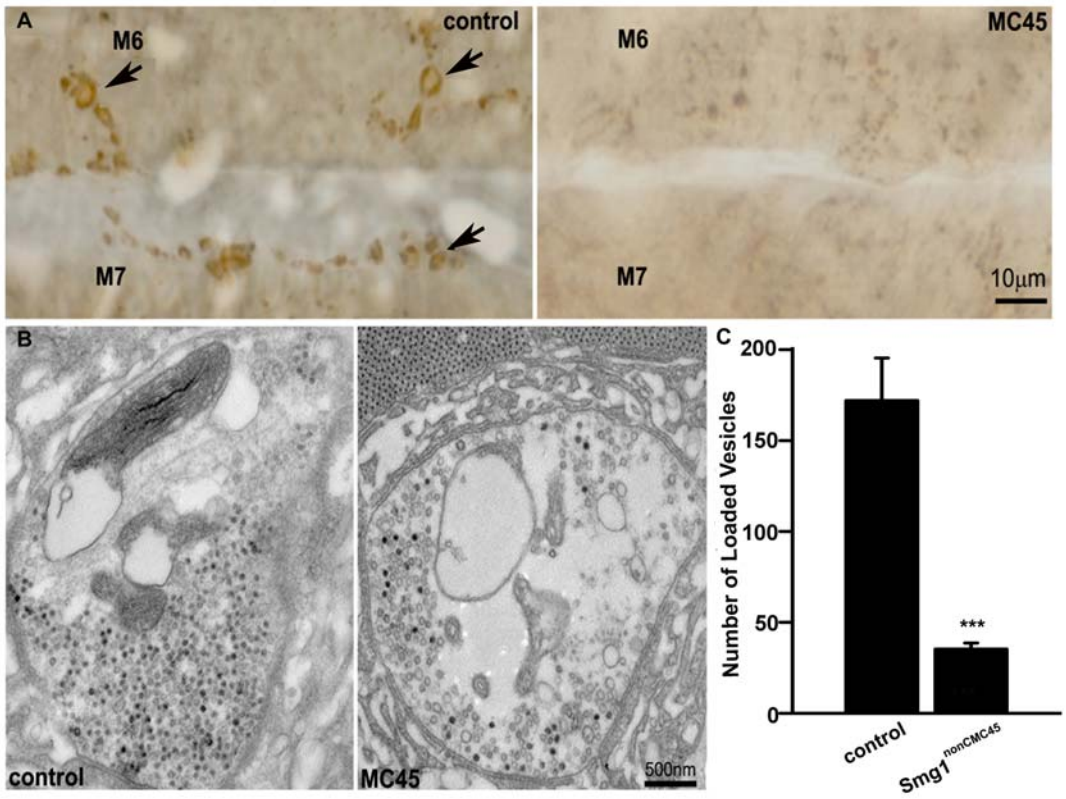
A
M6
control
M7
M6
MC45
M7
10μm
B
control
MC45
500nm
C
Number of Loaded Vesicles
200
150
100
50
0
***
control
Smg1 nonCMC45

values. In contrast, *Smg1* homozygous and transheterozygous mutants start out impaired by ~50% (see Fig. 3.3) and then experience further significant fatigue during the HFS train (Fig. 3.8A, bottom). Initially, normalized EJC amplitudes demonstrate a small amount of facilitation (<15 seconds), but this facilitation was not maintained (Fig. 3.8B). However, from ~20 seconds, *Smg1* mutants show an overall steady decline in transmission amplitudes for the remainder of the stimulus train (Fig. 3.8B). Upon return to basal (0.2 Hz) stimulation the *Smg1* mutant EJC amplitudes gradually recover towards their initial basal, with a timecourse mirroring (30-40s) the rate of fatigue during the HFS train (data not shown). Thus, under the same conditions used for FM1-43 dye loading, functional transmission in *Smg1* was reduced to ~20% of control levels.We next examined synaptic ultrastructure with the HFS train (20 Hz, 1 min). Figure 8C shows representative active zone images from wildtype control and *Smg1*^{nonCMC45} mutant with no stimulation (rest) and with HFS (stim). Synaptic vesicle and membrane trafficking parameters were quantified (n=21 wildtype control boutons, and n=20 *Smg1*^{nonCMC45} boutons) with remarkably different consequences in *Smg1* mutants compared to control. In regards to bouton size, HFS increased mean area from 3.1 ± 0.2 μm^2 to 4.8 ± 0.6 μm^2 in control, but rather decreased area from 5.4 ± 0.6 μm^2 to 3.8 ± 0.4 μm^2 in the *Smg1* mutant ($p>0.01$; Fig. 3.8D). While control boutons showed no significant change in the number of enlarged (>60 nm) membrane cisternae (mean 3.7 ± 1.4 following HFS), stimulated mutant boutons showed a highly significant elevation of these trafficking organelles (mean 6.3 ± 1.2; $p>0.01$; Fig. 3.8E). In regards to vesicle pools, the total synaptic vesicle number following HFS for controls was 248 ± 30 compared to 179 ± 18 in the mutant ($p>0.05$), but with no significant difference remaining in vesicle density ($p=0.3$). Stimulated wildtype controls maintained both the active zone clustered and membrane docked pools (Fig. 3.8F,G). In contrast, stimulated

Figure 3.8. Loss of Smg1 compromises high frequency transmission maintenance. Electrophysiological and ultrastructural analyses of NMJs during high frequency stimulation (HFS) of 20 Hz for 1 minute. **A)** Representative wildtype control (top) and *Smg1*^{nonCMC45} mutant EJC traces (bottom) at 0, 15, 30, and 60 sec time points during the HFS train. **B)** Quantification of EJC amplitudes during the HFS train, including the *Smg1* transheterozygous condition (rst2/p37) and the wildtype Smg1 genomic construct in the *Smg1*^{nonCMC45} homozygous mutant background (rescue). EJC amplitudes are shown at 5 sec intervals normalized to the mean EJC amplitude under basal (0.02 Hz) stimulation for each genotype. Sample size of n≥7 animals per genotype. **C)** Representative images of the active zone t-bar region in a resting terminal (rest) and with HFS (stim) in control and mutant. Arrows indicated SVs docked at active zones and arrowheads indicate cisternae (>60 nm). Quantification of synaptic bouton area **(D)**, trafficking cisternae **(E)**, clustered SVs <250 nm from the active zone t-bar **(F)** and docked SVs <20 nm from the active zone t-bar **(G)** in the resting and stimulated condition for each genotype. Significance: p range 0.005 to 0.001 (***), p range 0.01 to 0.005 (**), p range 0.05 to 0.01 (*). Sample sizes: 21 boutons for wildtype control and 20 boutons for *Smg1*^{nonCMC45}. Error bars indicate mean ± SEM.

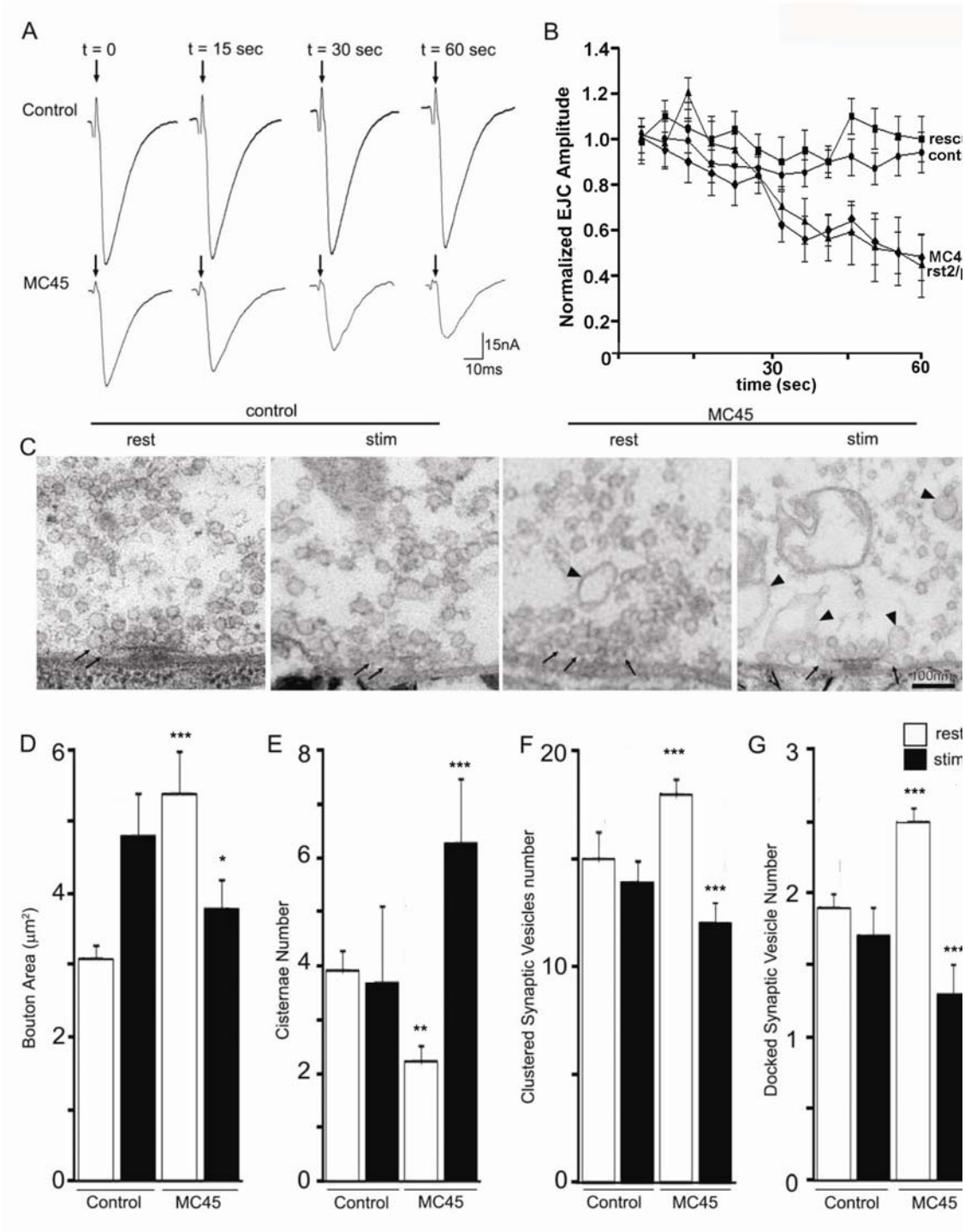
A
t = 0
t = 15 sec
t = 30 sec
t = 60 sec
Control
MC45
15nA
10ms
B
Normalized EJC Amplitude
time (sec)
control
MC45
rest
stim
rest
stim
C
100nm
D
Bouton Area (μm²)
Control
MC45
E
Cisternae Number
Control
MC45
F
Clustered Synaptic Vesicles number
Control
MC45
G
Docked Synaptic Vesicle Number
Control
MC45

Smg1^{nonCMC45} mutants showed a highly significant loss of clustered vesicles (from 12.0 ± 1.0 with HFS vs. 18.0 ± 0.8 at rest), resulting in a significantly (P>0.05) smaller pool compared to stimulated control. Similarly, *Smg1*^{nonCMC45} mutants lost docked vesicles from 2.5 ± 0.1 per active zone at rest to 1.3 ± 0.2 in the stimulated condition (Fig. 3.8G). Together, these data show that loss of Smg1 prevents the synaptic vesicle cycle from maintaining the rate required during periods of high frequency transmission demands.

The NMD pathway maintains synaptic function

Smg1 acts as a regulative kinase that triggers the formation of the mRNA surveillance complex during NMD. The above impairments were therefore hypothesized to result from loss of this NMD mechanism. However, it was possible that Smg1 may act independently of NMD in some unique role. In order to determine whether Smg1 acts as part of the NMD pathway, independent mutations in other components of the Smg complex were assayed. The *Upf2* (*Smg3*) mutant was isolated in a genetic mosaic screen of EMS–induced mutations. The *Upf2*^{25G} allele acts as a genetic null that abrogates NMD (M.M. Metzstein, unpublished data). The *Smg6* mutant was isolated in a genetic screen for mutations affecting NMD using an NMD-sensitive reporter construct. The *Smg6*^{292} allele acts as a genetic null with greatly reduced NMD activity (M.M. Metzstein, unpublished data). Figure 9 shows synaptic functional assays in these two mutants with both TEVC electrophysiology and FM1-43 dye imaging.

Evoked neurotransmission was assayed with 0.5 Hz nerve stimulation in 0.5 mM Ca^{2+} external saline (Fig. 3.9). Representative EJC traces for the wildtype control and the two null mutants are shown in Figure 3.9A. The controls displayed a mean EJC amplitude of 75.2 ± 7.89 nA, whereas *Upf2/Smg3* mutants exhibited average amplitudes of 36.1 ± 4.78 nA and *Smg6* mutants had average amplitudes of 41.3 ± 5.98 nA (p<0.004; n=8 animals for all 3 genotypes; Fig. 9B). The severity of the

Figure 3.9. The NMD pathway maintains synaptic transmission properties. Functional analyses of *Upf2* (*Smg3*) and *Smg6* mutants at the larval NMJ synapse using TEVC electrophysiology and FM1-43 dye imaging. **A)** Representative EJC records from 0.5 Hz basal stimulation in the wildtype control (WT) (left) and the two mutants, *Upf2/Smg3* (center) and *Smg6* (right). **B)** Quantifications of mean EJC amplitudes. Significance: p range 0.005 to 0.001 (***). Sample size: n $\geq$ 7 animals for each of the 3 genotypes. **C)** Representative FM1-43 dye loaded image in each genotype. The nerve was stimulated at 20 Hz for 1 minute. **D)** The plot shows quantified mean loading fluorescence intensities. Significance: p range 0.005 to 0.001 (***). Sample size: n$\geq$8 animals for each of the 3 genotypes. Error bars indicate mean ± SEM.

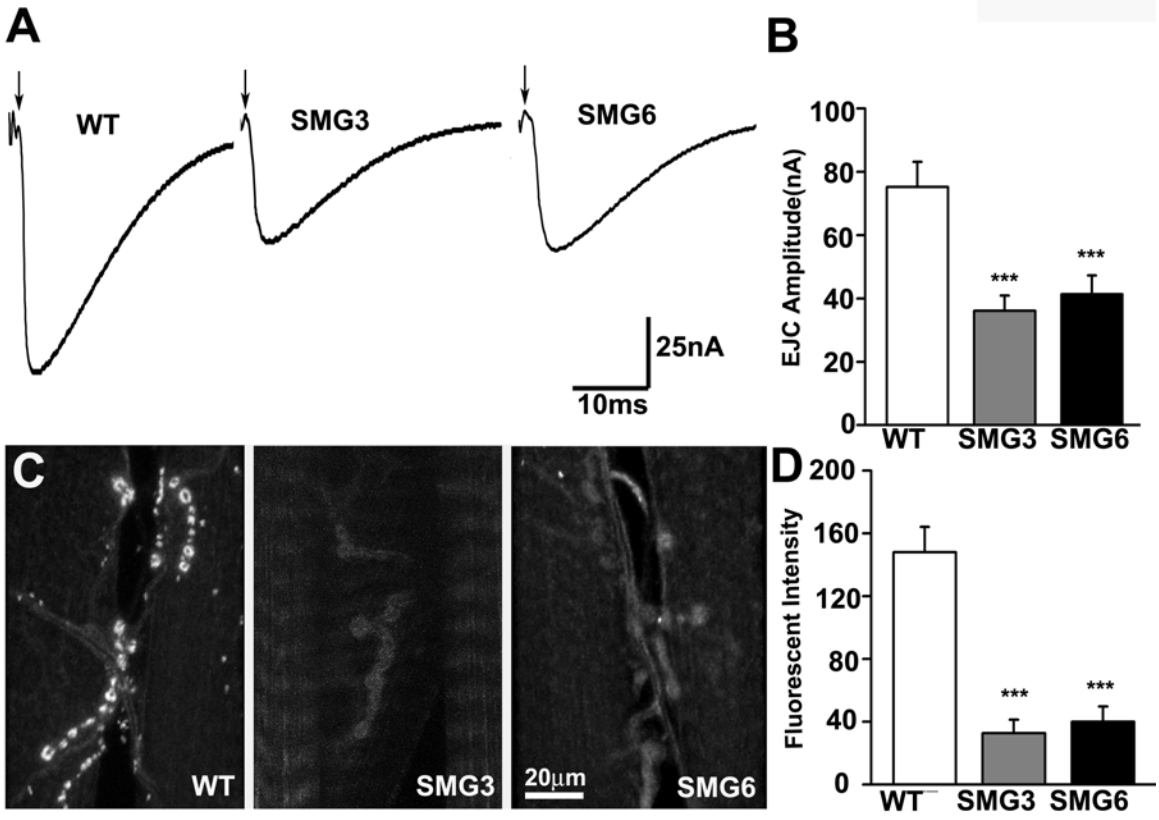
A
WT
SMG3
SMG6
25nA
10ms
B
EJC Amplitude(nA)
100
80
60
40
20
0
***
***
WT
SMG3
SMG6
C
WT
SMG3
20μm
SMG6
D
Fluorescent Intensity
200
160
120
80
40
0
***
***
WT
SMG3
SMG6

for both of these NMD pathway components was comparable to the *Smg1* mutants (see Fig. 3.3), indicating that NMD has an important role in the regulation of synaptic function, and that loss of Smg1 is equivalent to loss of NMD function in this requirement.The synaptic vesicle cycle was next assayed by FM1-43 dye incorporation following 20 Hz, 1 minute stimulation of the motor nerve in 0.5 mM Ca^{2+} saline. Representative NMJ images of the wildtype control and the two null mutants are shown in Figure 3.9C. The control loaded much more dye than either NMD pathway mutant, with a qualitatively clear difference in fluorescence intensity. Controls showed a mean fluorescent intensity of 148.1 ± 16.17 compared to *Upf2/Smg3* mutants at 32.8 ± 8.51 and *Smg6* mutants at 39.9 ± 9.68 (both $p<0.002$ compared to control; n=8 animals per genotype; Fig. 3.9D). These defects are similar too, albeit slightly more severe than, *Smg1* mutant phenotypes (compare to Fig. 3.6). Taken together, these data suggest that Smg1 operates in the same mechanism as *Upf2/Smg3* and *Smg6*, and therefore that the NMD pathway plays a critical role in the functional differentiation of the synapse.

Discussion

As part of a long-term, unbiased, forward genetic screen for synaptic dysfunction mutants in the *Drosophila* visual system, we have identified novel mutants in the phosphatidylinositol 3-kinase-like kinase (PIKK) Smg1, a key regulatory kinase in the nonsense mediated decay (NMD) pathway. NMD is an mRNA surveillance system critical to the maintenance of transcript integrity. The Smg proteins (Smg1-7) act together to degrade mRNA transcripts containing nonsense mutations that would produce truncated proteins with potentially deleterious activities. This study reveals that Smg1 functions to protect the development of synaptic morphological architecture and maintain high fidelity neurotransmission function, especially under conditions of heightened activity. Among isolated *Smg* mutants, only *Smg1* nulls are adult viable;

Smg5 mutants die as first instars, and *Upf2/Smg3* and *Smg6* die as pupae. These lethal periods have restricted our adult analyses to *Smg1* mutants, and our larval analyses to *Smg1*, *Smg3* and *Smg6* mutants, and may indicate that *Smg1* is less essential for NMD compared to the other complex components. Together, our studies indicate that NMD activity is required in at least two disparate synaptic classes, retinal photoreceptor synapses and neuromuscular junction, suggesting that a NMD-mediated protective mechanism is broadly important in synapses throughout the nervous system.

We and others have exerted a great deal of effort exploring the roles of mRNA regulation in synaptic mechanisms (Antar and Bassell, 2003; Gatto and Broadie, 2009; Pfeiffer and Huber, 2009; Tessier and Broadie, 2009; Yan et al., 2009). In particular, mechanisms of mRNA stabilization, trafficking, RISC-mediated degradation and localized translation have all been recently determined to occur in proximity to synapses, and/or with important roles in synapse regulation (Giorgi et al., 2007; Hengst and Jaffrey, 2007; Lin and Holt, 2007; Sebeo, et al., 2009; Yan et al., 2009;). These insights have raised the question of possible NMD involvement (Giorgi et al, 2007). In this study, we report that disruption of NMD-mediated mRNA regulation results in impaired morphological NMJ development, loss of functional transmission at central (histaminergic) synapses and peripheral (glutamatergic) synapses, and impaired synaptic vesicle cycling at the NMJ, especially under conditions of elevated demand. These results indicate that NMD plays an important role in maintaining synapse architecture and high fidelity synaptic efficacy.

NMD maintains synapse architecture: axon branching and bouton development

Synaptic morphological defects can be readily observed with the loss of appropriate mRNA regulation of synaptic components. This requirement has been characterized for a number of mRNA-binding

proteins, prominently including the fragile X mental retardation protein (FMRP) (Gatto and Broadie, 2008; Pan and Broadie, 2007; Pan et al., 2008; Tessier and Broadie, 2008; Tessier and Broadie, 2009). Here we show that loss of mRNA regulation via disruption of the NMD pathway also impairs synaptic architecture at the well-characterized *Drosophila* NMJ. In *Smg1* mutants, NMJ synaptic arbors appear underdeveloped and underelaborated, with limited differentiation outside the immediate vicinity of the initial point of muscle innervation. The range of morphological phenotypes includes overall reduction in synaptic terminal area, decrease in synaptic arbor branching by ~50% and decrease in synaptic bouton number by ~50%.

NMD mutant defects are presumably caused by the production of truncated proteins with dominant negative or deleterious gain of function activities that damage the machinery of synaptic development. Our model is that *Smg* mutants are unable to prevent translation of damaged transcripts, and thus the production of “toxic proteins” result in smaller, less developed and functionally compromised synapses. Where and when the NMD machinery performs this essential activity is uncertain; it could be wholly in the neuronal soma, or locally at synapses for transcripts that may undergo local translation. We note, however, that the *Smg1* mutant defects revealed here appear largely restricted to the presynaptic domain; postsynaptic scaffolding and glutamate receptor expression is not detectably altered, and there is no detectable change in postsynaptic physiological function (DiAntonio et al., 1999). Local mRNA translation in growth cones has been demonstrated to be critical for axon pathfinding and synapse maturation (Brittis et al., 2002; Hu et al., 2002; Hu et al., 2004, Lin and Holt, 2008; Sebeo, et al., 2009; Yan et al., 2009). The defects reported here could occur in the motor neuron growth cone or during later stages of synaptic maturation.

NMD maintains synaptic efficacy: the endo-exo vesicle cycling pool

The cyclic events that orchestrate the release of neurotransmitter at the synapse consist of a rapidly repeating series of vesicular trafficking, exocytosis and endocytosis steps. There are many molecular stages in this pathway susceptible to disruption, which when impaired cause similar outcome defects in vesicle cycling. Consistent with a protective mechanism for the NMD pathway in this mechanism, experimental introduction of peptide fragments of synaptic vesicle cycle proteins is a well established means of investigating molecular requirements (Gitler et al., 2008; Gitler et al., 2004; Hilfiker et al., 2005; Morgan et al., 2003). The multiple *Smg* gene mutants analyzed here all show profound disruptions in the endocytosis phase of the synaptic vesicle cycle, revealing an impairment in the ability to retrieve vesicular membrane and associated proteins from the plasma membrane after vesicle fusion. Moreover, disruption of the NMD pathway causes a significantly reduced functional readily releasable pool of vesicles, although the morphological releasable pool appears relatively intact in *Smg1* mutants after periods of both basal and intense synaptic activity. This suggests that the loss of neurotransmission in *Smg* mutants is due not only to impaired vesicle biogenesis, but perhaps also to the interruption of molecular functions underlying evoked vesicle exocytosis.

A long list of proteins have demonstrated roles in synaptic vesicle endocytosis and exocytosis (Owald and Sigrist, 2009; Sudhof, 2000; Sudhof, 2004; Sudhof and Rothman, 2009). Loss of NMD likely generates “toxic protein fragments” that interfere with many of these proteins, both individually and by preventing the formation of presynaptic molecular complexes. One of the predicted consequences of such fragmentary proteins is to act by interfering with (or out-competing) appropriate protein-protein interactions during complex formation. The *Smg* mutants show a more severe impairment of presynaptic function under conditions of high frequency stimulation. During such periods of elevated demand, the stress

placed on the synaptic vesicle machinery is obviously greater, demanding that proteins function more rapidly and that molecular complexes form and function at a faster rate. Our model predicts that mutant proteins produced in the absence of the NMD pathway would therefore have a greater deleterious impact under conditions of high frequency stimulation. The inhibition caused by truncated synaptic vesicle proteins presumably accounts for the very small amount of vesicle cycling evident at the *Smg* mutant synapse during high demand.

CHAPTER IV
SUMMARY AND FUTURE DIRECTIONS

In addition to the work presented in Chapters II and III, I have also characterized two additional synaptic vesicle cycle mutants in *Drosophila*, dTRPML and dRich. One of these studies is published (see Venkatachalam et al. 2008, in Cell), and the other is currently still under review. This work is summarized here, with the accompanying figures showing my contributions to both of these projects.

A *Drosophila* model of a mucolipidosis type IV

Disruption of the transient receptor potential (TRP) mucolipin 1 (TRPML) channel results in the neurodegenerative disorder mucolipidosis type IV (MLIV), a lysosomal storage disease with severe motor impairments (Bach, 2005; Venkatachalam and Montell, 2007). The mechanisms underlying MLIV are poorly understood and there is currently no treatment. In collaboration with Craig Montell's lab at Johns Hopkins University, I characterized a *Drosophila* MLIV model by providing electrophysiological analysis and FM1-43 vesicle cycle assays at the NMJ. This MLIV disease model recapitulates the key disease features, including abnormal intracellular accumuluation of macromolecules, and motor defects. The basis for the build up of macromoleculaes appears to be defective autophagy, which we proposed results in oxidative stress and impaired synaptic transmission (Figure 4.1).

We first noticed that the *trpml*^{1} flies remained immobilized longer than wild-type after exposure to CO_2 anesthesia. After four minutes, 90.7±9.3% of wild-type recovered mobility, in contrast to only 6.7±3.3% of *trpml*^{1}. The return of activity of all *trpml*^{1} flies required 9 minutes, twice as long as for wild-type (Figure 4.1). Since CO_2 immobilizes flies through inhibition of synaptic transmission at the NMJ (Badre et al., 2005), we tested whether there was a decrease in synaptic transmission in *trpml*^{1}.

To assess synaptic function, I made evoked excitatory junction current (EJC) recordings at the NMJ synapse of 3rd instar larvae, using the two-electrode voltage-clamp (TEVC) configuration. To reveal changes in basal synaptic function, we performed assays in a bath solution containing 0.5 mM extracellular [Ca^{2+}] (Rohrbough et al., 1999; Trotta et al., 2004; Long et al., 2008). Control animals exhibited a mean EJC amplitude of 64.1±5.2 nA, while *trpml*^{1} showed a ~50% decrease in transmission strength (32.3±4.6 nA).

To investigate whether the reduction in synaptic transmission was due to an alteration in the size or cycling of the endo-exo pool, I used the lipophilic fluorescent dye FM1-43 to assay endocytosis and exocytosis (Kuromi and Kidokoro, 2000; Fergestad and Broadie, 2001; Trotta et al., 2004; Long et al., 2008). I exposed NMJ preparations to FM1-43 in the presence of 90 mM [K^{+}] saline, which depolarized the nerve terminal and induced vesicular cycling and loading of FM1-43. I then depolarized the preparations in the absence of FM1-43 to assess dye unloading by SV exocytosis. Based on comparison of the initial mean fluorescence values, *trpml* mutant synaptic boutons displayed a four-fold decrease in loading (wild-type, 187.3±9.3; *trpml*^{1}, 48.2±3.2). This lower level of loading was sufficient to assess whether the loaded boutons in *trpml*^{1} unloaded properly. Following the second depolarization, the wild-type boutons displayed a >90% reduction in fluorescence (unloading), whereas the *trpml*^{1} mutants showed little decrease; wild-type, 29.2±3.5; *trpml*^{1}, 39.3±3.6). These data indicate that the diminished synaptic transmission in *trpml*^{1} was due to presynaptic impairment of SV cycling.

These results raise the possibility that a combination of neurodegeneration and loss of NMJ synaptic transmission accounts for diminished motor activity in MLIV patients. It will be of interest in future studies to determine if the impaired synaptic transmission in *trpml* is an indirect consequence of unhealthy neurons, or if the trpml protein is also

Figure 4.1. NMJ Deficits in *Drosophila* model of MLIV. A) Time-course of flies with restored mobility following a 3 min exposure to CO_2. n=3, 10 flies per experiment. (B) Representiive excitatory junctional current (EJC) from the 3rd instar NMJ. (C) Quantification of the EJC amplitudes in wt and trpml1. n=5 animals; 10 NMJs for each genotype; *, p≤0.001. (D) NMJ synapses following FM1-43 loading and unloading. Arrows indicate synaptic boutons. Panels below show enlarged magnification of synaptic boutons. (E) Quantification of FM1-43 fluorescence intensity in NMJ boutons following dye loading and unloading. n=5 animals, 10 NMJs for each genotype; *, difference from wt, p≤0.001.All statistical analyses, t-test.

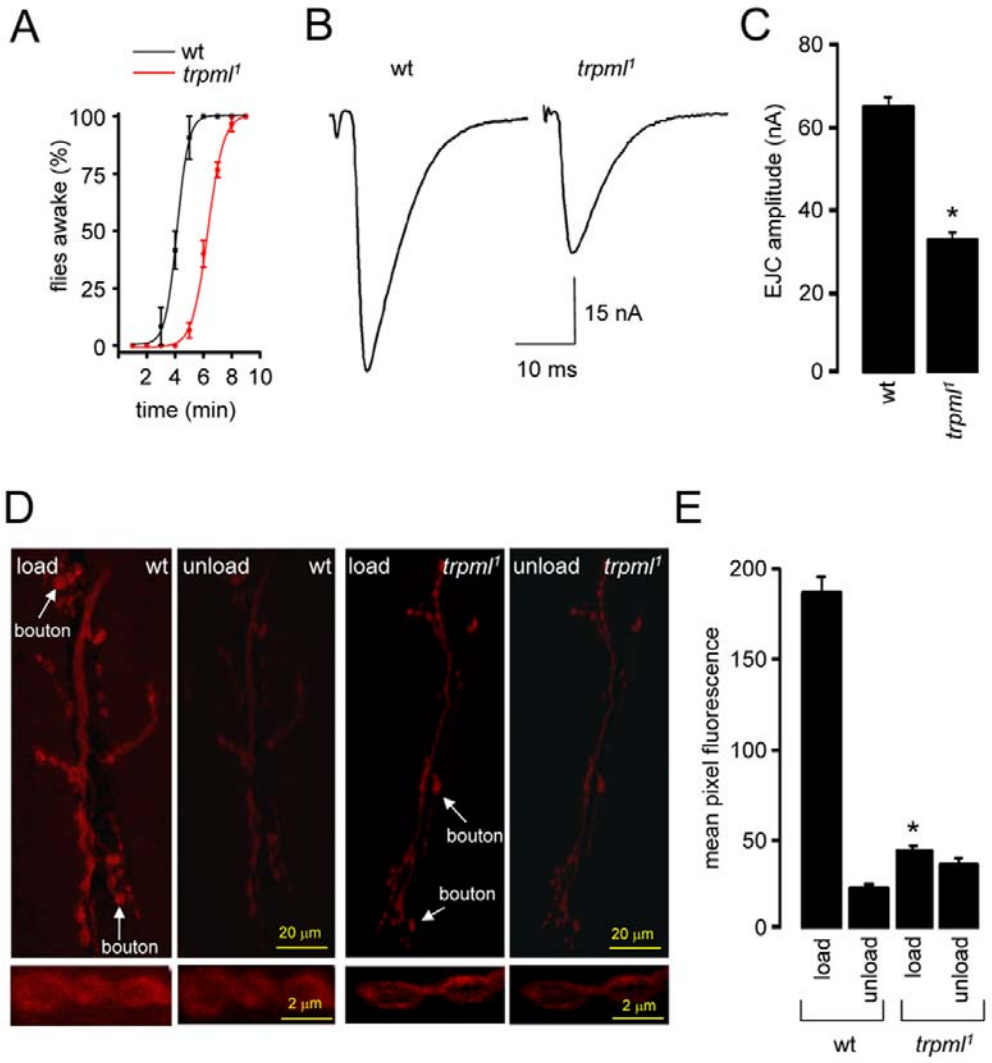
A
wt
trpml1
flies awake (%)
100
75
50
25
0
2 4 6 8 10
time (min)
B
wt
trpml1
15 nA
10 ms
C
EJC amplitude (nA)
80
60
40
20
0
*
wt
trpml1
D
load wt
unload wt
load trpml1
unload trpml1
bouton
bouton
bouton
bouton
20 μm
20 μm
2 μm
2 μm
E
mean pixel fluorescence
200
150
100
50
0
*
load
unload
load
unload
wt
trpml1

involved in synaptic vesicle cycling, similar to benchwarmer mutants in *Drosophila* with similar phenotypes of macromolecules accumulation, loss of NMJ funtion, neurodegeneration (Dermaut et al., 2005).

The cdc42-selective GAP Rich regulates postsynaptic development and Retrograde BMP Transynaptic Signaling

Retrograde BMP signaling mediated by the Glass bottom boat (Gbb) ligand modulates structural and functional synaptogenesis at the *Drosophila* NMJ (Wharton et al., 1999; Raftery and Sutherland, 1999; Baines, 2004; Nahm et al., 2010; Kim and Marques, 2010). However, the molecular mechanisms regulating postsynaptic Gbb release are poorly understood. In collaboration with Dr. Seungbok Lee's lab at Seoul National University in Korea, we showed that *Drosophila* Rich (dRich), a conserved Cdc42-selective GTPase activating protein (GAP), inhibits the Cdc42-Wiskott-Aldrich syndrome protein (Wsp) pathway to stimulate postsynaptic Gbb release. I provided the electrophysiological characterizations in this collaborative study. Loss of dRich strongly impairs neurotransmitter release, which is rescued by targeted postsynaptic expression of wildtype dRich but not a GAP-deficient mutant (Figure 4.2). dRich inhibits the postsynaptic localization of the Cdc42 effector Wsp, and manifestation of synaptogenesis defects in *drich* mutants requires Wsp signaling. Importantly, dRich increases Gbb release and elevates presynaptic P-Mad levels. In addition, dRich regulates postsynaptic organization independently of Cdc42. We propose that dRich coordinates the Gbb-dependent modulation of synaptic growth and function with postsynaptic development. This paper is currently under revision at Genes and Development.

To directly assess the functional consequence of *drich* mutations at the larval glutamatergic NMJ synapse, I recorded postsynaptic currents using the two-electrode voltage-clamp (TEVC) recording configuration

(Figure 4.2). At a basal stimulation frequency of 0.5 Hz in 0.5 mM extracellular Ca^{2+}, the amplitude of excitatory junctional currents (EJCs) in *drich* mutants were reduced by ~50% compared with wildtype controls (wildtype: 72.2 ± 6.2 nA; $drich^{1}/drich^{2}$: 32.2 ± 3.1 nA; $p < 0.01$) (Figure 4.2). Neuronal expression of dRich in *drich* mutants failed to restore synaptic transmission (Figure 4.2 A, B). In sharp contrast, targeted muscle expression of wildtype dRich in the null background completely restored synaptic transmission amplitude to wildtype levels (Figure 4.2 A, B). These data indicate that dRich acts postsynaptically to strongly facilitate synaptic function.

Either presynaptic or postsynaptic defects, or both, could potentially underlie impaired neurotransmission in *drich* mutants. One method to identify mechanistic defects is to assay spontaneous synaptic vesicle fusion, or miniature EJC (mEJC) events, occurring in the absence of evoked or endogenous action potentials (Trotta et al., 2004; Gatto and Broadie, 2008; Long et al., 2008). Representative mEJC records for wildtype and *drich* null mutants are shown in Figure 4.2. In *drich* mutants, mean mEJC amplitude was not altered compared with wildtype controls (Figure 4.2 C, D), suggesting no defect in basal postsynaptic function in the absence of dRich. In contrast, there was a small but significant increase in mEJC frequency in $drich^{1}/drich^{2}$ compared with wildtype animals (wildtype: 1.3 ± 0.2 Hz; $drich^{1}/drich^{2}$: 2.5 ± 0.4 Hz; $p < 0.01$) (Figure 4.2 C, E). Although this defect is presumably reflecting synaptic vesicle fusion probability, and is therefore presynaptic, the defect could only be rescued with postsynaptic introduction of wildtype dRich (Figure 4.2 C, E). Therefore, postsynaptic dRich has a retrograde transsynaptic effect on the regulation of synaptic neurotrasmitter release.

We demonstrate here that *Drosophila* Rich (dRich), a conserved Cdc42-selective GTPase activating protein (GAP), inhibits the Cdc42-Wsp pathway to stimulate postsynaptic Gbb release. Loss of dRich significantly

Figure 4.2 Postsynaptic Loss of dRich Impairs NMJ Synaptic Transmission

(A) Two-electrode voltage-clamp (TEVC; -60 mV) records from muscle 6 in segment A3 with 0.5 Hz nerve stimulation in 0.5 mM external Ca^{2+}. Representative excitatory junction current (EJC) records are shown for wild-type, *drich*^{1}*/drich*^{2}, *C155-GAL4*/+; *drich*^{2}*/UAS-drich*,*drich*^{1} (dRich rescue-pre), and *BG57-GAL4*,*drich*^{2}*/UAS-drich*,*drich*^{1} (dRich rescue-post) larvae. Arrows indicate time of nerve stimulation. (B) Quantified mean EJC amplitudes for all four genotypes. Transmission is reduced more than 50% in *drich* mutants. This defect is completely rescued by postsynaptic but not presynaptic expression of wild-type dRich. (C) Representative miniature EJC (mEJC) events following nerve transection; continuous recording in 0.5 mM external Ca^{2+} in the same genotypes as in (A). (D and E) Quantification of mean mEJC amplitude (D) and frequency (E). Sample size n > 5 animals per genotype. *p < 0.01; ** p < 0.01.

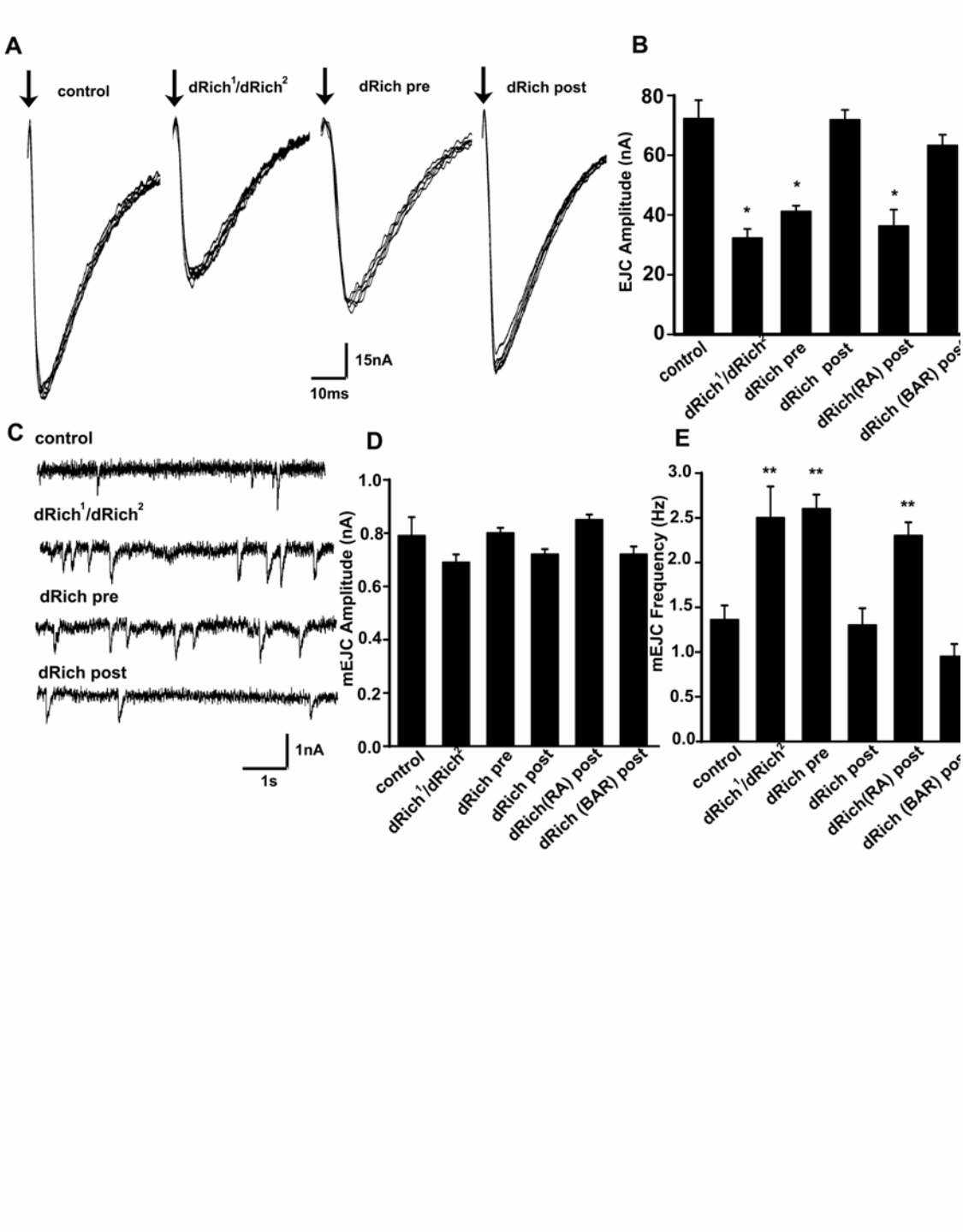
A
control
dRich1/dRich2
dRich pre
dRich post
15nA
10ms
B
EJC Amplitude (nA)
80
60
40
20
0
control
dRich1/dRich2
dRich pre
dRich post
dRich(RA) post
dRich (BAR) post
C
control
dRich1/dRich2
dRich pre
dRich post
1nA
1s
D
mEJC Amplitude (nA)
1.0
0.8
0.6
0.4
0.2
0.0
control
dRich1/dRich2
dRich pre
dRich post
dRich(RA) post
dRich (BAR) post
E
mEJC Frequency (Hz)
3.0
2.5
2.0
1.5
1.0
0.5
0.0
control
dRich1/dRich2
dRich pre
dRich post
dRich(RA) post
dRich (BAR) post

impairs neurotransmitter release and causes synaptic undergrowth, which is rescued by targeted postsynaptic expression of wildtype dRich but not a GAP-deficient mutant. dRich inhibits the postsynaptic localization of the Cdc42 effector Wsp, and manifestation of synaptogenesis defects in *drich* mutants requires Wsp signaling. In addition, dRich regulates postsynaptic organization independently of Cdc42. Future analysis of genetic and biochemical interactions between dRich and other post synaptic components will test the role of dRich in membrane morphogenesis and how that may impact synaptic function.

Presynaptic Calcium Channel Localization and Calcium Dependent Synaptic Vesicle Exocytosis Regulated by the Fuseless Protein

In Chapter II of this thesis, I described the indentification of Fuseless, a novel integral membrane protein associated with voltage-gated Ca^{2+} channels, using an unbiased, forward genetic screen for synaptic dysfunction mutants in the *Drosophila* visual system. The Fuseless protein is an 8-pass transmembrane protein whose closest known human homolog (~40% similarity) is the transmembrane protein Sialin, a transporter belonging to a group of anion/cation symporters (Yarovaya et al., 2005; Wreden et al., 2005). In *Drosophila*, *fuseless* mutants profoundly disrupt synaptic transmission, both at central histaminergic photoreceptor synapes and at peripheral glutamatergic synapses, indicating a conserved function, in multiple classes of chemical synapse (Chapter II).

Fuseless Protein Regulates Presynaptic Active Zones

The distribution of common synaptic proteins was also examined in *fuseless* mutants compared to controls. No detectable differences were observed in the localization, area or mean fluorescence intensities of Synaptotagmin 1 (Syt; SV pools) or in the postsynaptic glutamate receptor subunit (GluRIIA) (Figure 4.3A). These data show that Fuseless is not

required for synaptic morphogenesis or the gross molecular differentiation of pre- and postsynaptic compartments, or in postsynaptic compensations at the glutamate receptor level which may sometimes occur in response to synaptic mutations which reduce transmitter release levels (DiAntonio et al., 1999). One synaptic marker did show a pronounced difference in *fuseless* mutants; anti-NC82 (*bruschpilot*) which is known to specifically localize at presynaptic active zones (Wagh et al., 2006; Kittel et al., 2006). In wild-type terminals, anti-NC82 reveals numerous punctate active zone domains in each presynaptic bouton (Figure 4.3B). These punctate active zone domains appear normal in the *fuseless* mutant, but occur at a much lower density than in controls (Fig. 4.3 B, C). Active zone number was quantified by counting NC82 puncta in individual synaptic boutons. All *fuseless* mutants displayed a highly significant >40% reduction in active zone puncta compared to controls; 14.1 ± 1.3 (WT) and 12.4 ± 1.2 (+/Df) in controls, compared to 9.2 ± 1.1 ($fusl^1$), 8.1 ± 0.97 ($fusl^2$) and 7.2 ± 0.68 ($fusl^1$/Df) in mutants ($P<0.01$ for $fusl^1$ and $fusl^1$, $P<0.001$ for $fusl^1$/Df; N = 10 animals for each genotype; Figure 4.3C). These data indicate that Fusl plays an important role in either the development or maintenance of presynaptic active zones.

Loss of Fuseless Impairs *C*alcium Dynamics in the Presynaptic Terminal

The *fuseless* mutant phenotypes are consistent with an impaired Ca^{2+} trigger for SV exocytosis. All measurements of physiological defects, Ca^{2+}-cooperativity and Ca^{2+}-sensitivity suggest altered regulation by Ca^{2+}, perhaps due to impaired or mislocalized voltage-gated Ca^{2+} channels, or aberrant Ca^{2+} trafficking machinery involving Ca^{2+} transport or exchange (Littleton et al., 1994; Stewart et al., 2000; Bao et al., 2005). To test the possibility that a change in basal [Ca^{2+}] at rest and/or Ca^{2+} influx during

Figure 4.3: Null *fusl* mutant has fewer presynaptic active zones in a morphologically normal NMJ. A) Null *fusl* mutants have structurally normal NMJs.Representative images of mature larval NMJs probed with anti-HRP (presynaptic membrane; HRP, red), anti-GluRIIA (postsynaptic glutamate receptors; GluR, green) and anti-Synaptotagmin 1 (SV pools; Syt, blue). No major differences were observed between WT control (top row) and mutants (bottom row). Scale bar: 20 μm. **B)** Representative images of NMJ boutons probed with anti-NC82/Bruchpilot. Punctate active zone domainsappear normal in mutants, but occur at lower density. Scale bar: 2 μm. **C)** Quantificationof anti-NC82/Bruchpilot puncta number within individual type I synaptic boutons. Null *fusl* mutants display a ~40% reduction in active zone puncta, a highly significant decrease ($P<0.01$, N=10 animals, 20 boutons).

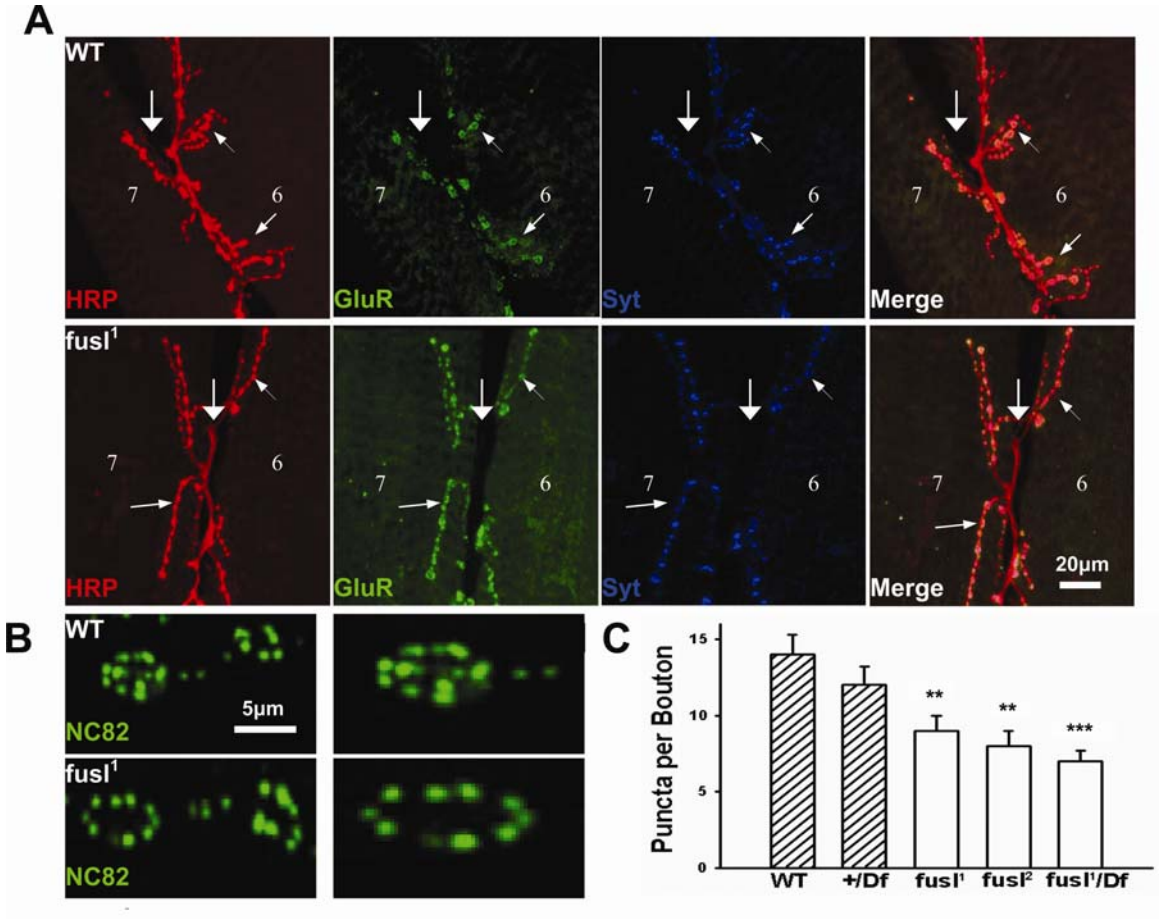
A
WT
HRP
GluR
Syt
Merge
7
6
fusl1
20μm
B
WT
5μm
NC82
fusl1
C
Puncta per Bouton
15
10
5
0
**
**
***
WT
+/Df
fusl1
fusl2
fusl1/Df

depolarization might occur, Ca^{2+} imaging was done at the NMJ using a genetically-encoded calcium indicator, gCAMP (GFP-tagged calmodulin) (Nakai et al., 2001).The gCAMP reporter undergoes a calcium-dependent conformational change upon Ca^{2+} binding (calmodulin, CaM), exciting the GFP fluorophore (Nakai et al., 2001; Reiff et al., 2005). This trangenic [Ca^{2+}] indicator was driven under control of a UAS promoter only in the presynaptic cell using the neural-specific elav-GAL4 (Fig. 4.4). The gCAMP fluorescence was assayed by confocal microscopy in physiological saline during unstimulated conditions ("resting"), during stimulation with 90 mM [K+] ("stimulated") and following return to physiological saline ("recovery") in controls and *fusl* mutants (Figure 4.4 A, B). At rest, mean gCAMP fluorescence intensities representing basal Ca^{2+} levels were slightly but significantly elevated in *fusl* mutants; 20.1 ± 4.7 (WT) and 17.5 ± 4.9 (+/Df) in controls, compared to 24.1 ± 1.4 (*fusl*^{1}), 23.8 ± 1.54 (*fusl*^{2}) and 21.8 ± 41.71 (*fusl*^{1}/Df) ($P<0.05$ for *fusl*^{1} and *fusl*^{2}, N=10 for each genotype); Figure 4.4C, left). This elevation in resting [Ca^{2+}] is similar to that observed in calcium transporter mutants (Liang, 1997). Ca^{2+} entry was stimulated by depolarizing the nerve terminal with 90 mM [K^{+}] saline (see Figure 4.4, middle panel, "stimulated"). These findings suggest an impairment in the maintenance of calcium levels in the neuron in *fuseless* mutants, both at basal and stimulated conditions. In control boutons, stimulation resulted in a striking 100-fold increase in mean gCAMP fluorescence within 5 seconds (Figure 4.4 A, middle). All *fuseless* mutants were dramatically impaired in the amount of Ca^{2+} influx; in controls, the mean stimulated gCAMP fluorescence intensity was 178.1 ± 2.7 (WT) and 172.5 ± 3.2 (+/Df), whereas in mutants it was only 23.5 ± 3.6 (*fusl*^{1}), 21.7 ± 3.1 (*fusl*^{2}) and 23.1 ± 3.5 (*fusl*^{1}/Df) ($P<0.001$, N=10 for all genotypes; Figure. 4.4 C, middle).

Figure 4.4: Impaired presynaptic Ca^{2+} influx in fusl mutants. Calcium imaging with the transgenic fluorescent [Ca^{2+}] indicator UAS-gCAMP driven by elav-GAL4 in the presynaptic NMJ terminal. A-B) Representative images at rest (left), during depolarization with 90 mM [K+] saline stimulation (center) and following recovery in physiological saline (right). Sample images from WT control (A) and fusl mutant (B) reveal a robust depolarization-triggered Ca^{2+} signal in control but a highly attenuated Ca^{2+} signal in the mutant. Scale: 20 .m. C) Mean fluorescent pixel intensity in synaptic boutons quantified during rest (left), during depolarization stimulation with 90 mM [K+] (center), and following recovery from stimulation in normal saline (right). Basal levels of UAS-gCAMP fluorescence are different as indicated ($P<0.05$) between controls (hatched bars) and mutants (white bars), and triggered UAS-gCAMP fluorescence levels are very significantly reduced ($P<0.001$) in fusl mutants compared to controls. Post stimulation UAS-gCAMP fluorescence also differs between fusl mutants and controls ($P<0.05$). Sample size of 10 animals for each genotype represented.

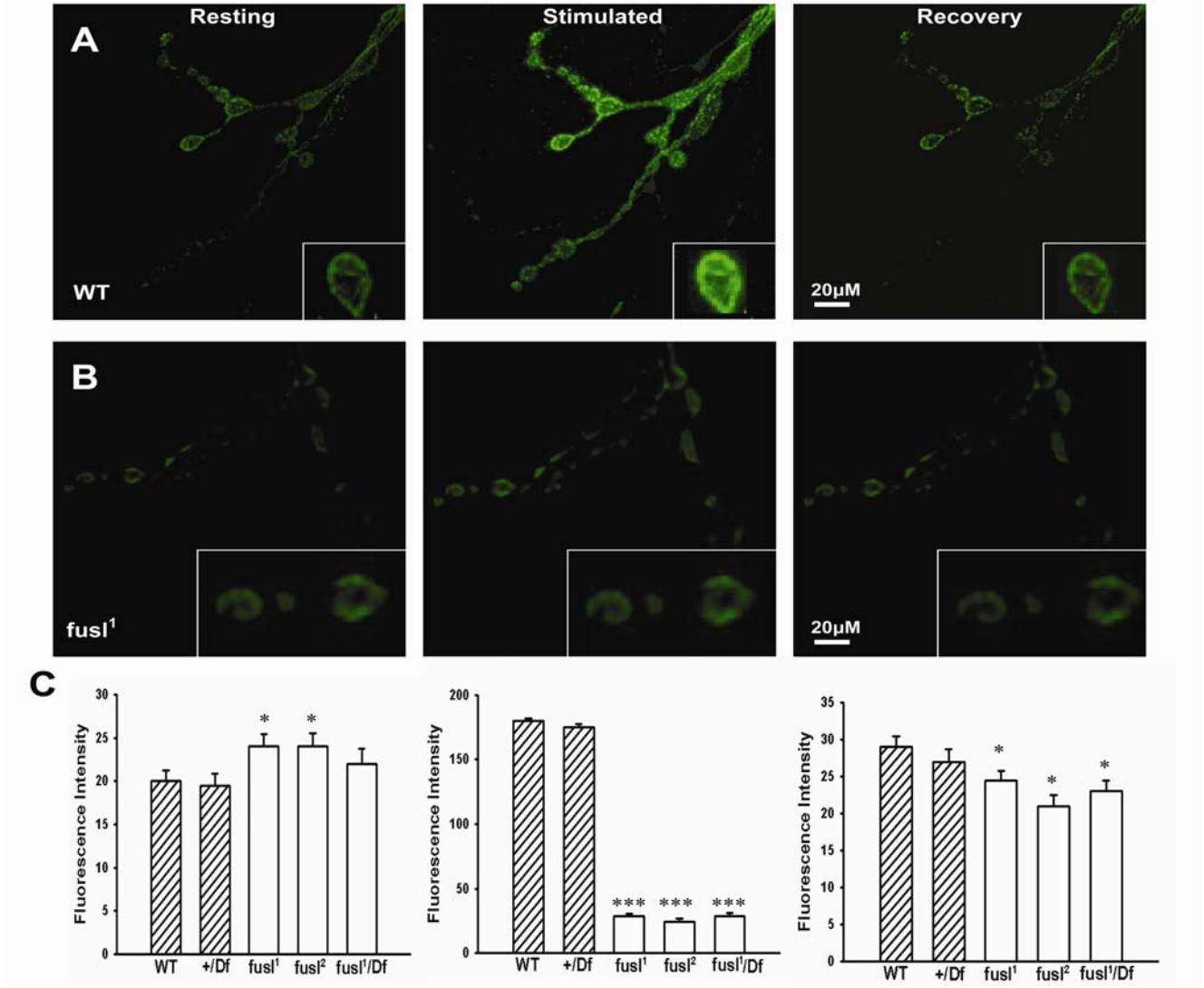
A
Resting
Stimulated
Recovery
WT
20μM
B
fusl1
20μM
C
Fluorescence Intensity
WT
+/Df
fusl1
fusl2
fusl1/Df
*
***

Thus, *fusl* mutants display a minimal [Ca^{2+}] increase during presynaptic depolarization, as detected utilizing this reporter technique. Following stimulation, gCAMP fluorescence rapidly declined in controls to near initial levels at 30 seconds (Figure 4.4 A, right, "recovery"). The fluorescence intensity 30 seconds after stimulation was still slightly higher in controls relative to mutants; 27.3 ± 4.3 (WT), 26.9 ± 4.9 (+/Df), 22.3 ± 4.5 (*fusl*^{1}), 21.9 ± 4.8 (*fusl*^{2}) and 22.8 ± 4.3 (*fusl*^{1}/Df) (Figure 4.4 C, right). These data indicate that *fusl* mutants display a profound impairment of Ca^{2+} dynamics in the presynaptic terminal, with higher Ca^{2+} levels at rest and a greatly attenuated Ca^{2+} influx during depolarization.

Loss of Fusl Causes Impaired Ca^{2+}-Dependent Facilitation

To further examine the prediction that Ca^{2+}-dependent transmission properties are impaired in the absence of Fuseless, we assayed the effect of [Ca^{2+}] on frequency-dependent facilitation (Figure 4.5). High frequency stimulation at lower calcium levels causes prominent Ca^{2+}-dependent, short-term facilitation (Rohrbough et al., 1999; Trotta et al., 2004). To assay facilitation, the NMJ was stimulated in 0.2 mM [Ca^{2+}] over a range of frequencies from 0.5 Hz to 20 Hz. Figure 4.5A shows sample traces from a 20 pulse 20 Hz stimulation train of wild-type controls and *fusl*^{1} mutants. Control synapses show a rapid, progressive facilitation over the first 5 stimuli and a 4-fold facilitation in EJC amplitude of the last 10 stimuli compared to the basal EJC amplitude (Figure 4.5A). In sharp contrast, *fuseless* mutants display no Ca^{2+}-dependent facilitation, and in fact exhibit responses that become slightly smaller during the stimulus train, showing synaptic depression (Figure 4.5A). These effects suggest that the mutant transmission machinery may already be working at maximum capacity, or that there is a selective defect in the Ca^{2+} trigger for facilitation. In Figure 4.5 B, the mean EJC amplitude normalized to basal EJC amplitude is displayed at 0.5, 5, 10 and 20 Hz in control and mutant conditions. Both controls display comparable facilitation at all frequencies, with a 3.5- to 4-

fold facilitation at 20 Hz. Both mutants display a complete lack of Ca^{2+}-dependent facilitation at all frequencies (Figure 4.5B). Taken together, the severely reduced Ca^{2+}-dependence of vesicular fusion and the loss of Ca^{2+}-dependent facilitation suggest that Ca^{2+} Entry into the nerve terminal and/or Ca^{2+} coupling to exocytosis must be impaired (Bao et al., 2005).

Fusl Protein is Required during Development in the Nervous System

To examine the temporal and spatial requirements of the Fusl protein, the elav-GeneSwitch-Gal4 system was employed (Gatto and Broadie, 2008). In this setting, driver lines expressing the transcriptional activator Gene Switch in a tissue-specific fashion are crossed to UAS-reporter lines with genomic inserts of a target gene (Gatto and Broadie, 2008). In the absence of an activator, the Gene Switch protein is expressed in target tissues but remains transcriptionally silent, and the target gene is therefore not expressed. However, after systemic application of RU486, the Gene Switch protein becomes transcriptionally active, mediating expression of the target gene in only those tissues expressing GeneSwitch (Osterwalder et al., 2001; Gatto and Broadie, 2008). Fusl null animals containing the genetic UAS-Fusl line were crossed to elav-GS and fed a high concentration of RU486 to induce a 12 hour “acute pulse,” of Fusl expression during the larval third instar stage. (Figure 4.6 A). Larvae were then assessed for phenotypic rescue using TEVC electrophysiology (Figure 4.6B). The elav-GS; UAS-fusl RU486-induced line revealed EJC amplitudes that were not statistically different from controls (64.1 $\pm$ 4.5 nA (control); 59.6 $\pm$ 3.9 nA (induced) (Figure 4.6C). When the elav-GS; UAS-fusl line was induced with ethanol (which is incapable of inducing the elav-GS-Gal4, and is classically used as a negative control (McGuire et al.,

Figure 4.5: Loss of Ca^{2+}-dependent facilitation in fusl mutant.
A) Representative EJC records of Ca2+-dependent synaptic facilitation protocol in fusl mutants (top row) and WT controls (bottom row). EJC responses are displayed to a 1 sec, 20 Hz stimulation train in 0.2 mM Ca^{2+}. The first five consecutive EJCs in the train are shown, with the 6th – 10th and 11th –20th responses averaged. Null fusl mutants show loss of facilitation. B) Quantification of EJC amplitudes plotted over a 0.5-20 Hz stimulation range. The EJC amplitude was averaged for the 11th-20th responses for a stimulation train at each frequency, and normalized to the mean EJC amplitude at the basal stimulation frequency (0.5 Hz). Four genotypes are shown; two controls (WT, Df/+) and two mutants (fusl1, fusl1/Df). Sample size 10 animals for each data point

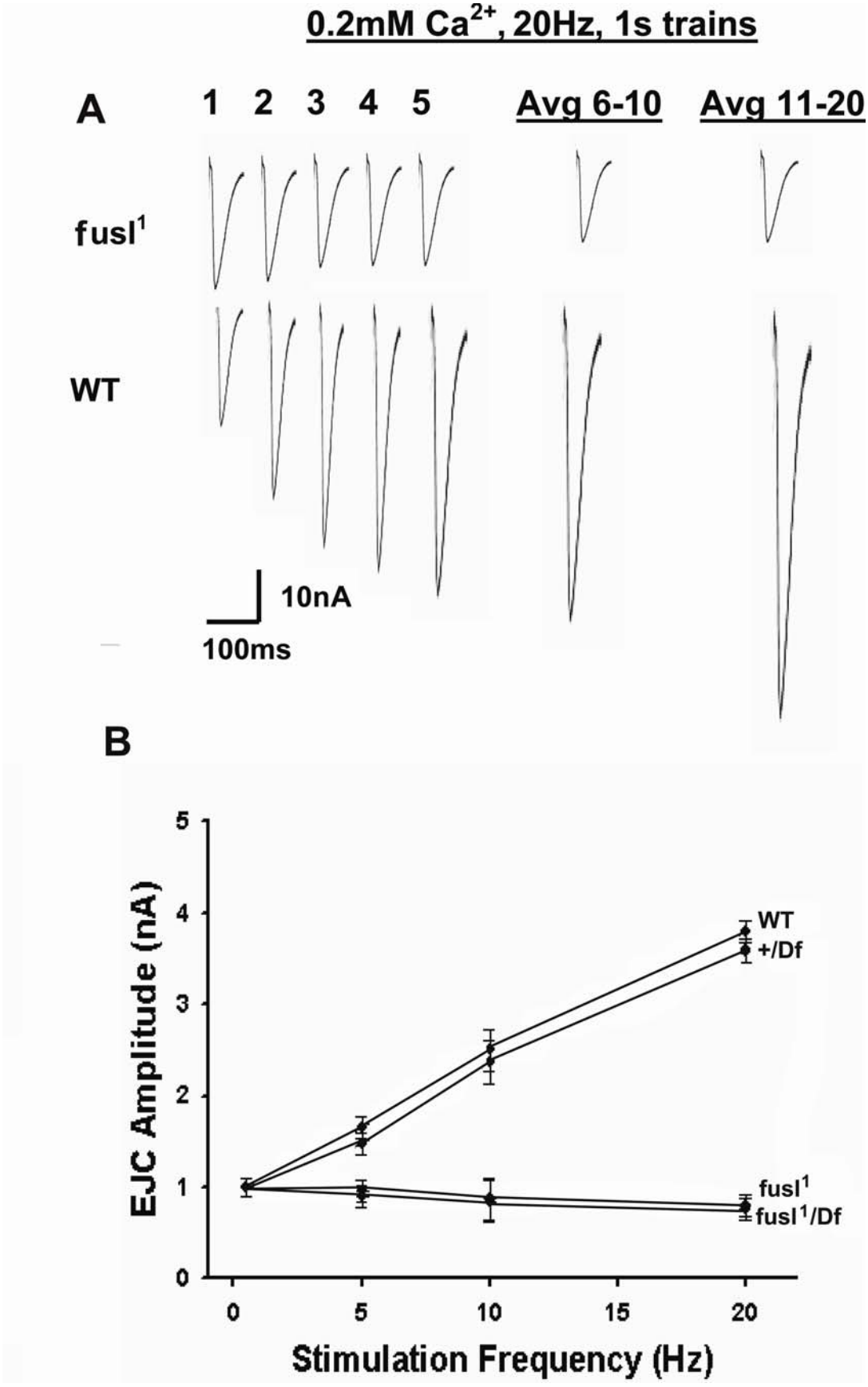
0.2mM Ca2+, 20Hz, 1s trains
A
1 2 3 4 5
Avg 6-10
Avg 11-20
fusl1
WT
10nA
100ms
B
EJC Amplitude (nA)
Stimulation Frequency (Hz)
WT
+/Df
fusl1
fusl1/Df
0
1
2
3
4
5
0
5
10
15
20

Figure 4.6: Acute rescue of fusl presynaptic transmission defect. The conditional GeneSwitch (GS) system was used to drive RU486-dependent expression of Fusl in the presynaptic cell only at the NMJ. A) Cartoon representation of elav-GS-GAL4 driver crossed to UAS-fusl to generate conditional expression in the fusl1 null background. Transgenic animals were raised on standard diet until 84 hrs of larval development , and then switched to food containing 200 mM RU486 for 12 hours, until the end of the 3rd larval instar at 96 hours, and then assayed by TEVC recording. B) Representative EJC traces of wild-type (control), RU486-induced (RU486), animals fed ethanol vehicle (ethanol control), and fusl1 homozygous mutant. C) Quantitation of EJC amplitude. Wild-type control and RU486-induced are not significantly different. N=10 animals for each genotype. Significance indicated as *** denotes P<0.001

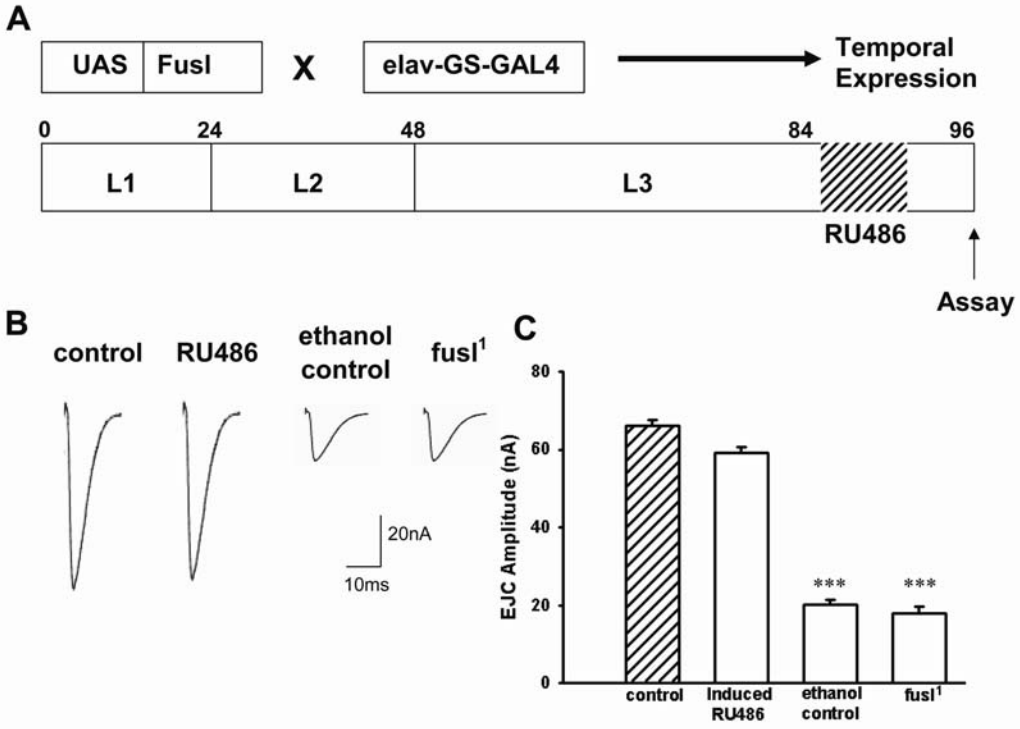
A
UAS
Fusl
X
elav-GS-GAL4
Temporal
Expression
0
24
48
84
96
L1
L2
L3
RU486
Assay
B
control
RU486
ethanol
control
fusl1
20nA
10ms
C
EJC Amplitude (nA)
80
60
40
20
0
***
***
control
Induced
RU486
ethanol
control
fusl1

2004), the results are comparable to that of the fusl1 mutant line 20.2 ± 3.2 nA (ethanol control), 18.4 ± 4.8 nA (fusl1), (Figure 4.6C). Thus, during development, the Fusl protein appears to play a critical role in the regulation of development and organization of the nerve terminal.

Expression of Cation Specific Channels Partially Rescues the *Fuseless* Phenotype

To further confirm an impairment in presynaptic calcium channels, light sensistive, rhodopsin-gated, cation specific channels were transgenically expressed in the Fusl mutant background by crossing flies containing the UAS-CHR2 construct (Nagel et al., 2005; Lima and Miesenbock, 2005) and driving expression in the nervous system using the neural-specific driver elav.TEVC evoked and nonevoked electrophysiology were carried out in high calcium (5mM) with a blue light diode in complete dark as described (Nagel et al., 2005). Animals were placed into one of two recording paradigms: evoked stimulation (using 0.5Hz) with additional light stimulation (0.5s of blue light exposure), or light stimulation only (0.5s). Representative traces in Figure 4.7A show representative traces from the dual stimulation or single light stimulation (Figure 4.7C). Control animals (elav;UAS-CHR2 in a wild type background) who received dual stimulations had EJC amplitudes that were significantly larger than $fusl^1$ mutants (151.1 ± 15.2nA (control), 62.4 ± 6.4nA ($fusl^1$) (Figure 4.7B). Interestingly, the dual stimulation of $fusl^1$ led to significantly higher EJC amplitudes compared to $fusl^1$ mutants who only received evoked stimulation in 5mM Ca^{2+} (62.4± 6.4nA ($fusl^1$, evoked plus expression of new channels in high calcium, not high calcium alone, which lessens the *fuseless* evoked phenotype (Figure 4.7A and 4.7C).

Figure 4.7: Exogenous Ca^{2+} trigger restores presynaptic function in fusl mutants. To introduce an alternative Ca^{2+} influx pathway, a transgenic rhodopsin, light-gated cation channel (UAS-CHR2) was driven with elav-GAL4 in the presynaptic NMJ terminal in control and fusl null mutant backgrounds. Both genotypes were assayed in 5 mM external [Ca^{2+}] with nerve stimulation alone (evoked), a blue light diode stimulus alone (light) or simultaneous nerve and light stimulation (evoked + light). A) Representative EJC traces from dual stimulation (light plus evoked) of the control and fusl1 null mutant. B) Quantification of evoked and light plus evoked dual stimulation in control and fusl1 mutant. Light stimulation enhanced EJC amplitude in both genotypes but resulted in a much greater increase in transmission amplitude in the mutant. A significant ($P<0.0001$) difference maintained between control and mutant in both conditions. C) Representative traces with light stimulation (0.5 sec) only in control and fusl null mutant backgrounds. D) Quantification of light-evoked current responses. The fusl1 mutant showed responses twice as large as control ($P<0.0001$, N=10 animals for each genotype).

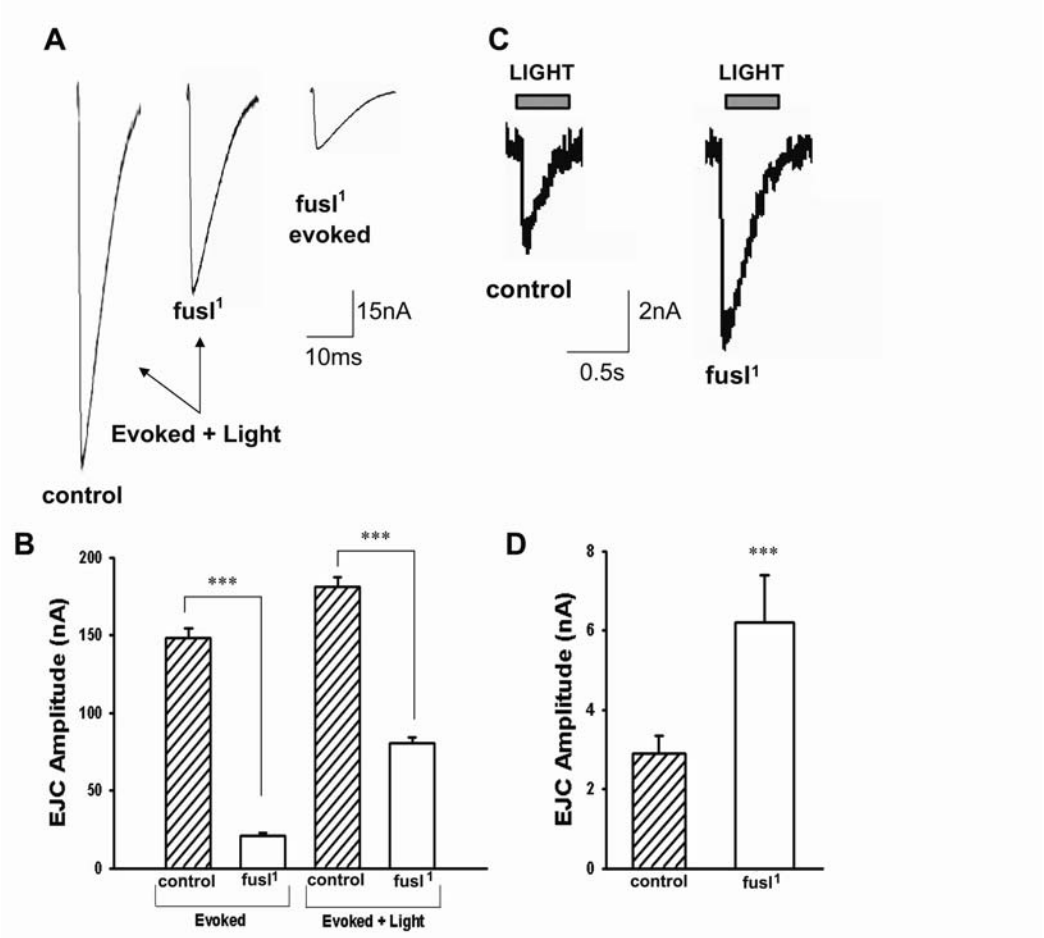
A
fusl1
evoked
15nA
10ms
fusl1
Evoked + Light
control
C
LIGHT
LIGHT
control
2nA
0.5s
fusl1
B
EJC Amplitude (nA)
200
150
100
50
0
***
***
control
fusl1
control
fusl 1
Evoked
Evoked + Light
D
EJC Amplitude (nA)
8
6
4
2
0
***
control
fusl1

That the expression of new channels did not rescue the evoked phenotype was not a great surprise, as the transgenic channels are not specifically calcium channels, and have dynamics and permeabilities to other ions which are not common to calcium channels found at the active zone. When a second group of animals were subjected to a light-only stimulation, the EJCs of control animals were significantly lower than that of $fusl^1$ mutants (Figure 4.7C and Figure 4.7D), 28.8 ± 4.3 nA (control), 62.5 ± 5.3 nA ($fusl^1$) (Figure 4.7D). light) versus 19.8 ± 2.1nA (evoked only), which demonstrates that it is the Thus, when not relying on the voltage gated calcium channels at the active zone, *fuseless* mutants are able to undergo vesicle fusion and transmitter exocytosis properly, and when calcium is made available through an alternate subset of channels to the *fuseless* active zone, the significantly enlarged pool of docked, unfused vesicles are able to fuse to create responses greater than that of controls.

Functional Relationship between Fuseless and Calcium Channels at the Active Zone

My studies strongly support a mechanistic role for the Fuseless protein in regulating the voltage-gated Ca^{2+} channels that trigger synaptic vesicle fusion. In the absence of this regulation, active zones may fail to form or be properly organized, but this occurs only some of the time, indicating that Fuseless may facilitate active zone assembly, but is not required for this process. Many ultrastructurally normal active zones persist in the complete absence of Fuseless, but lack the localized Ca^{2+} trigger for vesicle exocytosis, and therefore only inefficiently manage neurotransmitter release. One possible role for the Fuseless protein might be to serve as a direct interacting partner with the Ca^{2+} channel to enable its correct trafficking and/or localized maintenance at the active zone (Ambudkar, 2007). Arguing against this model is the fact that Fuseless is not restricted to active zones domains like the Ca^{2+} channel, but rather

shows a diffuse presynaptic plasma membrane localization, similar to the t-SNARE syntaxin. Another model, consistent with the predicted transmembrane transporter function, is that Fuseless might regulate the presynaptic environment in a way that facilitates Ca^{2+} channel localization. Arguing for this model, the closest human sequence homolog, Sialin, transports sialic acid (Yarovaya et al., 2005; Wreden et al., 2005). This modified sugar group is a component of transmembrane glycoproteins, typically as the terminal residue of cell surface oligosaccharides. Misregulation of this cargo transport could be envisioned to cause defects in Ca^{2+} channel trafficking in the presynaptic membrane. Future work should therefore examine the molecular function of the Fuseless protein by attempting to determine whether it functions as a transmembrane transporter, as predicted, and if so, the exact nature of the transported cargo.

The nonsense mediated decay pathway maintains NMJ synapse architecture and function

In Chapter III of this thesis, I described the identification of no-on-and-no-off - transient C (nonC), a phosphatidyl 3- kinase-like kinase (PIKK), identified in a systematic *Drosophila* forward genetic screen for photoreceptor synaptic transmission mutants based on loss of retinal synaptic responses to light stimulation. The cloned gene encodes Smg1 (Supressor with morphogenetic effects on genitalia-1), a regulatory kinase of the nonsense mediated decay pathway (NMD). The Smg proteins act in an mRNA quality control surveillance mechanism to selectively degrade transcripts containing premature stop codons, thereby preventing the translation of truncated proteins. At the NMJ, an allelic series of *Smg1* mutants show underdeveloped synaptic architecture, including reductions in NMJ area, arbor number, and number of synaptic boutons. Functionally, loss of Smg1 results in ~50% reduction in basal neurotransmission, strength, as well as progressive transmission fatigue and SV cycling

during high frequency stimulation physiology. Taken together, these findings suggest that the NMD pathway acts to regulate proper mRNA translation to safeguard synapse morphology and maintain synaptic functional efficacy.

Synaptic targets of NMD

We and others have exerted a great deal of effort exploring the roles of mRNA regulation in synaptic mechanisms (Antar and Bassell, 2003; Gatto and Broadie, 2009; Pfeiffer and Huber, 2009; Tessier and Broadie, 2009; Yan et al., 2009). In particular, mechanisms of mRNA stabilization, trafficking, RISC-mediated degradation and localized translation have all been recently determined to occur in proximity to synapses, and/or with important roles in synapse regulation (Giorgi et al., 2007; Hengst and Jaffrey, 2007; Lin and Holt, 2007; Yan et al., 2009; Sebeo, et al., 2009). These insights have raised the question of possible NMD involvement (Giorgi et al, 2007). In the absence of NMD regulation, synaptic morphological development is damaged, with reduced NMJ arbors and bouton formation, and an accompanying decrease in presynaptic neurotransmitter release due to impairment of synaptic vesicle cycling. Ultrastructurally, fairly normal synapses persist in the complete absence of NMD, but the inability to regulate the presence of truncated proteins at the synapse results in inefficiently managed neurotransmitter release. Thus, we suggest that the *S*mg genes working via NMD prevent the translation of aberrant proteins that disrupt synaptic stability and function. It has been shown previously that loss of the NMD initiating factor and exon-junction complex component eIF4AIII leads to synaptic functional impairments. Additionally, it is known that localized mRNAs encode receptors, cytoskeletal proteins and regulatory proteins critical for synaptic development, and that the localized translational regulation of these mRNAs is critical for synaptic stability and function. Our current work is focusing on the identification of the mRNA species encoding

synaptic proteins that accumulate in the absence of the NMD pathway, mRNAs locally translated in the late-maturing axonal growth cone and potentially presynaptic terminal. We plan to study how the production of these aberrant proteins synthesized in the absence of NMD activity impairs synaptic development, architecture and presynaptic function. Whole genome Affymetrix microarrays are currently being employed to determine if changes exist at the level of synaptic mRNAs in NMD mutants. Potential synaptic targets will be identified by screening for statistically significant mRNA levels between control and mutant. Several promising candidates have been identified in *Smg1* mutants (Table 4.1).

To determine if these changes could be evident at the level of synaptic protein, one of the most promising of these candidates, Secretory Carrier Membrane Protein (SCAMP), was selected for antibody staining at the larval NMJ (Figure 4.8). Though little is known about its function, SCAMP is considered to be a protein with a role in vesicular trafficking (Sudhof, 2008). In *Smg1* mutants, expression of SCAMP mRNA is upregulated compared to controls (Table 4.1). Quantification of anti-SCAMP antibody fluorescence at the NMJ is similarly increased by 41% compared to controls (Figure 4.8D). This increase is particularly evident at the level of the bouton (Figure 4.8C), where anti-SCAMP staining is punctate in control, and diffuse thoughout the mutant bouton.Though still in its beginning stages, this promises to be a potentially fruitful technique to determine how NMD is affecting synaptic structure and function. The characterizations of the newly identified proteins presented herein lay the groundwork for the discovery and establishment of more detailed mechanisms regarding Ca^{2+} - triggered SV fusion and clathrin-mediated endocytosis. In particular, it will be interesting to understand how the influx of Ca^{2+} or the presence of Ca^{2+} channel subunits can regulate the development of the active zone, if these effects can be compensated for during adulthood of the animal, and lastly, the breadth and diversity of synaptic targets at the NMJ synapse which are regulated by NMD activity.

Table 4.1. NMD Targets at the Synapse. An Affymetrix microarray screen looking for altered mRNA expression of synaptic candidates in *Smg1* and *Smg3* mutants, compared to control, reveals potential clues for NMD regulation of synaptic morphology and function.

NAME	Function	mRNA FOLD CHANGE
Sarah	Homolog of Downs Syndrome Critical Region 1 (DSCR1)	0.98
SCAMP	Vesicle Trafficking	0.52
Unc-13	Synaptic Vesicle Cycle	0.52
Calmodulin	Calcium Binding Protein	0.52
Syntaxin 4	Docking of Transport Vesicles	0.43
Synaptotagmin 12	Putative Calcium Sensor for Exocytosis	0.40
Blue Cheese	Adult Neural Survival	0.40
Calcyphosin	Calcium Binding Protein	0.39
SNAPIN	Membrane fusion; Putative Binding Partner of t-SNARE	-0.38
Eaat1	excitatory amino acid transporter	-0.39
Rab3-GAP	Vesicle Trafficking	-0.43
Synaptotagmin 7	Putative Calcium Sensor for Exocytosis	-0.43
Neurexin-1	Glutamatergic Synapse Cell Adhesion	-0.49
GluRIIC	Postsynaptic Excitatory Receptor	-0.58
Synaptogyrin	Vesicle Associated Protein; Synaptic Plasticity	-0.60
RIM	Active Zone Protein	-0.64

Figure 4.8: SCAMP levels at the NMJ are upregulated in *Smg1* mutants. Preliminary results using an anti-SCAMP polyclonal antibody reveal a ~40% increase in *Smg1*^{MC45} mutants compared to controls. (A) Low magnification images of controls labeled with anto-SCAMP (green) and anti-HRP (red), and (B) *Smg1*^{MC45} mutants. Arrows point to boutons. (C) High magnification images of single boutons labeled with anti-SCAMP. Staining appears more punctuate in control boutons (left) and more diffuse in mutants, right. Arrows point to punctae. D)Quantification of SCAMP fluorescence in controls and mutants. Significance as indicated by ** is characterized as $p<0.05$. N= 5 animals and 10 NMJs per genotype.

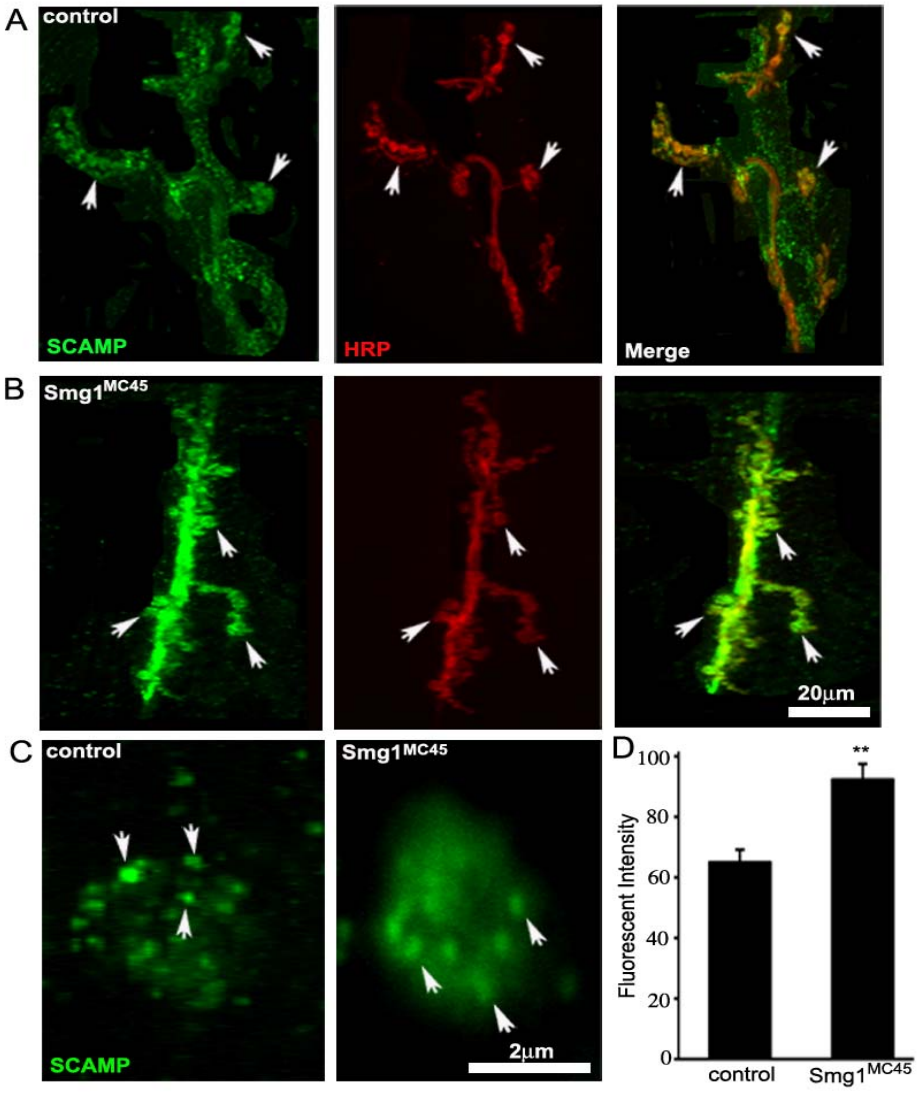
A
control
SCAMP
HRP
Merge
B
Smg1MC45
20μm
C
control
SCAMP
Smg1MC45
2μm
D
Fluorescent Intensity
100
80
60
40
20
0
**
control
Smg1MC45

References

Adler, E. M., Augustine, G. J., Duffy, S. N., and Charlton, M. P. (1991). Alienintracellular calcium chelators attenuate neurotransmitter release at the squid giantsynapse. *J. Neurosci.* 11, 1496-1507.

Ahle, S. and Ungewickell, E. (1986). Purification and properties of a new clathrin assembly protein. *Embo. J. 5*, 3143-3149.

Alfonso, A., Grundahl, K., Duerr, J.S., Han, H.P., and Rand, J.B. (1993). The Caenorhabditis elegans unc-17 gene: a putative vesicular acetylcholine transporter. *Science.* 261, 617-619.

Ambudkar, I. S. (2007). TRPC1: a core component of store-operated calcium channels. *Biochem. Soc. Trans. 35*, 96-100.

Amici, M., Doherty, A., Jo, J., Jane, D., Cho, K., Collingridge, G., and Dargan, S. (2009). Neuronal calcium sensors and synaptic plasticity. *Biochem. Soc. Trans.* 37,1359-1363.

Andrews, H. K., Zhang, Y. Q., Trotta, N., and Broadie, K. (2002). *Drosophila*, sec10 is required for hormone secretion but not general exocytosis or neurotransmission. Traffic *3*, 906-921.

Antar, L.N. and Bassell, G.J. (2003). Sunrise at the synapse: the FMRP mRNP shaping the synaptic interface. *Neuron*. 37, 555-558.

Aravamudan, B. and Broadie, K. (2003). Synaptic *Drosophila* UNC-13 is regulated by antagonistic G-protein pathways via a proteasome-dependent degradation mechanism.*J. Neurobiol. 54*, 417-438.

Aravamudan, B., Fergestad, T., Davis, W. S., Rodesch, C. K., and Broadie, K. (1999). *Drosophila* UNC-13 is essential for synaptic transmission. *Nat Neurosci 2*, 965-971.

Ashery, U., Varoqueaux, F., Voets, T., Betz, A., Thakur, P., Koch, H., Neher, E., Brose, N., and Rettig, J. (2000).Munc13-1 acts as a priming factor for large dense-core vesicles in bovine chromaffin cells. *EMBO J*. 19, 3586-3596.

Augustin, I., Rosenmund, C., Südhof, T.C., Brose, N. (1999). Munc13-1 is essential for fusion competence of glutamatergic synaptic vesicles. Nature. 400; 457-461.

Atwood, H.L., Govind, C.K., and Wu, C.F. (1993). Differential ultrastructure of synaptic terminals on ventral longitudinal abdominal muscles in Drosophila larvae. *J. Neurobiol.* 24,1008-1024

Bach, G. (2005). Mucolipin 1: endocytosis and cation channel--a review. *Pflugers. Arch*. 451, 313-317.

Baines, R.A. (2004). Synaptic strengthening mediated by bone morphogenetic protein-dependent retrograde signaling in the Drosophila CNS. *J. Neurosci.* 24,6904-6911.

Baker, P.F., Hodgkin, A.L., and Ridgway E.B. (1971). Depolarization and calcium entry in squid giant axons. *J. Physiol.* 218,709-755.

Bao, H., Daniels, R. W., MacLeod, G. T., Charlton, M. P., Atwood, H. L., and Zhang, B. (2005). AP180 maintains the distribution of synaptic and vesicle proteins in the nerve terminal and indirectly regulates the efficacy of Ca^{2+}-triggered exocytosis. *J. Neurophysiol. 94*, 1888-1903.

Barbee, S.A., Estes, P.S., Cziko, A.M., Hillebrand, J., Luedeman, R.A., Coller, J.M., Johnson, N., Howlett, I.C., Geng, C., Ueda, R., et al. (2006). Staufen- and FMRP-containing neuronal RNPs are structurally and functionally related to somatic P bodies. *Neuron.* 52, 997-1009.

Bassell, G.J. and Warren, S.T. (2008). Fragile X syndrome: loss of local mRNA regulation alters synaptic development and function. *Neuron*. 60, 201-214.

Becherer, U., Moser, T., Stuhmer, W., and Oheim, M. (2003). Calcium regulates exocytosis at the level of single vesicles. *Nat. Neurosci. 6*, 846-853.

Bekkers, J.M., Richerson, G.B., and Stevens, C.F (1990). Origin of variability in quantal size in cultured hippocampal neurons and hippocampal slices.*Proc. Natl. Acad. Sci. U. S. A.* 87, 5359-5362.

Benjamini, Y. and Hochberg, Y. (1995). Controlling the false discovery rate- a practical and powerful approach to multiple testing. *J.R.Stat.Soc.Ser.B. 57*, 289-300.

Bennett, M.K., Calakos, N., and Scheller, R.H. (1992). Syntaxin: a synaptic protein implicated in docking of synaptic vesicles at presynaptic active zones.*Science*. 257, 255-259.

Betz, A., Thakur, P., Junge, H.J., Ashery, U., Rhee, J.S., Scheuss, V., Rosenmund, C., Rettig, J., and Brose, N. (2001). Functional interactionn

of the active zone proteins Munc13-1 and RIM1 in synaptic vesicle priming. *Neuron*. 30,183 -196.

Betz, W.J. and Angleson, J.K. (1998). The synaptic vesicle cycle. *Annu. Rev. Physiol*. 60, 347-363.

Bleakman, D., Chard, P. S., Foucart, S., and Miller, R. J. (1991). Block of neuronal Ca++ influx by the anti-ischemic agent TA3090. *J. Pharmacol. Exp. Ther. 259*, 430-438.

Bourne, Y., Dannenberg, J., Pollmann, V., Marchot, P., and Pongs, O. (2001). Immunocytochemical localization and crystal structure of human frequenin (neuronal calcium sensor 1). *J. Biol. Chem. 276*, 11949-11955.

Bramham, C.R., Worley, P.F., Moore, M.J., and Guzowski, J. (2008). The immediate early gene arc/arg3.1: regulation, mechanisms, and function. *J. Neurosci.* 28, 11760-11767.

Brand, A.H. and Perrimon, N. (1993). Targeted gene expression as a means of altering cell fates and generating dominant phenotypes. *Development* 118, 401-415.

.**Brittis, P.A., Lu, Q., and Flanagan, J.G.** (2002). Axonal protein synthesis provides a mechanism for localized regulation at an intermediate target. *Cell.* 110, 223-235.

Broadie, K., Bellen, H. J., DiAntonio, A., Littleton, J. T., and Schwarz, T. L. (1994). Absence of synaptotagmin disrupts excitation-secretion coupling during synaptic transmission. Proc. Natl. Acad. Sci. U. S. A. *91*, 10727-10731.

Broadie, K., Prokop, A., Bellen, H. J., O'Kane, C. J., Schulze, K. L., and Sweeney, S. T. (1995). Syntaxin and synaptobrevin function downstream of vesicle docking in *Drosophila*. *Neuron. 15*, 663-673

Bronk, P., Deák, F., Wilson, M.C., Liu, X., Südhof, T.C., and Kavalali, E.T. (2007). Differential effects of SNAP-25 deletion on Ca2+ -dependent and Ca2+ independent neurotransmission. *J. Neurophysiol*. 98, 794-806

Bronk, P., Wenniger, J.J., Dawson-Scully, K., Guo, X., Hong, S., Atwood, H.L., and Zinsmaier, K.E. (2001). *Drosophila* Hsc70-4 is critical for neurotransmitter exocytosis in vivo. *Neuron.* 30, 475-88.

Brose, N., and Rosenmund, C. (2002). Move over protein kinase C, you've got company: alternative cellular effectors of diacylglycerol and phorbol esters.*J. Cell. Sci*.115, 4399-4411.

Bruneau, E.G. and Akaaboune, M. (2006). The dynamics of recycled acetylcholine receptors at the neuromuscular junction in vivo. *Development.* 133, 4485-4493.

Buchner, E. (1991). Genes expressed in the adult brain of *Drosophila* and effects of their mutations on behavior: a survey of transmitter- and second messenger-related genes. *J. Neurogenet.* 7, 153-192.

Bukharaeva, E.A., Samigullin, D., Nikolsky, E.E., and Magazanik, L.G. (2007). Modulation of the kinetics of evoked quantal release at mouse neuromuscular junctions by calcium and strontium. *J. Neurochem.* 100, 939-949.

Burg, M. G., Geng, C., Guan, Y., Koliantz, G., and Pak, W. L. (1996). *Drosophila* rosA gene, which when mutant causes aberrant photoreceptor oscillation, encodes a novel neurotransmitter transporter homologue. *J. Neurogenet*. 11, 59-79.

Burg, M. G., Sarthy, P. V., Koliantz, G., and Pak, W. L. (1993). Genetic and molecular identification of a *Drosophila* histidine decarboxylase gene required in photoreceptor transmitter synthesis. *Embo J.* 12, 911-919

Burgoyne, R.D., Barclay, J.W., Ciufo, L.F., Graham, M.E., Handley, M.T., and Morgan, A. (2009).The functions of Munc18-1 in regulated exocytosis. *Ann. N. Y. Acad. Sci*. 1152, 76-86.

.

Burgoyne, R.D., O'Callaghan, D.W., Hasdemir, B., Haynes, L.P., and Tepikin, A.V. (2004). Neuronal Ca2+-sensor proteins: multitalented regulators of neuronal function. *Trends. Neurosci.* 27, 203-209..

Burgoyne, R.D., and Weiss, J.L. (2001). The neuronal calcium sensor f amily of Ca2+-binding proteins. *Biochem. J.* 353, 1-12.

Campbell, D. L., Giles, W. R., and Shibata, E. F. (1988). Ion transfer characteristics of the calcium current in bull-frog atrial myocytes. *J. Physiol. 403*, 239-266.

Cesca F, Baldelli P, Valtorta F, Benfenati F. (2010). The synapsins: Key actors of synapse function and plasticity. *Prog. Neurobiol.* Ahead of Print.

Chapman, E.R., An, S., Edwardson, J.M., and Jahn, R.A (1996). Novel function for the second C2 domain of synaptotagmin. Ca^{2+}-triggered dimerization. *J. Biol. Chem.* 271, 5844-5849.

Chapman, E.R., Hanson, P.I., An, S., and Jahn, R. (1995). Ca^{2+} regulates the interaction between synaptotagmin and syntaxin 1. *J. Biol. Chem.* 270, 23667-23371.

Chapman, E.R. and Jahn, R. (1994).Calcium-dependent interaction of the cytoplasmic region of synaptotagmin with membranes. Autonomous function of a single C2-homologous domain. *J. Biol. Chem.* 269, 5735-41.

Cheever, A. and Ceman, S. (2009). Phosphorylation of FMRP inhibits association with Dicer. *RNA.* 15, 362-366.

Cheever, A. and Ceman, S. (2009). Translation regulation of mRNAs by the fragile X family of proteins through the microRNA pathway. *RNA Biol*. 6,2.

Chen, Y. A., Scales, S. J., Jagath, J. R., and Scheller, R. H. (2001). A discontinuous SNAP-25 C-terminal coil supports exocytosis. *J. Biol. Chem. 276*, 28503-28508

Chen, Z., Smith, K.R., Batterham, P., and Robin, C. (2005). *Smg1* nonsense mutations do not abolish nonsense-mediated mRNA decay in *Drosophila* melanogaster. *Genetics.* 171, 403-406.

Cheviet, S., Coppola, T., and Regazzi, R. (2005). Functional assays for he investigation of the role of Rab GTPase effectors in dense core granule release. *Methods. Enzymol.* 403, 57-71.

Collins, C.A., and DiAntonio, A. (2007). Synaptic development: insights from Drosophila. *Curr. Opin. Neurobiol*.17, 35-42.

Condrescu, M., Gardner, J. P., Chernaya, G., Aceto, J. F., Kroupis, C., and Reeves, J.P. (1995). ATP-dependent regulation of sodium-calcium exchange in Chinese hamster ovary cells transfected with the bovine cardiac sodium-calcium exchanger. *J.Biol. Chem*. *270*, 9137-9146.

Craig, E.A., Eisenman, H.C., Hundley, H.A. (2003). Ribosome-tethered molecular chaperones: the first line of defense against protein misfolding. *Curr. Opin. Microbiol.*157: 162.

Cremona, O. and De Camilli, P. (2001). Phosphoinositides in membrane traffic at the synapse. *J. Cell. Sci.* 114, 1041-1052.

Cremona, O. and De Camilli, P. (1997). Synaptic vesicle endocytosis. *Curr. Opin. Neurobiol.* 7, 323-330.

Daniels, R. W., Collins, C. A., Gelfand, M. V., Dant, J., Brooks, E. S., Krantz, D. E., and DiAntonio, A. (2004). Increased expression of the *Drosophila* vesicular glutamate transporter leads to excess glutamate release and a compensatory decrease in quantal content. *J. Neurosci.* 24, 10466-10474.

Davis, A.F., Bai, J., Fasshauer, D., Wolowick, M.J., Lewis, J.L., and Chapman, E.R. (1999). Kinetics of synaptotagmin responses to Ca^{2+} and assembly with the core SNARE complex onto membranes. *Neuron*. 24,363-376.

Deitcher, D.L., Ueda, A., Stewart, B.A., Burgess, R.W., Kidokoro, Y., and Schwarz, T.L. (1998). Distinct requirements for evoked and spontaneous release of neurotransmitter are revealed by mutations in the *Drosophila* gene neuronal-synaptobrevin. *J. Neurosci.* 18, 2028-2039

Del Castillo, J. and Katz, B. (1954). The failure of local-circuit transmission at the nerve-muscle junction. J. Physiol. *123*: 7-8P.

Demuro, A. and Parker, I. (2006). Imaging single-channel calcium microdomains. *Cell Calcium*. 40, 413-422.

Dermaut, B., Norga, K.K., Kania, A., Verstreken, P., Pan, H., Zhou, Y., Callaerts, P., and Bellen, H.J. (2005). Aberrant lysosomal carbohydrate storage accompanies endocytic defects and neurodegeneration in *Drosophila* benchwarmer. *J. Cell. Biol.* 170, 127-139.

DiAntonio, A. (2006). Glutamate receptors at the Drosophila neuromuscular junction. *Int. Rev. Neurobiol.* 75, 165-179.

DiAntonio, A., Petersen, S.A., Heckmann, M., and Goodman, C.S. (1999). Glutamate receptor expression regulates quantal size and quantal content at the *Drosophila* neuromuscular junction. *J. Neurosci.* 19, 3023-3032.

DiAntonio, A., and Schwarz, T. L. (1994). The effect on synaptic physiology ofsynaptotagmin mutations in *Drosophila*. *Neuron*. *12*: 909-920.

Dictenberg, J.B., Swanger, S.A., Antar, L.N., Singer, R.H., and Bassell, G.J. (2008). A direct role for FMRP in activity-dependent dendritic mRNA transport links filopodial-spine morphogenesis to fragile X syndrome. *Dev. Cell.* 14, 926-939.

Dodge, F. A. Jr. and Rahamimoff, R. (1967). Co-operative action a calcium ions in transmitter release at the neuromuscular junction. *J. Physiol.* 193, 419-432.

Dittman, J. and Ryan, T.A. (2009). Molecular circuitry of endocytosis at nerve terminals. *Annu. Rev. Cell Dev. Biol.* 25,133-160.

Duckles, S. P. and Budai, D. (1990). Stimulation intensity as critical determinant of presynaptic receptor effectiveness. *Trends. Pharmacol. Sci.* 11, 440-443.

Dulubova, I., Sugita, S., Hill, S., Hosaka, M., Fernandez, I., Südhof, T.C., and Rizo, J. (1999). A conformational switch in syntaxin during exocytosis: role of munc18. *EMBO J.* 18, 4372-4382.

Edwards, R.H. (2007). The neurotransmitter cycle and quantal size. *Neuron.* 20, 835-858.

Elbaz, Y., Danieli, T., Kanner, B.I., and Schuldiner, S. (2010). Expression of neurotransmitter transporters for structural and biochemical studies. *Protein Expr. Purif*. [Epub ahead of print].

Engels, W.R., Preston, C.R., Thompson, P., and Eggleston, W.B. (1989). In situ hybridization of *Drosophila* polytene chromosomes with digoxigenin-dUTP-labeled probes. *Trends Genetics.* 11, 366.

Farsad, K. and De Camilli, P. (2002). Neurotransmission and the synaptic vesicle cycle. *Yale. J. Biol. Med.* 75, 261-284.

Fdez, E. and Hilfiker, S. (2006). Vesicle pools and synapsins: new insights into old enigmas. *Brain Cell. Biol.* 35,107-115.

Featherstone, D. E., Davis, W. S., Dubreuil, R. R., and Broadie, K. (2001). *Drosophila* alpha- and beta-spectrin mutations disrupt presynaptic neurotransmitter release. J. Neurosci. 21, 4215-4224.

Featherstone, D.E., Rushton, E., Rohrbough, J., Liebl, F., Karr, J., Sheng, Q., Rodesch, C.K., and Broadie, K. (2005). An essential Drosophila glutamate receptor subunit that functions in both central neuropil and neuromuscular junction. *J. Neurosci*. 25, 3199-3208.

Fergestad, T. and Broadie, K. (2001). Interaction of stoned and synaptotagmin in synaptic vesicle endocytosis. *J. Neurosci*. *21*, 1218-1227.

Fon, E.A. and Edwards, R.H. (2001). Molecular mechanisms of neurotransmitter release. *Muscle Nerve.* 24, 581-601.

Frank, C.A., Kennedy, M.J., Goold, C.P., Marek, K.W., and Davis, G.W. (2006).Mechanisms underlying the rapid induction and sustained expression of synaptic homeostasis. *Neuron. 52*, 663-677.

Friedrich, R., Yeheskel, A., and Ashery, U. (2010). DOC2B, C2 domains, and calcium: A tale of intricate interactions. *Mol. Neurobiol.* 41, 42-51.

Fremeau, R.T. Jr, Burman, J., Qureshi ,T., Tran, C.H., Proctor, J., Johnson, J., Zhang, H., Sulzer, D., Copenhagen, D.R., Storm-Mathisen, J., Reimer, R.J., Chaudhry, F.A., and Edwards, R.H. (2002). The identification of vesicular glutamate transporter 3 suggests novel modes of signaling by glutamate. *Proc. Natl. Acad. Sci. U. S. A.* 99,14488-14893.

Frerking, M., Borges, S., and Wilson, M. (1995). Variation in GABA mini amplitude is the consequence of variation in transmitter concentration. Neuron. 15, 885-895.

Fykse, E.M. and Fonnum F. (1996). Amino acid neurotransmission: dynamics of vesicular uptake*. Neurochem. Res*. 21, 1053-1060.

Gawron, O., Keil, J. (1960).Competitive inhibition of acetylcholinesterase by several thiazolines and oxazolines. *Arch. Biochem. Biophys*. 89, 293-295.

Gatfield, D. and Izaurralde, E. (2004). Nonsense-mediated messenger RNA decay is initiated by endonucleolytic cleavage in *Drosophila*. *Nature*. 429, 575-578.

Gatto, C.L. and Broadie, K. (2008). Temporal requirements of the fragile X mental retardation protein in the regulation of synaptic structure. *Development.* 135, 2637-2648.

Gatto, C.L. and Broadie, K. (2009). The fragile X mental retardation protein in circadian rhythmicity and memory consolidation. *Mol. Neurobiol*. 39, 107-129.

Gearhart, J.M., Jepson, G.W., Clewell, H.J. 3rd, Andersen, M.E., and Conolly, R.B (1960). Physiologically based pharmacokinetic and pharmacodynamic model for the inhibition of acetylcholinesterase by diisopropylfluorophosphate. *Toxicol. Appl. Pharmacol.* 106, 295-310.

Gengs, C., Leung, H.T., Skingsley, D.R., Iovchev, M.I., Yin, Z., Semenov, E.P., Burg, M.G., Hardie, R.C. and Pak, W.L. (2002). The target of *Drosophila* photoreceptor synaptic transmission is a histamine-gated chloride channel encoded by ort (hclA). *J. Biol. Chem.* 277, 42113-42120.

Geppert, M., Goda, Y., Hammer, R. E., Li, C., Rosahl, T. W., Stevens, C. F., and Sudhof, T. C. (1994). Synaptotagmin I: a major Ca^{2+} sensor for transmitter release at a central synapse. *Cell*. 79, 717-727.

Gibbings, D.J., Ciaudo, C., Erhardt, M., and Voinnet, O. (2009). Multivesicular bodies associate with components of miRNA effector complexes and modulate miRNA activity. *Nat. Cell. Biol.* 11,1143-1149.

Giorgi, C., Yeo, G.W., Stone, M.E., Katz, D.B., Burge, C., Turrigiano, G., and Moore, M.J. (2007). The EJC factor eIF4AIII modulates synaptic strength and neuronal protein expression. *Cell.* 130, 179-191.

Gitler, D., Xu, Y., Kao, H.T., Lin, D., Lim, S., Feng, J., Greengard, P., and Augustine, GJ. (2004). Molecular determinants of synapsin targeting to presynaptic terminals. *J. Neurosci.* 24, 3711-3720.

Gitler, D., Cheng, Q., Greengard, P., and Augustine, G.J. (2008). Synapsin IIa controls the reserve pool of glutamatergic synaptic vesicles. *J. Neurosci.* 28, 10835-10843.

Goda, Y and Südhof, T.C. (1997). Calcium regulation of neurotransmitter release: reliably unreliable? *Curr. Opin. Cell. Biol*. 9, 513-518.

Gracheva, E.O, Burdina, A.O., Holgado, A.M., Berthelot-Grosjean, M., Ackley, B.D., Hadwiger, G., Nonet, M.L., Weimer, R.M., and Richmond JE. (2006). Tomosyn inhibits synaptic vesicle priming in Caenorhabditis elegans. *PLoS. Biol.* 4, e261.

Graham, M.E., Handley, M.T., Barclay, J.W., Ciufo, L.F., Barrow, S.L., Morgan, A., and Burgoyne, R.D. (2008). A gain-of-function mutant of Munc18-1 stimulates secretory granule recruitment and exocytosis and reveals a direct interaction of Munc18-1 with Rab3. *Biochem. J*. 409, 407-416.

Gras, C., Herzog, E., Bellenchi, G.C., Bernard, V., Ravassard, P., Pohl, M., Gasnier, B., Giros, B., and El Mestikawy, S. (2002). A third vesicular glutamate transporter expressed by cholinergic and serotoninergic neurons. *J. Neurosci.* 22, 5442-5451.

Greengard, P., Benfenati, F., and Valtorta, F. (1994). Synapsin I, an actin-binding protein regulating synaptic vesicle traffic in the nerve terminal.*Adv. Second Messenger Phosphoprotein Res*. 29, 31-45.

Groffen, A.J., Friedrich, R., Brian, E.C., Ashery, U., and Verhage, M. (2006). DOC2A and DOC2B are sensors for neuronal activity with unique calcium-dependent and kinetic properties. *J. Neurochem*. 97, 818-833.

Groth, A.C., Fish, M., Nusse, R., and Calos, M.P. (2004). Construction of transgenic *Drosophila* by using the site-specific integrase from phage phiC31. *Genetics.* 166, 1775-1782.

Gundelfinger, E.D., Kessels, M.M., and Qualmann, B. (2003).Temporal and spatial coordination of exocytosis and endocytosis. *Nat. Rev. Mol. Cell Biol.* 4, 127-139.

Gunter, T. E. and Pfeiffer, D. R. (1990). Mechanisms by which mitochondria transport calcium. Am. J. Physiol. 258, C755-786.

Haas, K.F. and Broadie, K. (2008). Roles of ubiquitination at the synapse. *Biochim. Biophys. Acta.* 1779, 495-506.

Haas, K.F., Miller, S.L., Friedman, D.B., and Broadie, K. (2007). The ubiquitin-proteasome system postsynaptically regulates glutamatergic synaptic function. *Mol. Cell. Neurosci.* 35, 64-75.

Haas, K.F., Woodruff, E. 3rd, and Broadie, K. (2007). Proteasome function is required to maintain muscle cellular architecture. *Biol. Cell* 11, 615-626.

Han, X., Wang, C.T., Bai, J., Chapman, E.R., and Jackson, M.B. (2004). Transmembrane segments of syntaxin line the fusion pore of Ca^{2+} - triggered exocytosis. *Science*. 304, 289-292.

Han, X. and Jackson, M.B. (2005). Electrostatic interactions between the syntaxin membrane anchor and neurotransmitter passing through the fusion pore. *Biophys. J.* 88(3), L20-22.

Hartveit, E., and Veruki ML. (2007). Studying properties of neurotransmitter receptors by non-stationary noise analysis of spontaneous postsynaptic currents and agonist-evoked responses in outside-out patches. *Nat. Protoc.* 2, 434-448.

Hay, J.C., and Martin, T.F. (1992). Resolution of regulated secretion into sequential MgATP-dependent and calcium-dependent stages mediated by distinct cytosolic proteins. *J. Cell. Biol.* 119,139-151.

Hengst, U. and Jaffrey, S.R. (2007). Function and translational regulation of mRNA in developing axons. *Semin. Cell. Dev. Biol.* 18, 209-215.

Heuser J, Katz B, and Miledi R. (1971). Structural and functional changes of frog neuromuscular junctions in high calcium solutions. *Proc. R. Soc. Lond. B. Biol. Sci*. 178, 407-415.

Heuser, J.E. and Reese, T.S. (1973). Evidence for recycling of synaptic vesicle membrane during transmitter release at the frog neuromuscular junction. *J. Cell Biol*. 57(2), 315-344.

Hilfiker, S., Benfenati, F., Doussau, F., Nairn, A.C., Czernik, A.J., Greengard, P., and Augustine, GJ. (2005). Structural domains involved in the regulation of transmitter release by synapsins. *J. Neurosci.* 25, 2658-2669.

Hille, B. (2001). Ion Channels of Excitable Membranes. (Sunderland, MA: Sinauer Associates.)

Hirota, S., Pertens, E., and Janssen, L. J. (2007). The reverse mode of theNa(+)/Ca(2+) exchanger provides a source of Ca(2+) for store refilling following agonist induced Ca(2+) mobilization. Am. J. Physiol. Lung. Cell. Mo.l Physiol. 292, L438-447.

Hodgkin, J., Papp, A., Pulak, R., Ambros, V., and Anderson, P. (1989). A new kind of informational suppression in the nematode Caenorhabditis elegans. *Genetics*. 123, 301-313.

Holm, S. (1979). A simple sequentially rejective multiple test procedure. *Scandanavian Journal of Statistics.* 6, 65-70.

Horrigan, F. T. and Bookman, R. J. (1994). Releasable pools and the kinetics of exocytosis in adrenal chromaffin cells. Neuron 13, 1119-1129.

Hosaka, M., Hammer, R.E., and Südhof, T.C. (1999). A phospho-switch controls the dynamic association of synapsins with synaptic vesicles. *Neuron*. 2, 377-387.

Hou, D., Suzuki, K., Wolfgang, W. J., Clay, C., Forte, M., and Kidokoro, Y. (2003). Presynaptic impairment of synaptic transmission in *Drosophila* embryos lacking Gs(alpha). *J. Neurosci.* 23, 5897-5905.

Hu, J.Y., Goldman, J., Wu, F., and Schacher, S. (2004). Target-dependent release of a presynaptic neuropeptide regulates the formation and maturation of specific synapses in Aplysia. *J. Neurosci*. 24, 9933-9943.

Hu, J.Y., Meng, X., and Schacher, S. (2002). Target interaction regulates distribution and stability of specific mRNAs. *J. Neurosci*. 22, 2669-2678.

Huang, F. D., Woodruff, E., Mohrmann, R., and Broadie, K. (2006). Rolling blackout is required for synaptic vesicle exocytosis. *J. Neurosci.* 26, 2369-2379

Jahn, R. (1999). Recycling of synaptic vesicle membrane within nerve terminals.*Brain Res. Bull*. 50, 313-314.

Jahn, R., Lang, T., and Südhof, T.C. (2003). Membrane fusion. *Cell*. 112, 519-33.

Jahn, R. and Südhof, T.C. (1999). Membrane fusion and exocytosis. *Annu. Rev. Biochem*. 68, 863-911.

James, D.J., Khodthong, C., Kowalchyk, J.A., and Martin, T.F. (2010). Phosphatidylinositol 4,5-bisphosphate regulation of SNARE function in membrane fusion mediated by CAPS. *Adv. Enzyme. Regul.* 50, 62-70.

Johnson, E. C. and Pak, W. L. (1986). Electrophysiological study of *Drosophila*rhodopsin mutants. *J. Gen. Physiol.* 88, 651-673

Jones, A.T, Mills, I.G., Scheidig, A.J., Alexandrov, K., and Clague, M.J. (1998). Inhibition of endosome fusion by wortmannin persists in the presence of activated Rab5. *Mol. Biol. Cell.* 9, 323-332.

Jordan, R., Lemke, E.A., and Klingauf, J. (2005).Visualization of synaptic vesicle movement in intact synaptic boutons using fluorescence fluctuation spectroscopy. *Biophys. J* 89, 2091-2102.

Jung, N. and Haucke, V. (2007). Clathrin-mediated endocytosis at synapses.*Traffic*. 8,1129-1136.

Kaeser, P.S., and Südhof, T.C. (2005). RIM function in short- and long-term synaptic plasticity. *Biochem. Soc. Trans.* 33,1345-1349.

Juranek, J., Mukherjee, K., Rickmann, M., Martens, H., Calka, J., Südhof, T.C., and Jahn, R. (2006). Differential expression of active zone proteins in neuromuscular junctions suggests functional diversification. *Eur. J. Neurosci.* 24, 3043-3052.

Kasri, N.N., Sienaert, I., Parys, J.B., Callewaert, G., Missiaen, L., Jeromin, A., and DeSmedt, H. (2003). A novel Ca^{2+} -induced Ca^{2+} release mechanism in A7r5 cells regulated by calmodulin-like proteins. *J. Biol. Chem.* 30, 27548-27555.

Kasuya, J., Ishimoto, H., and Kitamoto, T. (2009). Neuronal mechanisms of learning and memory revealed by spatial and temporal suppression of neurotransmission using shibire, a temperature-sensitive dynamin mutant gene in *Drosophila melanogaster*. *Front. Mol. Neurosci.* 2,11.

Katz, B. and Miledi, R. (1970). Further study of the role of calcium in synaptic transmission. *J. Physio*l. 207, 789-801

Katz, B. and Miledi, R. (1965). The Effect Of Calcium On Acetylcholine Release From Motor Nerve Terminals. *Proc. R. Soc. Lond. B. Biol. Sci.* 161, 496-503.

Katz, B. and Miledi, R. (1965). The effect of temperature on the synaptic delay at the neuromuscular junction. *J Physiol.* 181, 656-70.

Katz, B. and Miledi, R. (1968). The role of calcium in neuromuscular facilitation. *J. Physiol.*195, 481-492.

Kawasaki, F., Collins, S. C., and Ordway, R. W. (2002). Synaptic calcium-channel function in *Drosophila*: analysis and transformation rescue of temperature-sensitive paralytic and lethal mutations of cacophony. *J. Neurosci.* 22, 5856-5864.

Kawasaki, F., Felling, R., and Ordway, R. W. (2000). A temperature-sensitive paralytic mutant defines a primary synaptic calcium channel in *Drosophila*. *J. Neurosci.* 20, 4885-4889.

Kawasaki, F., Mattiuz, A. M., and Ordway, R. W. (1998). Synaptic physiology and ultrastructure in comatose mutants define an in vivo role for NSF in neurotransmitter release. *J. Neurosci*. 18, 10241-10249.

Kawasaki, F., Zou, B., Xu, X., and Ordway, R. W. (2004). Active zone localization of presynaptic calcium channels encoded by the cacophony locus of *Drosophila*. *J.Neurosci.* 24, 282-285.

Khare, P., White, A.R., Mulakaluri, A., and Parsons, S.M. (2010). Equilibrium binding and transport by vesicular acetylcholine transporter. *Methods Mol Biol.* 637,181-219.

Khvotchev, M. V., Ren, M., Takamori, S., Jahn, R., and Sudhof, T. C. (2003). Divergent functions of neuronal Rab11b in Ca^{2+} -regulated versus constitutive exocytosis. *J.Neurosci.* 23, 10531-10539.

Kidokoro, Y. (2003). Roles of SNARE proteins and synaptotagmin I in synaptic transmission: studies at the *Drosophila* neuromuscular synapse*. Neurosignals.* 12, 13-30.

Kidokoro, Y., Kuromi, H., Delgado, R., Maureira, C., Oliva, C., and Labarca, P. (2004). Synaptic vesicle pools and plasticity of synaptic transmission at the *Drosophila* synapse. *Brain Res Rev.* 47, 18-32.

Kiebler, M.A. and Bassell, G.J. (2006). Neuronal RNA granules: movers and makers. *Neuron.* 51, 685-690.

Kim, N.C., and Marqués, G. (2010). Identification of downstream targets of the Bone Morphogenetic Protein pathway in the Drosophila nervous system. Dev*. Dyn.* [Epub ahead of print].

Kittel, R. J., Wichmann, C., Rasse, T. M., Fouquet, W., Schmidt, M., Schmid, A., Wagh, D. A., Pawlu, C., Kellner, R. R., Willig, K. I.*, et al.* (2006). Bruchpilot promotes active zone assembly, Ca^{2+} channel clustering, and vesicle release. *Science.* 312, 1051-1054

Kiyonaka, S., Wakamori, M., Miki, T., Uriu, Y., Nonaka, M., Bito, H., Beedle, A.M., Mori, E., Hara, Y., De Waard, M., Kanagawa, M., Itakura, M., Takahashi, M., Campbell, K.P., and Mori, Y. (2007). RIM1 confers sustained activity and neurotransmitter vesicle anchoring to presynaptic Ca2+ channels. *Nat.Neurosci.* 10, 691-701.

Koenig, J.H. and Ikeda, K. (1996). Synaptic vesicles have two distinct recycling pathways. *J. Cell. Biol.* 135,797-808.

Koenig, J. H., Yamaoka, K., and Ikeda, K. (1998). Omega images at the active zone may be endocytotic rather than exocytotic: implications for the vesicle hypothesis of transmitter release. *Proc. Natl. Acad. Sci. U. S. A*. 95, 12677-12682.

Kosaka, T., and Ikeda, K. (1983). Reversible blockage of membrane retrieval and endocytosis in the garland cell of the temperature-sensitive mutant of Drosophila melanogaster, shibirets1. *J. Cell. Biol.* 97, 499-507.

Kurdyak, P., Atwood, H.L., Stewart, B.A., and Wu, C.F. (1994). Differential physiology and morphology of motor axons to ventral longitudinal muscles in larval *Drosophila*. *J. Comp. Neurol.* 350, 463-472.

Kuromi, H. and Kidokoro, Y. (1998). Two distinct pools of synaptic vesicles in single presynaptic boutons in a temperature-sensitive *Drosophila* mutant, shibire. *Neuron*. 20, 917-925

Kuromi, H. and Kidokoro, Y. (2000). Tetanic stimulation recruits vesicles from reserve pool via a cAMP-mediated process in *Drosophila* synapses. *Neuron.* 27, 133-143.

Lam, G. and Thummon C. S. (2002). Inducible expression of double stranded RNA directs specific genetic interference in *Drosophila*. *Current Biology*. 10, 957-963.

Larivee, D.C., Conrad, S.K., Stephenson, R.S., Pak, W.L. (1981). Mutation thatselectively affects rhodopsin concentration in the peripheral photoreceptors of*Drosophila* melanogaster. *J.Gen. Physiol.* 78, 521-545

Leung, H.T., Geng, C., and Pak, W.L. (2000). Phenotypes of trpl mutants and interactions between the transient receptor potential (TRP) and TRP-like channels in Drosophila. *J. Neurosci.* 20, 6797-6803.

Leung, H.T., Tseng-Crank, J., Kim, E., Mahapatra, C., Shino, S., Zhou, Y., An, L., Doerge, R.W., and Pak, W.L. (2008). DAG lipase activity is necessary for TRP channel regulation in *Drosophila* photoreceptors. *Neuron*. 58, 884-896.

Leveque, C., el Far, O., Martin-Moutot, N., Sato, K., Kato, R., Takahashi, M., and Seagar, M. J. (1994). Purification of the N-type calcium channel associated with syntaxin and synaptotagmin. A complex implicated in synaptic vesicle exocytosis. *J. Biol. Chem*. 269, 6306-6312.

Li, H., Peng, X., and Cooper R.L. (2002). Development of *Drosophila* larval neuromuscular junctions: maintaining synaptic strength. *Neuroscience*. 115, 505-513.

Li, Y.C., Bai, W.Z., Zhou, L., Sun, L.K., and Hashikawa, T. (2010). Nonhomogeneous distribution of filamentous actin in the presynaptic terminals on the spinal motoneurons. *J. Comp. Neurol*. 518, 3184-3192.

Liang, F., Cunningham, K. W., Harper, J. F., and Sze, H. (1997). ECA1 complements yeast mutants defective in Ca^{2+} pumps and encodes an endoplasmic reticulum-type Ca^{2+} -ATPase in Arabidopsis thaliana. *Proc. Natl. Acad. Sci. U. S. A*. 94, 8579-8584.

Lima, S.Q. and Miesenbock, G. (2005). Remote control of behavior through genetically targeted photostimulation of neurons. Cell. 121:141-152.

Lin, A.C. and Holt, C.E. (2007). Local translation and directional steering in axons. *EMBO*. 26, 3729-3736.

Lin, A.C. and Holt, C.E. (2008). Outsourcing CREB translation to axons to survive. *Nat. Cell. Biol.* 10, 115-118.

.**Lin, R.C. and Scheller, R.H.** (2000). Mechanisms of synaptic vesicle exocytosis*Annu. Rev. Cell. Dev. Biol*. 16,19-49.

Lin, X.G., Ming, M., Chen, M.R., Niu, W.P., Zhang, Y.D., Liu, B., Jiu, Y.M., Yu, J.W., Xu, T., and Wu, Z.X. (2010). UNC-31/CAPS docks and primes dense core vesicles in C. elegans neurons. *Biochem. Biophys. Res. Commun*. [Epub Ahead of Print].

Lindsley, D.L. and Zimm, G.G. (1992). The genome of *Drosophila* melanogaster. Academic Press, New York.

Littleton, J. T., Bai, J., Vyas, B., Desai, R., Baltus, A. E., Garment, M. B., Carlson, S. D.,Ganetzky, B., and Chapman, E. R. (2001). Synaptotagmin mutants reveal essential functions for the C2B domain in Ca^{2+} -triggered fusion and recycling of synaptic vesicles in vivo. *J. Neurosci.* 21, 1421-1433.

Littleton, J.T., Barnard. R.J., Titus, S.A., Slind , J., Chapman, E.R, and Ganetzky, B. (2001). SNARE-complex disassembly by NSF follows synaptic-vesicle fusion. *Proc. Natl. Acad. Sci. U S A.* 98,12233-12238

Littleton, J. T., Bellen, H. J., and Perin, M. S. (1993). Expression of synaptotagmin in *Drosophila* reveals transport and localization of synaptic vesicles to the synapse. *Development.* 118, 1077-1088.

Littleton, J. T., Chapman, E. R., Kreber, R., Garment, M. B., Carlson, S. D., and Ganetzky, B. (1998). Temperature-sensitive paralytic mutations demonstrate that synaptic exocytosis requires SNARE complex assembly and disassembly. *Neuron.* 21,401-413.

Littleton, J. T. and Ganetzky, B. (2000). Ion channels and synaptic organization: analysis of the *Drosophila* genome. *Neuron*. 26, 35-43.

Littleton, J. T., Stern, M., Perin, M., and Bellen, H. J. (1994). Calcium dependence of neurotransmitter release and rate of spontaneous vesicle fusions are altered in *Drosophila* synaptotagmin mutants. *Proc. Natl. Acad. Sci. U. S. A*. 91, 10888-10892.

Liu, G., Choi, S., and Tsien, R.W. (1999).Variability of neurotransmitter concentration and nonsaturation of postsynaptic AMPA receptors at synapses in hippocampal cultures and slices. *Neuron*. 2, 395-409.

Liu, G., and Tsien, R.W. (1995).Synaptic transmission at single visualized hippocampal boutons. Neuropharmacology. 34, 1407-1421.

Liu, Y.L., Connoley, I.P., Harrison, J., Heal, D.J., and Stock, M.J. (2002).Comparison of the thermogenic and hypophagic effects of sibutramine's metabolite 2 and other monoamine reuptake inhibitors. *Eur. J. Pharmacol.* 452, 49-56.

Liu, Y., Peter, D., Roghani, A., Schuldiner, S., Privé, G.G., Eisenberg, D., Brecha, N., and Edwards, R.H. (1992). A cDNA that suppresses MPP+ toxicity encodes a vesicular amine transporter. *Cell*. 70, 539-551

Llinas, R., Steinberg, I. Z., and Walton, K. (1976). Presynaptic calcium currents and their relation to synaptic transmission: voltage clamp study in squid giant synapse and theoretical model for the calcium gate. *Proc. Natl. Acad. Sci. U. S. A.* 73, 2918-2922.

Llinas, R., Sugimori, M., and Silver, R. B. (1992). Microdomains of high calcium concentration in a presynaptic terminal. *Science.* 256, 677-679.

Lnenicka, G. A., Grizzaffi, J., Lee, B., and Rumpal, N. (2006). Ca^{2+} dynamics along identified synaptic terminals in *Drosophila* larvae. *J. Neurosci*. 26, 12283-12293.

Long, A.A., Kim, E., Leung, H.T., Woodruff, E. 3rd, An, L., Doerge, R.W., Pak, W.L., and Broadie, K. (2008). Presynaptic calcium channel localization and calcium-dependent synaptic vesicle exocytosis regulated by the Fuseless protein. *J. Neurosci.* 28, 3668-3682.

Loyet, K.M., Kowalchyk, J.A., Chaudhary, A., Chen, J., Prestwich, G.D., and Martin, T.F. (1998). Specific binding of phosphatidylinositol 4, 5-bisphosphate to calcium-dependent activator protein for secretion (CAPS), a potential phosphoinositide effector protein for regulated exocytosis. *J. Biol. Chem.* 273, 8337-43.

Madison, J.M., Nurrish, S., and Kaplan, J.M. (2005). UNC-13 interaction with syntaxin is required for synaptic transmission. *Curr. Biol.* 15, 2236-2242.

Markow, T. A., and Merriam, J. (1977). Phototactic and geotactic behavior of countercurrent defective mutants of *Drosophila* melanogaster. *Behav. Genet*. 7, 447-455.

Martelli, A.M., Baldini, G., Tabellini, G., Koticha, D., Bareggi, R., and Baldini, G. (2000). Rab3A and Rab3D control the total granule number and the fraction of granules docked at the plasma membrane in PC12 cells. *Traffic.* 1, 976-986.

Maruyama, I.N., and Brenner, S. (1991). A phorbol ester/diacylglycerol-binding protein encoded by the unc-13 gene of Caenorhabditis elegans. *Proc. Natl. Acad. Sci. U. S. A.* 88, 5729-5733.

Maximov, A., and Bezprozvanny, I. (2002). Synaptic targeting of N-type calcium channels in hippocampal neurons. *J. Neurosci*. *22*, 6939-6952.

Maycox, P.R., Deckwerth, T., Hell, J.W., and Jahn, R. (1998). Glutamate uptake by brain synaptic vesicles. Energy dependence of transport and functional reconstitution in proteoliposomes. *J. Biol. Chem.* 263,15423-15428.

McIntyre, D.C., Hutcheon, B., Schwabe, K., and Poulter, M.O. (2002). Divergent GABA(A) receptor-mediated synaptic transmission in genetically seizure-prone and seizure-resistant rats. *J. Neurosci.* 22, 9922 -9931.

Merrifield, C.J., Perrais, D., and Zenisek, D. (2005). Coupling between clathrin-coated-pit invagination, cortactin recruitment, and membrane scission observed in live cells. *Cell.* 121, 593-606.

Messa, M., Congia, S., Defranchi, E., Valtorta, F., Fassio, A., Onofri, F., and Benfenati, F. (2010).Tyrosine phosphorylation of synapsin I by Src regulates synaptic-vesicle trafficking. *J. Cell. Sci.* Ahead of Print.

McEwen, J.M., Madison, J.M., Dybbs, M., and Kaplan, J.M. (2006). Antagonistic regulation of synaptic vesicle priming by Tomosyn and UNC-13. *Neuron.* 51, 303-315.

Metzstein, M.M. and Krasnow, M.A. (2006). Functions of the nonsense-mediated mRNA decay pathway in *Drosophila* development. *PLoS Genet*. 2, e180.

Miller, R. J. (1991). The control of neuronal Ca^{2+} homeostasis. *Prog. Neurobiol.* 37, 255-285.

Miller, T.M. and Heuser, J.E. (1984). Endocytosis of synaptic vesicle membrane at the frog neuromuscular junction. *J. Cell Biol.* 98, 685-698

Mirotznik, R. R., Zheng, X., and Stanley, E. F. (2000). G-Protein types involved in calcium channel inhibition at a presynaptic nerve terminal. *J.*

Neurosci. 20, 7614-7621.

Miyoshi, K., Okada, T.N., Siomi, H., and Siomi, M.C. (2009). Characterization of the miRNA-RISC loading complex and miRNA-RISC formed in the *Drosophila* miRNA pathway. *RNA.* 15, 1282-1291.

Mochida, S., Kobayashi, H., Matsuda, Y., Yuda, Y., Muramoto, K., and Nonomura Y. (1994). Myosin II is involved in transmitter release at synapses formed between rat sympathetic neurons in culture. *Neuron.* 13,1131-1142.

Mochida, S., Sheng, Z. H., Baker, C., Kobayashi, H., and Catterall, W. A. (1996). Inhibition of neurotransmission by peptides containing the synaptic protein interaction site of N-type Ca^{2+} channels. *Neuron.* 17, 781-788.

Morgan, J.R., Prasad, K., Jin, S., Augustine, G.J., and Lafer, E.M. (2003). Eps15 homology domain-NPF motif interactions regulate clathrin coat assembly during synaptic vesicle recycling. *J. Biol. Chem.* 278, 33583-33592.

Morimoto, T., Nobechi, M., Komatsu, A., Miyakawa, H., and Nose, A. (2010). Subunit-specific and homeostatic regulation of glutamate receptor localization by CaMKII in Drosophila neuromuscular junctions. *Neuroscience.* 165,1284-1292.

Murthy, V.N., and Stevens, C.F. (1999). Reversal of synaptic vesicle docking at central synapses. *Nat. Neurosci.* 6, 503-507

Nagel, G., Brauner, M., Liewald, J.F., Adeishvili, N., Bamberg, E., Gottschalk, A. (2005). Light activation of channelrhodopsin-2 in excitable cells of *C. Elegans* triggers rapid behavioral responses. *Curr.Biol.* 15: 2279-2284.

Nagerl, U. V. and Mody, I. (1998). Calcium-dependent inactivation of high-threshold calcium currents in human dentate gyrus granule cells. *J. Physiol*. 509 *(*Pt 1), 39-45.

Nahm, M., Kim, S., Paik, S.K., Lee, M., Lee, S., Lee, Z.H., Kim, J., Lee, D., Bae, Y.C., and Lee, S. (2010). dCIP4 Drosophila Cdc42-interacting protein 4restrains synaptic growth by inhibiting the secretion of the retrograde Glass bottom boat signal. *J.Neurosci.* 30, 8138-8150.

Nakai, J., Ohkura, M., and Imoto, K. (2001). A high signal-to-noise Ca(2+) probe composed of a single green fluorescent protein. *Nat. Biotechnol.* 19, 137-141.

Nakata, K., Abrams, B., Grill, B., Goncharov, A., Huang, X., Chisholm AD, and Jin, Y. (2005). Regulation of a DLK-1 and p38 MAP kinase pathway by the ubiquitin ligase RPM-1 is required for presynaptic development. *Cell.* 120, 407-420.

Nicholls, D. G. (1985). A role for the mitochondrion in the protection of cells against calcium overload? *Prog. Brain Res.* 63, 97-106.

Nishimune, H., Sanes, J. R., and Carlson, S. S. (2004). A synaptic laminin-calcium channel interaction organizes active zones in motor nerve terminals. *Nature* 432, 580-587.

Nojiri, M., Loyet, K.M., Klenchin, V.A., Kabachinski, G., and Martin, T.F. (2009). CAPS activity in priming vesicle exocytosis requires CK2 phosphorylation. *J. Biol. Chem*. 284,18707-18714.

Nonet, M.L., Staunton, J.E., Kilgard, M.P., Fergestad, T., Hartwieg, E., Horvitz, H.R., Jorgensen, E.M., and Meyer, B.J. (1997). Caenorhabditis elegans rab-3 mutant synapses exhibit impaired function and are partially depleted of vesicles. *J. Neurosci.* 17, 8061-8073

Ohnishi, O. (1977). Spontaneous and ethyl methanesulfonate-induced mutations controlling viability in *Drosophila* melanogaster. III. Heterozygous effect of polygenic mutations. *Genetics.* 87, 547-556.

Onoa, B., Li, H., Gagnon-Bartsch, J.A., Elias, L.A., and Edwards, R.H. (2010). Vesicular monoamine and glutamate transporters select distinct synaptic vesicle recycling pathways. *J. Neurosci.* 30, 7917-7927.

Opazo, F., and Rizzoli, S.O. (2010).Studying synaptic vesicle pools using photoconversion of styryl dyes. *J. Vis. Exp*. 36, 1790.

Osborne, S.L., Herreros, J., Bastiaens, P.I., and Schiavo, G. (1999). Calcium-dependent oligomerization of synaptotagmins I and II. Synaptotagmins I and II are localized on the same synaptic vesicle and heterodimerize in the presence of calcium. *J. Biol. Chem.* 274, 59-66

Owen, D. J., Vallis, Y., Noble, M. E., Hunter, J. B., Dafforn, T. R., Evans, P. R., and McMahon, H. T. (1999). A structural explanation for the binding of multiple ligands by the alpha-adaptin appendage domain. *Cell*. 97, 805-815.

Owald, D. and Sigrist, S.J. (2009). Assembling the presynaptic active zone. *Curr. Opin. Neurobiol.* 19, 311-318.

Oyler, G.A., Higgins, G.A., Hart, R.A., Battenberg, E., Billingsley, M., Bloom, F.E., and Wilson, M.C. (1989). The identification of a novel synaptosomal-associated protein, SNAP-25, differentially expressed by neuronal subpopulations. *J. Cell. Biol.* 109, 3039-3052.

Pak, W.L. (1995). *Drosophila* in vision research. The Friedenwald Lecture. *Invest. Ophthalmol. Vis. Sci.* 36, 2340-2357.

Pak, W.L. 1975. Mutations affecting the vision of *Drosophila melanogaster*. pp. 703-733. In R.C. King (ed.), Handbook of Genetics, Vol. 3. Plenum, New York.

Pak, W.L. and Boes, R.J. (1967). Rhodopsin: responses from transient intermediates formed during its bleaching. *Science.* 155, 1131-1133.

Pak, W.L., Grossfield, J., and Arnold, K.S. (1970). Mutants of the visual pathway of *Drosophila* melanogaster. *Nature*. 227, 518-520

Pak, W.L., Grossfield, J., and White, N.V. (1969). Nonphototactic mutants in a study of vision of *Drosophila*. *Nature*. 222, 351-354.

Pak, W.L. and H.-T. Leung (2003). Genetic Approaches to Visual Transduction in *Drosophila melanogaster.* In Emerging aspects of heterotrimeric G protein-mediated signaling, *P. Chidiac, ed. Receptors Channels* 9, 149-167.

Pan, C. Y., Jeromin, A., Lundstrom, K., Yoo, S. H., Roder, J., and Fox, A. P. (2002). Alterations in exocytosis induced by neuronal Ca^{2+} sensor-1 in bovine chromaffin cells. *J. Neurosci.* 22, 2427-2433

Pan, L., Zhang, Y.Q., Woodruff, E. 3rd, and Broadie, K. (2004). The *Drosophila* fragile X gene negatively regulates neuronal elaboration and synaptic differentiation. *Curr. Biol*. 14, 1863-1870.

Pan, L. and Broadie, K. (2007). *Drosophila* fragile X mental retardation protein and metabotropic glutamate receptor A convergently regulate the synaptic ratio of ionotropic glutamate receptor subclasses. *J. Neurosci.* 27, 12378-12389.

Pan, L., Woodruff, E. 3rd, Liang, P., and Broadie, K. (2008). Mechanistic relationships between *Drosophila* fragile X mental retardation protein and metabotropic glutamate receptor A signaling. *Mol. Cell. Neurosci.* 37, 747-760.

Pang, Z.P., and Südhof, T.C. (2010). Cell biology of Ca(2+)-triggered exocytosis. *Curr. Opin. Cell. Biol.* [Epub Ahead of Print].

Park, E.C., Glodowski, D.R., and Rongo, C. (2009). The ubiquitin ligase RPM-1 and the p38 MAPK PMK-3 regulate AMPA receptor trafficking. *PLoS One* 4(1), e4284.

Perin, M.S., Fried, V.A., Mignery, G.A., Jahn, R., and Südhof TC. (1990). Phospholipid binding by a synaptic vesicle protein homologous to the regulatory region of protein kinase C. *Nature*. 345,260-263

Pfeiffer, B.E. and Huber, K.M. (2009). The State of Synapses in Fragile X Syndrome. *Neuroscientist*. 15, 549-567.

Pillai, R.S., Bhattacharyya, S.N., Artus, C.G., Zoller, T., Cougot, N., Basyuk, E., Bertrand, E., and Filipowicz, W. (2005). Inhibition of translational initiation by Let-7 MicroRNA in human cells. *Science.* 309, 1573-1576.

Piper, M. and Holt, C. (2004). RNA translation in axons. *Annu. Rev. Cell. Dev. Biol*. 20, 505-523.

Pongs, O. (1993). Structure-function studies on the pore of potassium channels. *J.Membr. Biol*. 136, 1-8.

Poodry, C.A., and Edgar, L. (1979). Reversible alteration in the neuromuscular junctions of Drosophila melanogaster bearing a temperature-sensitive mutation, shibire.*J. Cell. Biol.* 81, 520-527.

Prasad, V., Okunade, G., Liu, L., Paul, R.J., Shull, G.E. (2007). Distinct phenotypes among plasma membrane Ca^{2+} -ATPase knockout mice. Ann N Y Acad Sci *1099*, 276-286.

Pucadyil, T.J. and Schmid, S.L. (2009). Conserved functions of membrane active GTPases in coated vesicle formation. *Science*. 325,1217-1220.

Pyle, J.L., Kavalali, E.T., Piedras-Rentería, E.S., and Tsien, RW. (2000). Rapid reuse of readily releasable pool vesicles at hippocampal synapses. *Neuron*. 28, 221-231.

Raastad, M., Storm, J.F., and Andersen, P. (1992). Putative Single Quantum and Single Fibre Excitatory Postsynaptic Currents Show Similar Amplitude Range and Variability in Rat Hippocampal Slices. *Eur. J. Neurosci.* 4,113-117.

Raftery, L.A., and Sutherland, D.J. (1999). TGF-beta family signal transduction in Drosophila development: from Mad to Smads. *Dev. Biol.* 210, 251-268.

Rao, S.S., Stewart, B.A., Rivlin, P.K., Vilinsky, I., Watson, B.O., Lang, C., Boulianne, G., Salpeter, M.M., and Deitcher, D.L. (2001). Two distinct effects on neurotransmission in a temperature-sensitive SNAP-25 mutant. *EMBO J.* 20, 6761-6771.

Reiff, D. F., Ihring, A., Guerrero, G., Isacoff, E. Y., Joesch, M., Nakai, J., and Borst, A. (2005). In vivo performance of genetically encoded indicators of neural activity in flies. *J.Neurosci. 25*, 4766-4778.

Renden, R., Berwin, B., Davis, W., Ann, K., Chin, C.T., Kreber, R., Ganetzky B., Martin, T.F., and Broadie, K. (2001). Drosophila CAPS is an essential gene that regulates dense-core vesicle release and synaptic vesicle fusion. *Neuron*. 31,421–437.

Repicky, S. and Broadie, K. (2009). Metabotropic glutamate receptor-mediated use-dependent down-regulation of synaptic excitability involves the fragile X mental retardation protein. *J. Neurophysiol.* 101, 672-687.

Rhee, J.S., Betz, A., Pyott, S., Reim, K., Varoqueaux, F., Augustin, I., Hesse, D., Südhof, T.C., Takahashi, M., Rosenmund, C., and Brose, N. (2002). Beta phorbol ester- and diacylglycerol-induced augmentation of transmitter release is mediated by Munc13s and not by PKCs. *Cell*. 108,121-133.

Richards, D.A., Guatimosim, C., and Betz, W.J. (2000). Two endocytic recycling routes selectively fill two vesicle pools in frog motor nerve terminals. *Neuron*. 27,551-559.

Richmond, J. E., and Broadie, K. S. (2002). The synaptic vesicle cycle: exocytosis and endocytosis in *Drosophila* and *C. elegans*. *Curr. Opin. Neurobiol.* 12, 499-507.

Richmond, J.E., Davis, W.S., and Jorgensen, E.M. (1999). UNC-13 is required for synaptic vesicle fusion in *C. elegans Nat. Neurosci*. 2, 959-964.

Richmond JE, Weimer RM, and Jorgensen EM. (2001). An open form of syntaxin bypasses the requirement for UNC-13 in vesicle priming. *Nature.* 19, 412338-412441

Rickman, C., and Davletov, B. (2005). Arachidonic acid allows SNARE complex formation in the presence of Munc18. *Chem. Biol.* 12, 545-553.

Rickman, C., Hu, K., Carroll, J., and Davletov, B. (2005).Self-assembly of SNARE fusion proteins into star-shaped oligomers. *Biochem. J*. 388, 75-79.

Rizo, J., and Sudhof, T. C. (2002). Snares and Munc18 in synaptic vesicle fusion. *Nat. Rev. Neurosci*. 3, 641-653.

Rizzoli, S.O. and Betz, W.J. (2005). Synaptic vesicle pools. *Nat. Rev. Neurosci*. 6,57-69.

Roghani, A., Feldman, J., Kohan, S.A., Shirzadi, A., Gundersen, C.B., Brecha, N., and Edwards, R.H. (1994). Molecular cloning of a putative vesicular transporter for acetylcholine. *Proc. Natl. Acad. Sci. U. S. A.* 91,10620-10624.

Rohrbough, J. and Broadie, K. (2005). Lipid regulation of the synaptic vesicle cycle. *Nat. Rev. Neurosci.* 2, 139-50.

Rohrbough, J., Pinto, S., Mihalek, R.M., Tully, T., and Broadie, K. (1999). latheo, a *Drosophila* gene involved in learning, regulates functional synaptic plasticity. *Neuron*. 23, 55-70.

Rosenmund, C., Rettig, J., and Brose, N. (2003). Molecular mechanisms of active zone function. *Curr. Opin. Neurobiol.* 13, 509-519.

Rosenmund, C., Sigler, A., Augustin, I., Reim, K., Brose, N., and Rhee, J.S. (2002). Differential control of vesicle priming and short-term plasticity by Munc13 isoforms. *Neuron.* 33, 411-424.

Sagné, C., El Mestikawy, S., Isambert, M.F., Hamon, M., Henry, J.P., Giros, B., and Gasnier, B. (1997). Cloning of a functional vesicular GABA and glycine transporter by screening of genome databases.*F.E.B.S Lett*. 417,177-183.

Sánchez-Gracia, A., Romero-Pozuelo, J., and Ferrús, A. (2010). Two frequenins in Drosophila: unveiling the evolutionary history of an unusual neuronal calcium sensor (NCS) duplication. *BMC. Evol. Biol.* 10, 54.

Schacher, S. and Wu, F. (2002). Synapse formation in the absence of cell bodies requires protein synthesis. *J. Neurosci.* 22, 1831-1839.

Schäfer, M.K., Varoqui, H., Defamie, N., Weihe, E., and Erickson, J.D. (2002).Molecular cloning and functional identification of mouse vesicular glutamate transporter 3 and its expression in subsets of novel excitatory neurons.*J. Biol. Chem.* 277, 50734-50748.

Schiavo, G., Matteoli, M., and Montecucco, C. (2000). Neurotoxins affecting neuroexocytosis. *Physiol Rev*. 80,717-766.

Schiavo, G., Stenbeck, G., Rothman, J.E., and Söllner, T.H. (1997). Binding of the synaptic vesicle v-SNARE, synaptotagmin, to the plasma membrane t-SNARE, SNAP-25, can explain docked vesicles at neurotoxin-treated synapses. *Proc. Natl. Acad. Sci. U. S. A.* 94, 997-1001.

Schoch, S., Deák, F., Königstorfer A., Mozhayeva, M., Sara, Y., Südhof, T.C., and Kavalali, E.T. (2001). SNARE function analyzed in synaptobrevin/VAMP knockout mice. *Science.* 294,1117-1122.

Schorge, S., Gupta, S., Lin, Z., McEnery, M. W., and Lipscombe, D. (1999). Calcium channel activation stabilizes a neuronal calcium channel mRNA. Nat*. Neurosci*. 2, 785-790.

Schulze, K.L., Broadie, K., Perin, M.S., and Bellen, H.J. (1995). Genetic and electrophysiological studies of *Drosophila* syntaxin-1A demonstrate its role in nonneuronal secretion and neurotransmission. *Cell.* 80, 311-320.

Schwarz, E. M., and Benzer, S. (1997). Calx, a Na-Ca exchanger gene of *Drosophila* melanogaster. *Proc. Natl. Acad. Sci. U. S. A* .94, 10249-10254.

Sebeo, J., Hsiao, K., Bozdagi, O., Dumitriu, D., Ge, Y., Zhou, Q., and Benson, D.L. (2009). Requirement for protein synthesis at developing synapses. *J. Neurosci.* 31, 9778-9793.

Sheng, Z. H., Westenbroek, R. E., and Catterall, W. A. (1998). Physical link and functional coupling of presynaptic calcium channels and the synaptic vesicle docking/fusion machinery. *J. Bioenerg. Biomembr*. 30, 335-345.

Sherff, C.M. and Carew, T.J. (1999). Coincident induction of long-term facilitation in Aplysia: cooperativity between cell bodies and remote synapses. *Science* 285, 1911-1914.

Sherff, C.M. and Carew, T.J. (2002). Coincident induction of long-term facilitation at sensory-motor synapses in Aplysia: presynaptic and postsynaptic factors. *Neurobiol. Learn. Mem.* 78, 498-507.

Shibuya, T., Tange, T., Sonenberg, N., and Moore, M.J. (2004). eIF4AIII binds spliced mRNA in the exon junction complex and is essential for nonsense-mediated decay. *Nat. Struct. Mol. Biol.* 11, 346-351.

Shibuya, T., Tange, T., Stroupe, M.E., and Moore, M.J. (2006). Mutational analysis of human eIF4AIII identifies regions necessary for

exon junction complex formation and nonsense-mediated mRNA decay. *RNA.* 12, 360-374.

Silver, R.A., Cull-Candy, S.G., and Takahashi, T. (1996). Non-NMDA glutamate receptor occupancy and open probability at a rat cerebellar synapse with single and multiple release sites. *J. Physiol.* 494, 231-250.

Sippy, T., Cruz-Martin, A., Jeromin, A., and Schweizer, F. E. (2003). Acute changes in short-term plasticity at synapses with elevated levels of neuronal calcium sensor-1. *Nat. Neurosci*. 6, 1031-1038.

Slepnev, V.I. and De Camilli, P. (2000). Accessory factors in clathrin-dependent synaptic vesicle endocytosis. *Nat. Rev. Neurosci.* 3, 161-172.

Smith, D. O. (1988). Muscle-specific decrease in presynaptic calcium dependence and clearance during neuromuscular transmission in aged rats. *J. Neurophysiol*. 59, 1069-1082.

Söllner, T., Bennett, M.K., Whiteheart, S.W., Scheller, R.H., and Rothman, J.E. (1993). A protein assembly-disassembly pathway in vitro that may correspond to sequential steps of synaptic vesicle docking, activation, and fusion. *Cell*. 75, 409-418.

Sørensen, J.B. (2005). SNARE complexes prepare for membrane fusion. *Trends Neurosci.* 28,453-455.

Speese, S., Petrie, M., Schuske, K., Ailion, M., Ann, K., Iwasaki, K., Jorgensen, E.M., and Martin, T.F. (2007). UNC-31 (CAPS) is required for dense-core vesicle but not synaptic vesicle exocytosis in Caenorhabditis elegans. *J. Neurosci.* 27, 6150-6162.

Speese, S.D., Trotta, N., Rodesch, C.K., Aravamudan, B., and Broadie, K. (2003). The ubiquitin proteasome system acutely regulates presynaptic protein turnover and synaptic efficacy. *Curr. Biol.* 13, 899-910.

Speidel, D., Varoqueaux, F., Enk, C., Nojiri, M., Grishanin, R.N., Martin, T.F., Hofmann, K., Brose, N., and Reim, K. (2003). A family of Ca2+-dependent activator proteins for secretion: comparative analysis of structure, expression, localization, and function. *J. Biol. Chem.* 278, 52802-52809.

Stadler, H. and Tsukita, S. (1984). Synaptic vesicles contain an ATP-dependent proton pump and show 'knob-like' protrusions on their surface. *EMBO J.* 3, 3333-3337.

Stewart, B.A., Atwood, H.L., Renger, J.J., Wang, J., Wu, C.F. (1994).

Improved stability of *Drosophila* larval neuromuscular preparations in haemolymph-like physiological solutions. *J. Comp. Physiol*. 2, 179-191.

Stewart, B. A., Mohtashami, M., Trimble, W. S., and Boulianne, G. L. (2000). SNARE proteins contribute to calcium cooperativity of synaptic transmission. *Proc. Natl. Acad. Sci. U. S. A.* 97, 13955-13960.

Strehler, E. E., and Zacharias, D. A. (2001). Role of alternative splicing in generating isoform diversity among plasma membrane calcium pumps. *Physiol. Rev*. 81, 21-50.

Sudhof, T.C. (2008). Neurotransmitter release. Handb Exp Pharmacol. 184,1-21.

Sudhof, T.C. (2001). The synaptic vesicle cycle revisited. *Neuron*. 28, 317-320.

Sudhof, T.C. (2004). The synaptic vesicle cycle. *Annu. Rev. Neurosci.* 27, 509-547.

Sudhof, T.C. and Rothman, J.E. (2009). Membrane fusion: grappling with SNARE and SM proteins. *Science*. 323, 474-477.

Sutton, M.A. and Schuman, E.M. (2009). Partitioning the synaptic landscape: distinct microdomains for spontaneous and spike-triggered neurotransmission. *Sci. Signal.* 2,65.

Sutton, R.B., Fasshauer, D., Jahn, R., and Brunger, A.T. (1998).Crystal structure of a SNARE complex involved in synaptic exocytosis at 2.4 A resolution. *Nature*. 395, 347-353

Suzuki, D. T., and Procunier, D. (1969). Temperature-sensitive mutations in *Drosophila* melanogaster. Dominant lethals and semilethals on chromosome 2 *Proc. Natl.Acad.Sci U. S. A*. 62, 369-376.

Sweeney, S.T., Broadie, K., Keane, J., Niemann ,H., and O'Kane CJ. (1995). Targeted expression of tetanus toxin light chain in *Drosophila* specifically eliminates synaptic transmission and causes behavioral defects. *Neuron*. 14, 341-351.

Takamori, S., Holt, M., Stenius, K., Lemke, E. A., Gronborg, M., Riedel, D., Urlaub, H.,Schenck, S., Brugger, B., Ringler, P.*, et al.* (2006). Molecular anatomy of a trafficking organelle. *Cell.* 127, 831-846.

Taverna, E., Saba, E., Rowe, J., Francolini, M., Clementi, F., and Rosa, P. (2004). Role of lipid microdomains in P/Q-type calcium channel

(Cav2.1) clustering and function in presynaptic membranes. *J. Biol. Chem.* 279, 5127-5134.

Tessier, C.R. and Broadie, K. (2008). *Drosophila* fragile X mental retardation protein developmentally regulates activity-dependent axon pruning. *Development* 135, 1547-1557.

Tessier, C.R and Broadie, K. (2009). Activity-dependent modulation of neural circuit synaptic connectivity. *Front. Mol. Neurosci.* 2, 8.

Thayer, S. A. and Miller, R. J. (1990). Regulation of the intracellular free calcium concentration in single rat dorsal root ganglion neurones in vitro. *J. Physiol*. 425, 85-115.

Trimble WS, Cowan DM, and Scheller RH. (1988). VAMP-1: a synaptic vesicle-associated integral membrane protein. Proc. Natl. Acad. Sci. U. S. A. 85, 4538-4542.

Tsujimoto, T., Jeromin, A., Saitoh, N., Roder, J. C., and Takahashi, T. (2002). Neuronal calcium sensor 1 and activity-dependent facilitation of P/Q-type calcium currents at presynaptic nerve terminals. *Science*. 295, 2276-2279.

Trotta, N., Rodesch, C.K., Fergestad, T., and Broadie, K. (2004). Cellular bases of activity-dependent paralysis in *Drosophila* stress-sensitive mutants. *J. Neurobiol.* 60, 328-347.

Tucker, W.C., Weber, T., and Chapman, E.R. (2004). Reconstitution of Ca^{2+} -regulated membrane fusion by synaptotagmin and SNAREs. *Science*. 304, 435-438.

Ule, J. and Darnell, R.B. (2006). RNA binding proteins and the regulation of neuronal synaptic plasticity. *Curr. Opin. Neurobiol.* 16, 102-110.

van der Bliek, A.M., and Meyerowitz, E.M. (1991). Dynamin-like protein encoded by the Drosophila shibire gene associated with vesicular traffic. *Nature*. 351, 411-414.

Venkatachalam, K, and Montell, C. (2007). TRP channels. *Annu. Rev. Biochem.* 76, 387-417.

Venken, K.J., He, Y., Hoskins, R.A., and Bellen, H.J. (2006). P[acman]: a BAC transgenic platform for targeted insertion of large DNA fragments in D. melanogaster. *Science*. 314, 1747-1751.

Verhage, M., de Vries, K.J., Røshol, H., Burbach, JP, Gispen, W.H., and Südhof, T.C. (1997). DOC2 proteins in rat brain: complementary distribution and proposed function as vesicular adapter proteins in early stages of secretion. *Neuron*. 18, 453-461.

Verhage, M., Maia, A.S., Plomp, J.J., Brussaard, A.B., Heeroma, J.H., Vermeer, H., Toonen, R.F., Hammer RE, van den Berg TK, Missler M, Geuze HJ, and Südhof TC. (2000). Synaptic assembly of the brain in the absence of neurotransmitter secretion. *Science*. 287, 864-869.

Verhage, M. and Sørensen, J.B. (2008). Vesicle docking in regulated exocytosis**.***Traffic*. 9,1414-1424.

Vijayakrishnan, N., Woodruff, E., 3rd, and Broadie, K. (2009). Rolling blackout is required for bulk endocytosis in non-neuronal cells and neuronal synapses. *J. Cell. Sci.* 122, 114-125.

Vilensky, J.A., and Gilman, S. (2002). Neurognostics question 16: the size principle. *J. Hist. Neurosci.* 11, 183-184.

Virmani T, Han W, Liu X, Südhof TC, Kavalali ET.EMBO J. 2003 Oct Synaptotagmin 7 splice variants differentially regulate synaptic vesicle recycling 15;22(20):5347-57.

Voets, T., Toonen, R.F., Brian, E.C., de Wit, H., Moser, T., Rettig, J., Südhof, T.C., Neher, E., and Verhage, M. (2001). Munc18-1 promotes large dense-core vesicle docking. *Neuron*. 31, 581-591

Von Schilcher, F. (1976). The behavior of cacophony, a courtship song mutant in *Drosophila* melanogaster. *Behav. Biol*. 17, 187-196.

Wagh, D. A., Rasse, T. M., Asan, E., Hofbauer, A., Schwenkert, I., Durrbeck, H., Buchner, S., Dabauvalle, M. C., Schmidt, M., Qin, G.*, et al.* (2006). Bruchpilot, a protein with homology to ELKS/CAST, is required for structural integrity and function of synaptic active zones in *Drosophila*. *Neuron*. 49, 833-844.

Walent, J.H., Porter, B.W., Martin, and T.F. (1992). A novel 145 kd brain cytosolic protein reconstitutes Ca(2+)-regulated secretion in permeable neuroendocrine cells. *Cell.* 70,765-775.

Wan, H.I., DiAntonio, A., Fetter, R.D., Bergstrom, K., Strauss, R., and Goodman, C.S. (2000). Highwire regulates synaptic growth in *Drosophila*. *Neuron.* 26, 313-329.

Wang, C. Y., Yang, F., He, X., Chow, A., Du, J., Russell, J. T., and Lu, B. (2001). Ca(2+) binding protein frequenin mediates GDNF-induced potentiation of Ca(2+) channels and transmitter release. *Neuron*. 32, 99-112

Wang, H., Frelin, L., and Pevsner, J. (1997).Human syntaxin 7: a Pep12p/Vps6p homologue implicated in vesicle trafficking to lysosomes. *Gene.* 199, 39-48.

Waung, M.W., Pfeiffer, B.E., Nosyreva, E.D., Ronesi, J.A., and Huber, K.M. (2008). Rapid translation of Arc/Arg3.1 selectively mediates mGluR-dependent LTD through persistent increases in AMPAR endocytosis rate. *Neuron*. 59, 84-97.

Weber, T., Zemelman, B.V., McNew, J.A., Westermann, B., Gmachl, M., Parlati, F., Söllner, T.H., and Rothman, J.E. (1998). SNAREpins: minimal machinery for membrane fusion. *Cell*. 92, 759-772.

Weimer, R.M., and Richmond, J.E. (2005). Synaptic vesicle docking: a putative role for the Munc18/Sec1 protein family. *Curr. Top. Dev. Biol.* 65, 83 -113.

Weimer RM, Richmond JE, Davis WS, Hadwiger G, Nonet ML, and Jorgensen EM. (2003).Defects in synaptic vesicle docking in unc-18 mutants. *Nat. Neurosci.* 10,1023-1030.

Wenk, M.R. and De Camilli, P. (2004). Protein-lipid interactions and phosphoinositide metabolism in membrane traffic: insights from vesicle recycling in nerve terminals. *Proc. Natl. Acad. Sci. U S A.* 101: 8262-8269.

Wharton. K.A., Cook, J.M., Torres-Schumann, S., de Castro, K., Borod, E., and Phillips, D.A. (1999). Genetic analysis of the bone morphogenetic protein-related gene, gbb, identifies multiple requirements during Drosophila development. *Genetics*. 152,629-640.

Wickner, W. (2010). Membrane Fusion: Five Lipids, Four SNAREs, Three Chaperones, Two Nucleotides, and a Rab, All Dancing in a Ring on Yeast Vacuoles. *Annu. Rev. Cell. Dev. Biol.* Ahead of print.

Wilson, I.B., and Alexander, J. (1962). Acetylcholinesterase: reversible inhibitors, substrate inhibition. *J. Biol. Chem.* 237, 1323-1326.

Witcher, D. R., De Waard, M., Sakamoto, J., Franzini-Armstrong, C., Pragnell, M., Kahl, S. D., and Campbell, K. P. (1993). Subunit identification and reconstitution of the N-type Ca^{2+} channel complex

purified from brain. *Science*. 261, 486-489.

Wreden, C. C., Wlizla, M., and Reimer, R. J. (2005). Varied mechanisms underlie the free sialic acid storage disorders. *J. Biol. Chem.* 280, 1408-1416.

Wu, C., Daniels, R.W., and DiAntonio, A. (2007). Dfsn collaborates with Highwire to down-regulate the Wallenda/DLK kinase and restrain synaptic terminal growth. *Neural Dev*. 2,16-27.

Wu, M. N., Fergestad, T., Lloyd, T. E., He, Y., Broadie, K., and Bellen, H. J. (1999). Syntaxin 1A interacts with multiple exocytic proteins to regulate neurotransmitter release in vivo. *Neuron*. 23, 593-605.

Venkatachalam, K., Long, A.A., Elsaesser, R., Nikolaeva, D., Broadie, K., and Montell, C. (2008). Motor deficit in a Drosophila model of mucolipidosis type IV due to defective clearance of apoptotic cells. *Cell.* 135, 838-851.

Xing, B., Ashleigh Long, A., Harrison, D. A., and Cooper, R. L. (2005). Developmental consequences of neuromuscular junctions with reduced presynaptic calcium channel function. *Synapse*. 57, 132-147.

Xu, H., Jun, Y., Thompson, J., Yates, J.,and Wickner, W. (2010). HOPS prevents the disassembly of trans-SNARE complexes by Sec17p/Sec18p during membrane fusion*. EMBO J.* Ahead of Print.

Xu, X.L., Li, Y., Wang, F., and Gao, F.B. (2008). The steady-state level of the nervous-system-specific microRNA-124a is regulated by dFMR1 in *Drosophila. J. Neurosci.* 28, 11883-11889.

Yan, D., Wu, Z., Chisholm, A.D., and Jin, Y. (2009). The DLK-1 kinase promotes mRNA stability and local translation in *C. elegans* synapses and axon regeneration. *Cell.* 138, 1005-1018.

Yang, Y., Xia, Z., and Liu, Y. (2000). SNAP-25 functional domains in SNARE core complex assembly and glutamate release of cerebellar granule cells.*J. Biol. Chem.* 275, 29482-29487.

Yarovaya, N., Schot, R., Fodero, L., McMahon, M., Mahoney, A., Williams, R., Verbeek, E., de Bondt, A., Hampson, M., van der Spek, P.*, et al.* (2005). Sialin, an anion transporter defective in sialic acid storage diseases, shows highly variable expression in adult mouse brain, and is developmentally regulated. *Neurobiol. Dis*. 19, 351-365.

Yoshihara, M., and Littleton, J. T. (2002). Synaptotagmin I functions as

a calcium sensor to synchronize neurotransmitter release. *Neuron*. 36, 897-908.

Yoshihara, M., Suzuki, K., and Kidokoro, Y. (2000). Two independent pathways mediated by cAMP and protein kinase A enhance spontaneous transmitter release at *Drosophila* neuromuscular junctions. *J. Neurosci.* 20, 8315-8322.

Zhang, B., Koh, Y. H., Beckstead, R. B., Budnik, V., Ganetzky, B., and Bellen, H. J. (1998). Synaptic vesicle size and number are regulated by a clathrin adaptor protein required for endocytosis. *Neuron.* 21, 1465-1475.

Zhang, C., Atasoy, D., Araç, D., Yang, X., Fucillo, M.V., Robison, A.J., Ko, J., Brunger, A.T., and Südhof, T.C. (2010). Neurexins physically and functionally interact with GABA(A) receptors. *Neuron*. 66, 403-416.

Zhang, Y.Q., Bailey, A.M., Matthies, H.J., Renden, R.B., Smith, M.A., Speese, S.D., Rubin, G.M., and Broadie, K. (2001). *Drosophila* fragile X-related gene regulates the MAP1B homolog Futsch to control synaptic structure and function. *Cell.* 107, 591-603.

Zhang, Y.Q., Friedman, D.B., Wang, Z., Woodruff, E. 3rd, Pan, L., O'donnell, J., and Broadie, K. (2005). Protein expression profiling of the *drosophila* fragile X mutant brain reveals up-regulation of monoamine synthesis. Mol. Cell. Proteomics 4, 278-290.

Zhong, Y., and Wu, C. F. (1991). Altered synaptic plasticity in *Drosophila* memory mutants with a defective cyclic AMP cascade. *Science*. 251, 198-201.

Zhou, J., Olcese, R., Qin, N., Noceti, F., Birnbaumer, L., and Stefani, E. (1997).Feedback inhibition of Ca^{2+} channels by Ca^{2+} depends on a short sequence of the C terminus that does not include the Ca^{2+} -binding function of a motif with similarity to Ca^{2+} -binding domains. *Proc. Natl. Acad. Sci. U. S. A.* 94, 2301-2305.

Zucker, R. S. (1993). Calcium and transmitter release at nerve terminals. *Biochem. Soc. Trans*. 21, 395-401.

Zucker, R. S. (1996). Exocytosis: a molecular and physiological perspective. *Neuron***.** 17, 1049-1055.